

New Applications of Fluorescence Correlation Spectroscopy in Materials Science

DISSERTATION

zur Erlangung des akademischen Grades eines

Doktors der Naturwissenschaften

- Dr. rer. nat. -

der Fakultät Biologie, Chemie und Geowissenschaften

der Universität Bayreuth

vorgelegt von

Heiko Zettl

aus Schwarzhofen

Bayreuth, 2006

Die vorliegende Arbeit wurde in der Zeit von Mai 2000 bis Juni 2006 am Lehrstuhl für Physikalische Chemie der Universität Bayreuth in der Arbeitsgruppe von Herrn Prof. Dr. Georg Krausch angefertigt.

1. Gutachter: Prof. Dr. G. Krausch

Meiner Familie

*Damit das Mögliche entsteht,
muß immer wieder das
Unmögliche versucht werden*

Hermann Hesse

Contents

1	Introduction	1
1.1	Fluorescence Correlation Spectroscopy	2
2	Theoretical Basis	9
2.1	Fluorescence Correlation Spectroscopy	9
2.2	Experimental Setup	20
2.3	Confocal Observation Volume	23
2.3.1	Calculations of Shape and Size	23
2.3.2	Determination of the Observation Volume in Water	26
2.4	Setup for Temperature-Dependent Measurements	27
2.4.1	Sample Chamber	27
2.4.2	Temperature Control SetUp	28
3	Observation Volume	31
3.1	Possible Paths for the Determination of the Observation Volume	32
3.2	Synthesis of Dye-labelled Polystyrene	34
3.2.1	Anionic Polymer Synthesis	34
3.2.2	Synthesis of the Acid Chloride of Rhodamine B	35
3.2.3	Coupling of the Polymer with the Dye Molecules	35
3.2.4	Characterisation of the Polymer by GPC and MALDI-ToF	36
3.3	Observation Volume in Organic Solvents	39
4	Overlap Concentration	43
4.1	Dilute and Semi-Dilute Polymer Solutions	44
4.2	Overlap concentration	48
5	Aggregation of Surfactants	57
5.1	Theory of Surfactant Aggregation	58
5.2	Experimental Methods for the CMC Determination	62
5.3	Aggregation Studis of Surfactants with FCS	62
5.3.1	Sample Preparation	63
5.3.2	Results of the FCS Measurements	64
5.3.3	Discussion	75

6	Aggregation of Block Copolymers	79
6.1	Theoretical basis for the aggregation of polymers	80
6.2	Aggregation of Polystyrene-block-Amylose in THF	80
6.2.1	Investigated sample	81
6.2.2	Results and Discussion	82
6.3	Aggregation of Janus micelles in THF	84
6.3.1	Investigated polymer	84
6.3.2	Results and Discussion	85
6.4	Amphiphilic Janus Micelles	86
6.4.1	Experimental Setup	87
6.4.2	Results and Discussion	87
7	Temperature dependent measurement	91
7.1	Binding of protein to DNA	91
8	Summary	97
9	Zusammenfassung	101

Chapter 1

Introduction

The importance of experiments that deal with single-molecule aspects has strongly increased over the past years. The possibility of studying the dynamics of individual molecules and their mechanical and photo-physical properties has provided new insights into a broad variety of physical processes and led to a profound understanding of effects that occur on the nanometer scale. Single-molecule studies allow to observe reactions inside cells or to follow the self organisation of molecules. Such studies are first steps towards the development of molecular motors, to the formation of structures for liquid handling, and to electronics on the nanometer scale.

Various experimental methods have been developed and improved to address individual particles on the nanometer scale. Imaging methods like scanning force microscopy (AFM), scanning tunnelling microscopy (STM) and cryo-transmission electron microscopy (cryo-TEM) are used to study conformations of single molecules [Lin97, Ike01, Mul02, Gon05, Gal04], to investigate the interaction and complex-formation of molecules [Kam94, Sti01, Lys05, Lys02] or to study the adsorption of individual molecules on surfaces [Lop98, Pfa99, Kim02, Dun02]. Modified AFM setups were used to determine inter- and intra-molecular forces of single molecules [Jan00, Sen01, Tro02]. Optical methods like single-molecule track-

ing and fluorescence correlation spectroscopy (FCS) give new insights in the motion and mobility of molecules. With single-molecule tracking it was possible for the first time to visualise the infection pathway of a virus [Sei01] and various other elementary processes inside cells [Moe99, Sak00, Sch00b, Har01, Dei04]. In contrast to this technique, fluorescence correlation spectroscopy does not follow the motion of an individual molecule. Instead, it relies on the ensemble average of a large number of single-molecule events and from this determines the diffusion of molecules. This way changes in the mobility of molecules can be detected with very high sensitivity. The origin of such changes can be the aggregation of molecules, chemical reactions or conformational changes of the molecules.

In this thesis FCS is used to investigate interactions between polymer chains and to study the aggregation of molecules. For this purpose a commercial FCS setup was modified to allow measurements in organic liquids and a calibration system for the modified optics was developed. In addition, the setup was expanded by a temperature control unit, which opened a way to determine reaction constants and reaction enthalpies of very small amounts of material.

1.1 Fluorescence Correlation Spectroscopy

The theoretical background of fluorescence correlation spectroscopy (FCS) was developed in the early 1970th by Elson and Madge adapted from the theory of dynamic light scattering (DLS) [Mag72, Els74, Mag74]. In analogy to DLS correlations in the temporal fluctuations of a signal are analysed. In FCS the fluorescence signal of the sample is correlated to obtain information on the processes that cause the fluctuations. To measure the fluorescence of the sample a small part of it is illuminated by a focussed laser beam. Figure 1.1 presents the conceptual basis of FCS and shows three examples for the possible origin of fluctuations in the fluorescence signal. First, transport of fluorescent molecules through the illuminated

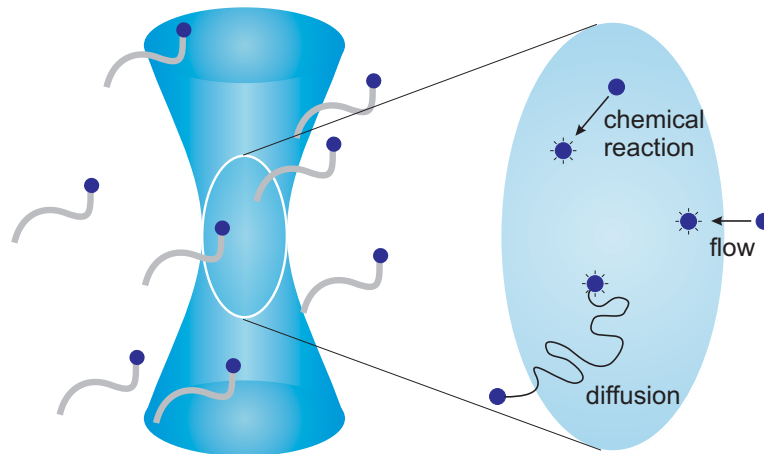


Figure 1.1: Conceptual basis of FCS. Fluorescent molecules move through an illuminated volume by diffusion or flow or they undergo a chemical reaction and change therefore their fluorescent properties.

volume can be the cause of fluctuations of fluorescence. In thermodynamic equilibrium the origin of such motion can be thermally-induced concentration fluctuations, which occur on the microscopic scale, and are known as Brownian motion. Also an external flow of the liquid transports molecules through the illuminated volume and therefore causes fluctuations in the fluorescence signal. Second, transitions between two states of different fluorescent yield can lead to fluctuations in the fluorescence if the transition occurs while the molecule traverse the excitation beam [Wid00]. The stability of such states and the change between different states is often dependent on the local environment of the molecules. Therefore FCS can be used to probe the local environment of the fluorescent molecules on a microscopic scale [Wid95].

As mentioned above, FCS can be set up to only detect thermally induced Brownian motion of the molecules [Rig79, Gee82, dIT01]. In this case the sample stays in the thermodynamic equilibrium and it is not necessary to induce external perturbations of the system.

Dynamic light scattering (DLS) also investigates concentration fluctuations by analysing the dynamics of the dielectric constants in liquids. Hence, also this technique determines

the mobility of molecules. But in contrast the detection efficiency of FCS exceeds that of DLS due to the high signal-to-background ratio of fluorescence compared to the dielectric contrast used in DLS.

The theoretical introduction of FCS was soon followed by first experiments. In the early work, the mobility of marker molecules in cell membranes are discussed as well as several in-vitro and in-vivo applications [Mag72, Ara76, Ehr76, Kop76, Mad76, Web76]. These first FCS experiments suffer from poor signal quality, which arises from a low photon detection efficiency. In addition, the weak background suppression and the large ensemble of molecules impaired the signal. It is obvious that fluctuations can be resolved the better the smaller the number of molecules is in the illuminated volume. Ideally the experiments take place on the single-molecule level. In the 1990ies this aim was reached with the development of lasers as efficient light sources and highly-efficient and fast avalanche photo diodes for the detection of the fluorescence. Koppel *et al.* were the first who suggest a confocal microscopy geometry to minimise the illuminated volume [Kop76, Web76]. In this geometry a laser beam is focussed by an objective with high numerical aperture ($NA > 0.9$) to a diffraction-limited focus which is of the order of the wavelength in size. Figure 1.2 A shows the isointensity surface of a diffraction-limited laser beam at which the intensity of the laser is dropped to $\frac{1}{e^2}$. Only fluorescent molecules inside the volume enclosed by the isointensity area emit enough photons to give a contribution to the fluorescent signal. The size of the focus volume perpendicular to the optical axis is of the order of the wavelength. The axial dimension of the focus is about one order of magnitude larger. This resolution can be improved by placing a field aperture (pinhole) in the image plane of the objective. This yields a volume for the observation of the motion of fluorescent molecules of around 1 fL. Figure 1.2 B shows the isointensity surface and the corresponding observation volume of a typical confocal FCS setup. Rigler and Eigen were the first to use this geometry for FCS experiments and to integrate avalanche photo diodes in the experimental setup for

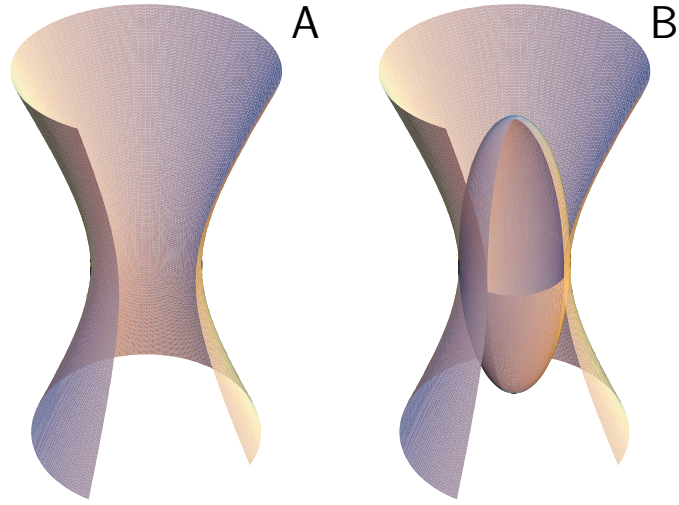


Figure 1.2: Isointensity surface of a focused laser beam. The intensity is dropped to $\frac{1}{e^2}$ to the intensity in the optical axis. On the right side additionally the observation volume restricted by a field aperture is shown.

single-molecule detection [Eig94, Mai97].

For the description of the mobility of molecules it is necessary to determine the time a molecule needs to move through the observation volume. For this purpose the fluctuations of the detected fluorescence is correlated with a time shifted replica of itself at different values of time shift τ . The resulting function is called autocorrelation function and is a measure of the self similarity of the fluctuation signal. Mathematically, the autocorrelation function reads

$$g(\tau) = \langle I(t)I(t + \tau) \rangle \quad (1.1)$$

where $I(t)$ is the intensity of the signal at time t . The angle brackets denote the averaging over all times t . From a physics point of view the above-defined autocorrelation function describes the probability to detect a second photon at time τ after a first photon was detected at time zero. For a proper interpretation of the correlation function we need to discuss the possible origins of these two photons.

Case I: The two photons detected at time zero and at time τ are emitted by two different

fluorescing molecules. When we assume that the motion of each molecule is independent from the other molecule, we expect that there is no average correlation between the two events and these photons only contribute an offset to the autocorrelation function.

Case II: The photons originate from a constant background fluorescence of the solution. Also in this case no correlation between the two photons is expected and hence the background fluorescence will also contribute a constant offset to the autocorrelation function.

Case III: The two photons originate from the same molecule. These photons are then physically correlated and lead to a time-dependent contribution to $g(\tau)$. They reflect the residence time of the fluorescent species inside the illuminated volume.

This considerations show that only photons originating from the same molecule lead to time-dependent contributions of the autocorrelation function. This classifies FCS as a single-molecule method [End04], although the characteristic relaxation time a molecule needs to move through the observation volume is not extracted from the signal of a single molecule. In contrast to DLS where the averaging is done over a large area and, hence, by observing a big ensemble of molecules *simultaneously* here the averaging is done over many single-molecule events that occur *non-simultaneously*.

A key motivation for the development of FCS was the possibility to measure kinetic constants of biochemical reactions without a perturbation of the system. Therefore all the early FCS work concentrate on biochemical systems [Mag72, Els74, Mag74, Ehr74]. Also the further improvement of this technique was done by groups with their main interest in biochemical questions. Several review articles and one book show the high potential of FCS in the analytical and diagnostic work in life science [Web76, Rig01, Kri02, Sch01a, Hes02a]. In the 1990ies Carl Zeiss offered the first commercial FCS setup. In the following years a few groups started to use this technique to monitor the aggregation of synthetic polymers and to investigate polymer surfactant aggregates [Sch00a, VR01, Zha01]. However, this technique is barely used so far in materials science and its potential is still under-utilised

yet.

With this thesis I try to reveal the potential of FCS in materials science by utilising it for the investigation of aggregation processes and by expanding the common setup to organic solvents and to temperature-controlled samples. I show exemplarily that the high sensitivity of FCS in determining the mobility of molecules makes it an ideal method to study the aggregation of molecules.

In a first part of the work a modified FCS setup is configured for the investigation of polymers in organic solvents. To determine the size of the observation volume dye-labelled polystyrene chains of different molecular weight and a narrow weight distribution were synthesised. The modified and optically characterised setup is then used to investigate the molecular-weight dependence of the overlap concentration of polystyrene in a range of molecular weights from 4 to 1550 kg/mol.

In a second part I concentrate on the detailed study of micelle formation of low molecular weight surfactants and on the aggregation of block-copolymers. For these investigations I developed a new concept of non-covalent labelling of micelles and polymers to follow the aggregation formation in various systems from low molecular weight surfactant molecules up to complex block copolymers. The high sensitivity and the fact that FCS relies on the detection of single-molecule events makes it possible to study the aggregation in a concentration range not accessible by other methods.

In addition the setup was modified to enable FCS measurements at various temperatures. In the last part of this thesis very different systems synthesised and characterised by co-workers were presented. With the modifications and labelling methods developed in this thesis new insights about the systems are won.

Chapter 2

Theoretical Basis and Experimental Setup

2.1 Fluorescence Correlation Spectroscopy

Polymers and colloids are often characterised solution and are processed in solutions. Therefore a detailed knowledge of the static and dynamic properties of solutions and the dissolved molecules is desirable. The investigation of these properties can be done using different approaches. One possibility is to investigate the samples with macroscopic methods averaging over a large ensemble of molecules. Two methods often used in material science to characterise solutions are rheological measurements and scattering experiments. From these experiments inference on the behaviour of single polymer molecules is mostly difficult. This lack can be circumvented by a direct observation of the motion of single molecules. This second approach for the characterisation of polymer solutions give insight in the behaviour of an individual molecule, but also provide a measure for macroscopically relevant parameters like viscosity. For the observation of single molecules a signal with high selectivity is necessary. in other words it is important to be able to distinguish the signal

originating from a specific molecule from unspecific background signal. In our case we use fluorescent labels to mark a certain molecular species. The fluorescence of the label gives an intense signal which can clearly be separated from Raman-scattered light and other background signals. As mentioned in the introduction we follow molecules entering and leaving the observation volume to obtain information on the dynamic behaviour of these molecules. The fluorescence signal carries this information in its fluctuation dynamics. The distribution of the molecules in the observation volume can be described by a Poissonian [Kri02, Saf03]. Hence the root mean square fluctuation of the particle number is given by

$$\frac{\sqrt{\langle(\delta N)^2\rangle}}{\langle N\rangle} = \frac{\sqrt{\langle(N - \langle N\rangle)^2\rangle}}{\langle N\rangle} = \frac{1}{\sqrt{\langle N\rangle}} \quad (2.1)$$

The relative fluctuations in the signal increase with a decreasing average number of particles $\langle N\rangle$ observed at a time . Therefore a minimisation of the average number of fluorescent molecules that is at a time in the observation volume is essential for an effective detection of fluctuations. This aim can be reached either by decreasing the concentration of fluorescent molecules in the solution or by minimising the observation volume. Schwille *et al.* claims 0.1 to 1000 fluorescent particles in the observation volume to be the ideal range for FCS experiments. Our experiments indicate that only a range of 0.1 to 10 particles is useful. Having more than one particle in the observation volume decreases the amplitude of the relative fluctuations, having much less than one particle increases the required measurement time for an experiment with sufficient signal-to-noise ratio. Hence the optimum concentration of fluorescent molecules is predetermined mainly by the size of the observation volume. Minimising the observation volume has the additional advantage of lowering the background fluorescence as well as the Raman scattering. For this purpose a confocal observation volume of around 1 fL is the smallest volume achievable at present. The improvements of optical components like lenses and filters together with the progress

in the field of photo diodes during the past decade allow to detect single dye molecules. An important parameter characterising an FCS experiments is the number of photon counts η_i recorded from a single molecule i . The photon counts depend on the photo physical properties of the molecule described by the absorption cross section σ_i and the quantum yield q_i of the molecule. Furthermore the total detection efficiency κ of the setup has to be considered. The multiplication of these efficiency parameters with the intensity I of the exciting light gives the number of counts per molecule:

$$\eta_i = \sigma_i q_i \kappa I \quad (2.2)$$

Koppel showed that this value is directly proportional to the signal-to-noise ratio of an FCS measurement. Therefore, a high value of η_i is necessary to yield a good FCS measurement [Kop74]. The emitted fluorescence density is calculated by multiplying η_i with the particle concentration c_i .

$$F_{em} = \eta_i \cdot c_i \quad (2.3)$$

The detected fluorescence is the integral of the emitted fluorescence density given in equation 2.3 weighted with the molecule detection function (MDF) $W(\vec{r})$ of the optical setup.

$$F_{i,det}(t) = \int_V W(\vec{r}) F_{em} \cdot dV = \int_V W(\vec{r}) \eta_i c_i \cdot dV \quad (2.4)$$

The MDF is a product of the intensity profile of the incident laser beam $I_{ex}(\vec{r})$ and the collection efficiency function (CEF) $S(\vec{r})$ describing the combination of objective and pinhole. The normalisation on the intensity I_0 at the focus point gives an intensity independent function [Sch01b].

$$W(\vec{r}) = \frac{I_{ex}(\vec{r})}{I_0} S(\vec{r}) \quad (2.5)$$

$W(\vec{r})$ is independent of the investigated species and describes the properties of the optical setup. Determining $W(\vec{r})$ experimentally is extremely difficult or even impossible. Instead, the MDF is commonly approximated by a three-dimensional Gaussian intensity distribution [Hes02b]. This distribution is characterised by the distances where the initial intensity I_0 drops to $\frac{1}{e^2}$. In the direction of the beam this distance is called the focus length w_z , perpendicular to the optical axis it is called the waist radius $w_{x,y}$.

$$W(\vec{r}) = \frac{I_{ex}(\vec{r})}{I_0} S(\vec{r}) = \exp\left(\frac{-2(x^2 + y^2)}{w_{x,y}^2}\right) \exp\left(\frac{-2z^2}{w_z^2}\right) \quad (2.6)$$

The volume comprised by the iso-intensity surface $\frac{I(\vec{r})}{I_0} = \frac{1}{e^2}$ has the shape of an ellipsoid with the axes $w_{x,y}$ and w_z and is often referred to as observation volume. The signal detected in an FCS experiment originates predominantly from this volume. Therefore the size and shape of the observation volume is a key parameter for FCS. A more detailed description of this volume is given in chapter 2.3. Inserting equation 2.5 and 2.2 into equation 2.4 yields

$$F_{i,det}(t) = \int_V I_{ex}(\vec{r}) S(\vec{r}) \kappa \sigma_i q_i c_i(\vec{r}, t) \cdot dV \quad (2.7)$$

All three parameters σ_i , q_i and $c_i(\vec{r})$ can vary with time and hence lead to fluctuations in the fluorescence signal. For the further considerations we assume constant optical properties of the fluorescent molecules. Hence the absorption cross section σ_i and the quantum yield q_i of the molecules do not change during the experiment. Only the local concentration of the molecule fluctuates. Therefore the fluorescence fluctuations can then be written as

$$\delta F_i(t) = \kappa \int_V I_{ex}(\vec{r}) S(\vec{r}) \sigma_i q_i \delta c_i(\vec{r}, t) \cdot dV \quad (2.8)$$

Figure 2.1 shows a typical fluorescence signal in an FCS experiment. For further analysis it is helpful to split the fluorescence signal into the time-independent average fluorescence

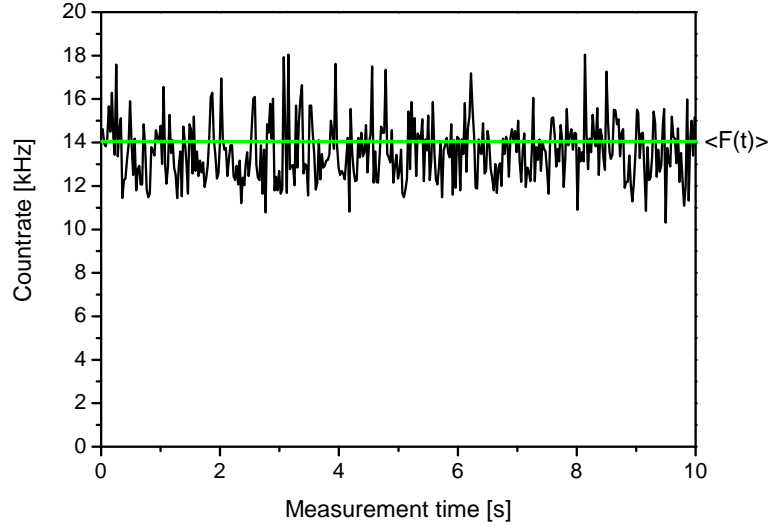


Figure 2.1: Typical curve of the fluorescence intensity in an FCS experiment. The green line indicates the average signal intensity.

intensity and the time-dependent fluctuations around this average value.

$$F(t) = \langle F \rangle + \delta F(t) \quad (2.9)$$

The autocorrelation of this signal quantifies the time-dependent fluctuations in the fluorescence signal. The basis for this analysis was done in the 1970ties by Madge *et al.* [Mag72, Mag74, Els74]. The autocorrelation function analyses the signal with respect to its self similarity after the lag time τ [Sch01a] and is defined as:

$$G_{allg}(\tau) = \langle F(t)F(t + \tau) \rangle \quad (2.10)$$

Equation 2.10 is normalized to the time-independent fluorescence intensity $\langle F(t) \rangle$ in order to remove the background fluorescence and scattered light.

$$G(\tau) = \frac{\langle F(t)F(t + \tau) \rangle}{\langle F(t) \rangle^2} = \frac{\langle \delta F(t)\delta F(t + \tau) \rangle}{\langle F(t) \rangle^2} + 1 \quad (2.11)$$

To obtain information on the observed molecules a detailed analysis of the origin of the fluctuations has to be done. In the case that the molecules do not show any change in their optical properties we observe only fluctuations in the local concentration of the fluorescent molecules. In an undisturbed system the motion of molecules is caused by Brownian motion only [dlT01].

For a small number of fluorescent particles in the observation volume the signal increases significantly if a dye molecule enters the observation volume and decreases when it leaves. This is the case for small observation volumes and low dye concentrations. The time-dependent and position-dependent concentration can be written as

$$C(\vec{r}, t) = \langle C \rangle + \delta C(\vec{r}, t) \quad (2.12)$$

In FCS experiments a length scale of a few nanometer and volume elements of around 1 fL are observed. In dilute solutions on these scales a concentration gradient of the fluorescent molecules can be observed. Hence the time-dependent concentration fluctuations $\delta C(\vec{r}, t)$ can be described and analysed by means of Fick's law of diffusion:

$$\frac{\partial \delta C_j(\vec{r}, t)}{\partial t} = D_j \nabla^2 \delta C_j(\vec{r}, t) \quad (2.13)$$

where D_j is the diffusion constant of component j and C_j is the concentration of this component at \vec{r} at time t . For an analysis of the time-dependent fluctuations equation 2.13 is Fourier transformed and the autocorrelation of the concentration fluctuations is calculated (for details see [Kri02, Els74]).

$$\langle \delta C(\vec{r}, 0) \delta C(\vec{r}', \tau) \rangle = \langle C \rangle \frac{1}{(4\pi D\tau)^{3/2}} \cdot e^{-\frac{(\vec{r}-\vec{r}')^2}{4D\tau}} \quad (2.14)$$

A combination of equations 2.6, 2.8, 2.14 and 2.11 leads to the autocorrelation function for freely diffusing molecules.

$$G(\tau) = \frac{1}{\langle N \rangle} \frac{1}{1 + \frac{\tau 4D}{w_{x,y}}} \frac{1}{\sqrt{1 + \frac{\tau 4D}{w_z}}} + 1 = \frac{1}{\langle N \rangle} \frac{1}{1 + \frac{\tau}{\tau_D}} \frac{1}{\sqrt{1 + S^2 \frac{\tau}{\tau_D}}} + 1 \quad (2.15)$$

where $\langle N \rangle$ is the average number of fluorescent molecules in the observation volume, $S = \frac{w_z}{w_{x,y}}$ is the structure parameter of the observation volume and

$$\tau_D = \frac{w_{x,y}}{4 \cdot D} \quad (2.16)$$

is the average time a molecule needs to diffuse through the illuminated volume. In case of a spherical particle the hydrodynamic radius of the measured molecules can be related to D by the Einstein-Stokes relationship

$$D = \frac{kT}{6\pi\eta R_h} \quad (2.17)$$

where k is the Boltzmann constant, T the temperature and η is the viscosity of the solution. With these calculations we obtain the number average of the hydrodynamic radius R_h of the molecules. A typical autocorrelation curve expected for a solution with a single dye molecule diffusing through the observation volume described by equation 2.15 is presented in figure 2.2.

In the theory presented so far only fluorescence is considered as origin for the emission of photons. The photo physics of dye molecules, however, is often more complex [Dit01, Egg05]. The excitation of an electron by absorption of a photon can be followed by different relaxation steps. A description of the molecular energetic states is given in figure 2.3 by a Jablonski diagram. Starting from the ground state S_0 of the molecule a photon is absorbed and the molecule undergoes a transition into the first excited singlet state

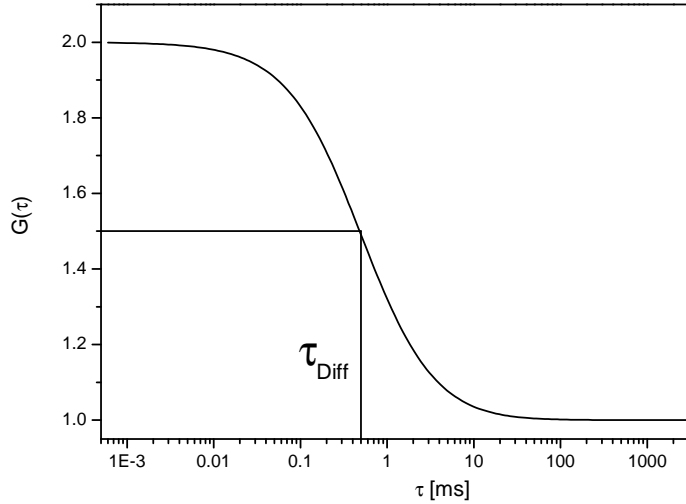


Figure 2.2: Typical autocorrelation curve of a freely diffusing dye molecule with a diffusion time τ_{Diff} of $50 \mu\text{s}$. The number of particles in the observation volume in this example is one.

S_1 . This state has a typical lifetime of a few nanoseconds. The relaxation of the excited state can happen in two different ways. The molecule can emit a photon and return back to the ground state. This emitted photon is called fluorescence. The second way is an intersystem crossing in the first excited triplet state T_1 . From the point of quantum mechanics this transition is forbidden. In case of spin-orbit coupling this transition is possible. A relaxation of the molecule from the triplet state to the ground state is forbidden for the same reasons. Therefore the life time of the excited triplet state is of the order of several micro seconds. Light originating from a relaxation of the triplet state to the ground state is called phosphorescence. The long life time of these states also increases the probability of photobleaching. The fluctuations in the detected light occurring from molecules trapped in the triplet state can be achieved by FCS measurements and also contribute to the autocorrelation function [Egg98]. Triplet relaxation and the diffusion process of molecules occur at different time scales and can to first approximation be treated separately. In this case the expected autocorrelation curve $G(\tau)$ is a product of the two

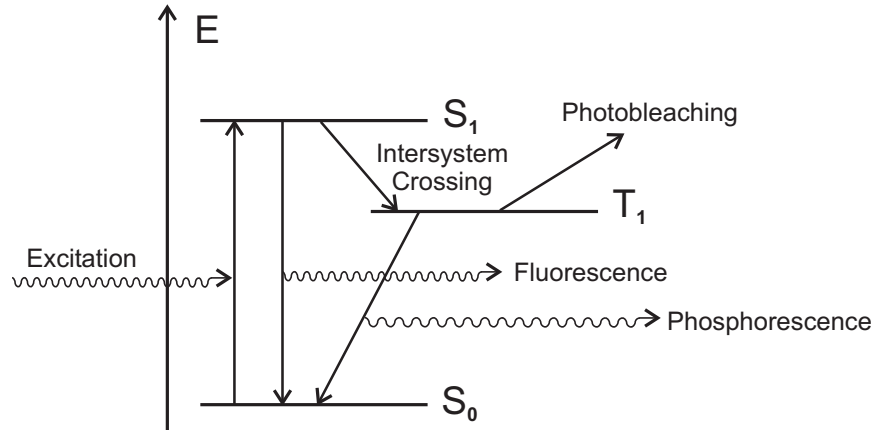


Figure 2.3: Jablonski diagramm of a dye molecule. The energy levels of an dye molecule and the possible transitions between the different state are shown.

contributions describing the diffusion $G_{\text{diffusion}}(\tau)$ and the triplet relaxation $G_{\text{triplet}}(\tau)$ of the molecule

$$G(\tau) = G_{\text{diffusion}}(\tau) \cdot G_{\text{triplet}}(\tau) \quad (2.18)$$

The triplet decay of a dye is a first order kinetics and can be described by an exponential decay.

$$G_{\text{triplet}}(\tau) = 1 - T + T \cdot e^{-\frac{\tau}{\tau_{\text{triplet}}}} \quad (2.19)$$

where T is the fraction of molecules in the triplet state and τ_{triplet} is the decay time of the triplet state [Wid95]. The product of equation 2.15 and 2.19 describes a freely diffusing particle including triplet excitation as well. The total autocorrelation function is then given by

$$G(\tau) = (1 - T + T \cdot e^{-\frac{\tau}{\tau_{\text{triplet}}}}) \cdot \frac{1}{\langle N \rangle} \frac{1}{1 + \frac{\tau}{\tau_D}} \frac{1}{\sqrt{1 + S^2 \frac{\tau}{\tau_D}}} + 1 \quad (2.20)$$

In figure 2.4 an autocorrelation curve for particles with a diffusion time of 1 ms and a triplet life time of 10 μs is depicted. 20% of the particles are in the triplet state and the average number of the fluorescent molecules in the observation volume is one. The two

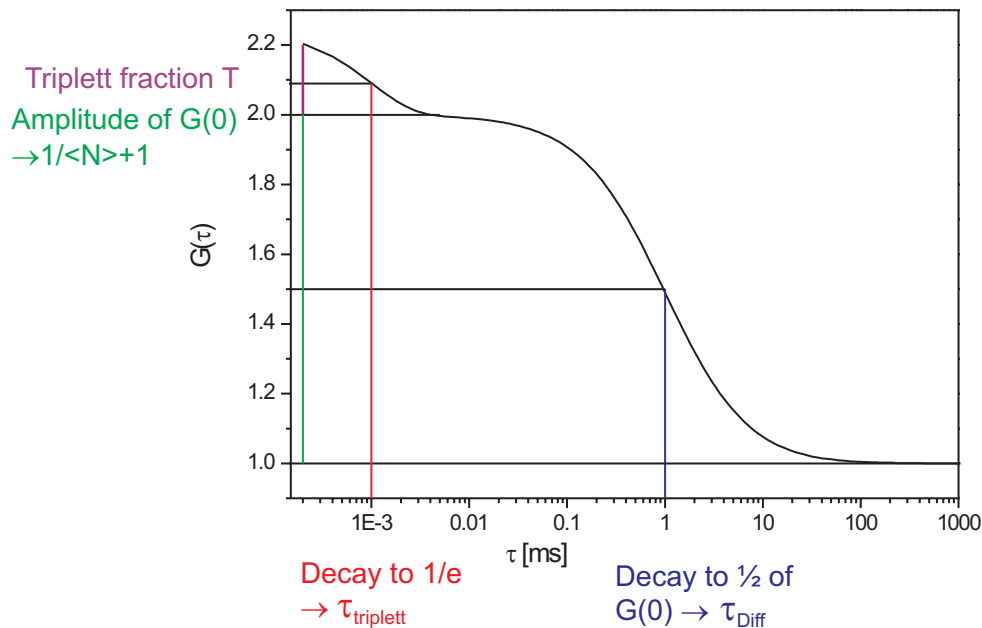


Figure 2.4: Typical autocorrelation curve of a freely diffusing dye molecule with a triplet fraction T of 20% a triplet time $\tau_{triplett}$ of $10 \mu s$ and a diffusion time of $1 ms$.

different parts of the curve resulting from the triplet excitation and the diffusion of the molecules are clearly separated. With this graph we show how the key values T , $\langle N \rangle$, τ_{Diff} , $\tau_{triplett}$ can be obtained by an FCS experiment.

For a quantitative determination of the concentration of fluorescent molecules and an absolute value for the diffusion coefficient it is essential to know the size of the observation volume. Only then the values obtained by FCS are comparable with other methods measuring the diffusion coefficients and concentrations. For this reason we have to determine the observation volume of the FCS setup. The diffusion of a dye molecule with a well known diffusion coefficient is investigated. Using the obtained diffusion time and the known diffusion coefficient leads to the waist radius using equation 2.16.

In order to follow the aggregation of molecules or the binding of molecules it is necessary to distinguish between fractions of particles with different diffusion times. Therefore the

description of the autocorrelation function has to be expanded to i different fractions. If we assume that the photo physical properties of the dye molecules do not change during aggregate formation we get an autocorrelation function for k different molecules.

$$G(\tau) = (1 - T + T \cdot e^{\frac{\tau}{\tau_{triplet}}}) \cdot \frac{1}{\langle N \rangle} \sum_{i=1}^k \frac{\Phi_i}{1 + \frac{\tau}{\tau_{D_i}}} \cdot \frac{1}{\sqrt{1 + S^2 \frac{\tau}{\tau_{D_i}}}} + 1 \quad (2.21)$$

From a fit of equation 2.21 to the experimental data the dynamic and photo physical parameters of the system are obtained. In case of aggregation we have good reasons to assume that there are two fractions: freely diffusing dye molecules and dye molecules attached to the aggregates. In this case it is necessary to find a method to distinguish between systems where a fit with only one diffusion time τ_D is sufficient or if two different fractions with two different τ_{Diff_i} are necessary. A first possibility is to compare the two χ^2 values resulting from a single-particle model and from the more complicated model with two fractions. A more advanced but more accurate method is a hypothesis test [Mes99, Woh01]. This so called F-test compares the χ^2 values weighted with the number of parameters varied during the fitting of the different fit models. The details of this method and the mathematical background are described by Bevington and Robinson [Bev92].

The ability of FCS to distinguish two fractions of molecules with different diffusion times is limited. A detailed analysis of the boundaries of FCS was done by Meseth *et al.* [Mes99]. He found that a fraction of 10% can be evaluated if the respective diffusion times differ by a factor of two. As $\tau_{Diff} \propto R_h$ and the volume of the aggregates is proportional to R_h^3 the molecular weight of the aggregates has to differ by a factor of eight for two aggregates distinguished by FCS [Mes99].

2.2 Experimental Setup

From the theory presented in chapter 2.1 we learned that it is essential to maximise the relative fluctuations of the fluorescence signal (equation 2.1). It can be mathematically shown that the highest signal-to-noise ratio is achieved when the averaged number of particles in the observation volume is one. Therefore it is necessary to work with highly-diluted solutions of dye molecules and to minimise the observation volume. These two goals can be achieved by a confocal setup, where the excitation of the molecules and the collection of the fluorescence light is done by the same objective. The efficiency of a confocal setup was first presented by Koppel *et al.* [Kop76]. Decisive improvements in optics (development of new objectives with high numerical aperture and low chromatic and spherical aberration), in the detection of the fluorescence (fast and highly sensitive avalanche photo diodes), and in the data evaluation (fast electronics for counting and storing the photo diode signal) [Eig94, Mai97] during the past years made FCS a very powerful experimental single-molecule technique.

A sketch of a confocal FCS setup is shown in figure 2.5. A collimated excitation laser is reflected by a dichroic mirror and focussed to the sample by an objective with a high numerical aperture. The emitted fluorescence light is collected by the same objective. As the focus of the excitation and emission beam path is identical such configuration is named “confocal”. The fluorescence light is separated from the residual scattered light by a dichroic mirror and is focussed onto a pinhole which eliminates all light emitted from outside the focal volume. The fluorescence light is detected by an avalanche photo diode in single-photon-counting mode. For FCS application the resulting signal is autocorrelated.

Since the early 1990ies setups for Fluorescence Correlation Spectroscopy are commercially available. They are typically equipped with water immersion objectives and are optimised for the work with aqueous samples. In this work we used the commercially available

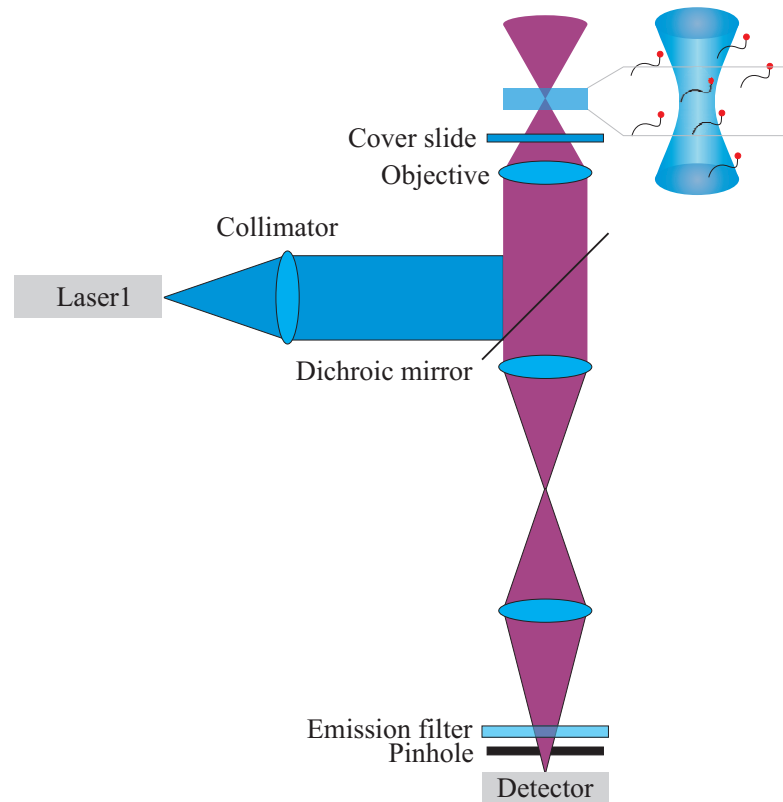


Figure 2.5: Scheme of a confocal set up for Fluorescence Correlation Spectroscopy.

ConfoCor 2 from Carl Zeiss Jena, which was optimised for aqueous samples as well. A view of the optical beam path of this instrument is shown in figure 2.6 [Rig01]. This setup based on the three subunits: the laser unit, the FCS detection unit with the microscope and the APD unit for detection. For the excitation of the molecules three light sources are available in the laser unit: an Ar-ion laser in multi-line mode, a green and a red HeNe laser. These lasers cover the wavelengths of 458 nm, 488 nm, 514 nm, 543 nm and 633 nm. The excitation sources are coupled into a optical single-mode fibre which is connected to the FCS detection unit. In this unit the whole optics of the FCS setup is integrated. A collimation lens creates an expanded parallel laser beam. This beam is reflected by the main beamsplitter, which can be chosen from a variety of different dichroic mirrors optimised for the corresponding wavelength. A cover-slide-corrected 40× C-Apochromat

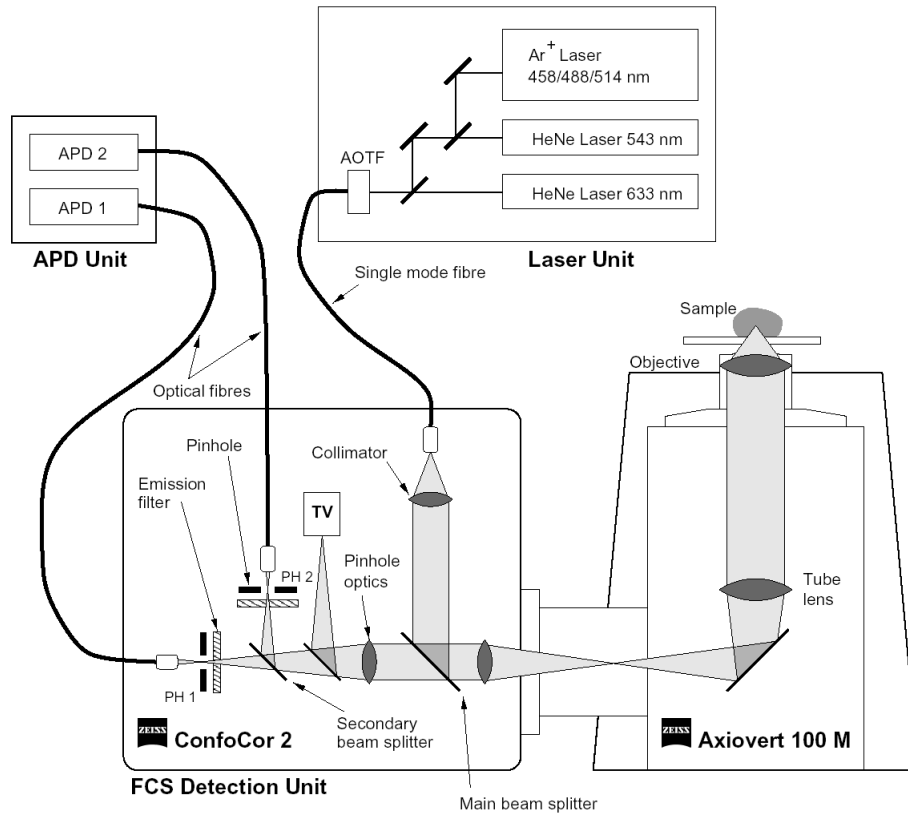


Figure 2.6: Scheme of the beam path of the commercial FCS setup Confocor 2. The laser is coupled to the microscope head by a glass fibre. The selection of the laser wavelength and the control of the intensity is done by an acousto-optical tunable filter (AOTF).

water immersion objective with a numerical aperture of 1.2 is used to focus the laser beam into the sample. Objectives with high numerical aperture are very sensitive to small changes in the thickness of the coverslide. To correct such deviations a correction ring at the objective is available. As the fluorescence light has a longer wavelength compared to the excitation light of the laser, it passes the dichroic mirror and is focussed onto a pinhole by a special pinhole optic mounted in the image plane of the objective–tube lens combination. In front of the pinhole emission filters are used to further suppress scattered laser light and Raman-scattered light. For this purpose different long-pass and band-pass filters can be placed into the beam path. The collected light is detected by avalanche

photo diodes coupled via optical fibres to the FCS detection unit. The signal is counted by a special counter card and autocorrelated by a software correlator. The accessible correlation times range from 10 ns to 100 s. The analysis of the obtained autocorrelation curve is done by fitting equation 2.21 to the data. Therefore a LabView program using the Levenberg-Marquardt algorithm was developed.

2.3 Confocal Observation Volume

2.3.1 Calculations of Shape and Size

For the detected fluorescence described by equation 2.4 and therefore for the resulting autocorrelation curve of an FCS experiment (equation 2.21) the size and the shape of the observation volume represented by the *molecule detection function* (MDF) $W(\vec{r})$ plays an important role. In the following section this volume will be analysed in more detail by calculations on the basis of fundamental wave optical considerations.

The MDF can be separated in a part describing the excitation beam and a part for detection of the fluorescence. For the description of optical beampaths and effects of optical components on laser beams commonly a paraxial approximation and a Gaussian beam is used. But these common approximations are only valid for lenses and objectives with numerical apertures clearly below 0.9. In case of a confocal geometry objective with high numerical aperture up to 1.45 are used. Therefore an exact wave-optical calculation is necessary. Wolf and Richards [Wol59, Ric59] have done these seminal calculations for the first part of the MDF describing the excitation beampath. They evaluated the spatial distribution of the electromagnetic field of a laser focus in the object space of an objective with high numerical aperture.

For the second part describing the optical components for the detection of the fluorescence light these calculations were done much more recently. The collection efficiency func-

tion (CEF) is calculated by Sheppard, Török and Enderlein [She97, Tor98, Tor00, End00, End03]. These calculations describe the intensity distribution at the pinhole generated by a single dipole emitter in the object plane of the objective. The product of the CEF and the excitation beam profile yields the MDF. The evaluation of the MDF allows a detailed theoretical insight in the optical effects of changes in the FCS setup and the investigated samples. Enderlein used the calculated MDF to study the effect of variations of the refractive index of the sample on the size and the shape of the MDF and the effect on the autocorrelation curve. Therefore he simulated the deviation of the autocorrelation function caused by this changes and compared these results with the respective measurements. He found for a difference of the refractive index of 4% a change in the diffusion coefficient of 12% [End04]. In the present work his calculations were used to evaluate the shape and the size of the observation volume of the used setup for different samples and therefore to decide which configuration is the best for the experiments.

Figure 2.7 A shows the MDF for a water immersion objective with a numerical aperture

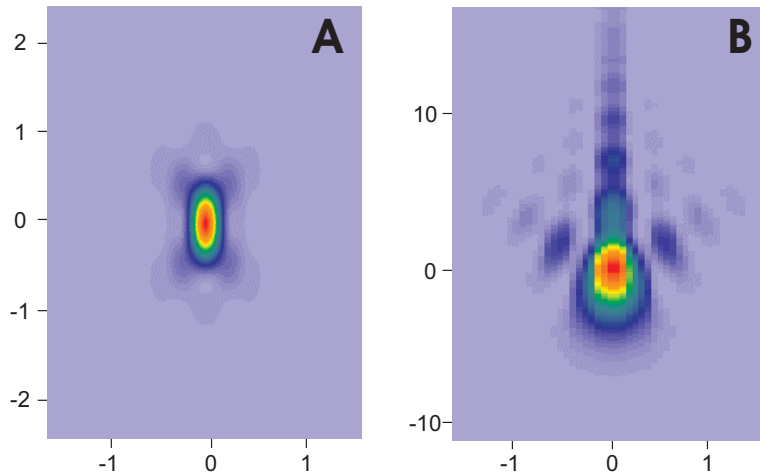


Figure 2.7: Molecule detection function of a water immersion objective with a numerical aperture of 1.2. The focus was chosen $200\ \mu\text{m}$ above the cover slide. Figure A and B show the calculation with a refractive index of 1.333 (water) and 1.49 (toluene) respectively. Note the different y-scales for figure A and B.

of 1.2 and a sample with a refractive index of 1.333. The resulting MDF enclose a volume of 0.42 fL. This calculation represents the normally used configuration of the ConfoCor2. In this thesis most studies were done in toluene with an refractive index of 1.49, i.e. 12% larger compared to aqueous solutions. Therefore the MDF shows as well a dramatic change. In figure 2.7 B the calculated MDF for a sample with refractive index 1.49 is shown. We see that in the case of organic solvents the shape of the volume is no more well defined and the size of the volume (15.44 fL) is more than 30 times bigger than the observation volume in water. Hence, for solvents with a refractive index much larger than 1.33 we have to adapt our setup.

It has been shown that the correction ring at the objective for the correction of the glass thickness (see chapter 2.2) can as well be used to compensate for little variations in the refractive index of the sample solution [Zei01]. In the case of the water immersion objective correction ring can not compensate refractive indices up to 1.49. Instead, we choose a Plan Neofluar 40 \times multi-immersion objective. Multi-immersion objectives are designed to be used with immersion media with refractive indices varying from 1.333 to 1.5. The correction is, once more, achieved with the help of a correction ring. A calculation in analogy to the one for the water immersion objective was done for the Plan Neofluar objective. Figure 2.8 A shows the intensity distribution for a sample with refractive index 1.49. We see that the calculation predicts a well-defined volume and the size of 1.2 fL should be excellent for FCS experiments.

For the analysis of the measured autocorrelation curves equation 2.21 is used. For the derivation of this equation the observation volume was approximated by a three dimensional Gaussian intensity distribution. Figure 2.8 B shows the shape of a three dimensional Gaussian intensity distribution. A comparison of the shape of this approximation with the calculated MDF for the multi-immersion objective (figure 2.8 A) shows a reasonable match. Mainly the shape of the regions with high intensity are nearly identical. Thus the approx-

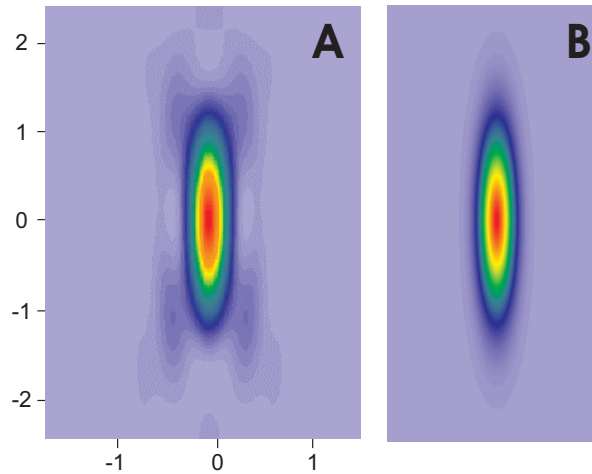


Figure 2.8: Figure A shows the calculated intensity distribution for a multi-immersion objective. This objective has a magnification of $40\times$ and a numerical aperture of 0.9. The dye was dissolved in toluene. The volume has a size of 1.2 fL. Figure B represents the intensity distribution approximated by a Gaussian distribution in all directions.

imation of the observation volume by a three dimensional Gaussian intensity distribution is valid for FCS experiments. The calculations show that with the two available objectives we are able to measure in water as well as in organic solvents. A FCS setup applicable for such a large variety of solvents is unique.

2.3.2 Determination of the Observation Volume in Water

In the previous section calculations for the size of the observation volume of an FCS setup were presented. Already small changes in the setup lead to variations in the observation volume [End04]. For the determination of concentrations and diffusion coefficients it is therefore necessary to measure the size of the observation volume. For aqueous solutions there is a well established route to do this. A dilute solution of Rhodamine 6G is measured and the diffusion time is determined. The diffusion coefficient of this dye is known to be $2.8 \cdot 10^{-6} \text{ cm}^2/\text{s}$ [Zei01]. Inserting this two values in equation 2.16 lead to the waist radius

of the observation volume. For our setup we obtain for the different laser lines waist radii in the range of 190 to 300 nm.

2.4 Setup for Temperature-Dependent Measurements

The setups presented so far are useful for measurements at room temperature. For the study of reaction enthalpies, activation energies or of the gelation of polymers a measurement at variable temperatures is necessary. For this purpose a new sealed sample chamber and a temperature control unit for the FCS setup were designed.

2.4.1 Sample Chamber

The new sample chamber has to fulfill several premises. To avoid evaporation and therefore induced concentration changes the chamber has to be sealed tightly. In the experiments different solvents were investigated. Hence, to avoid contamination of the sample and corrosion of the chamber the chamber must be resistant against most solvents. In addition, for some investigations a variation of the temperature is done. To heat and cool the sample fast a high heat conductance is desirable.

The sample chambers were made of stainless steel. This material is resistant against water and most organic solvent and has a sufficiently high heat conductance. Figure 2.9 A shows a sketch of this chamber. At the bottom a 140 μm thick cover glass (Marienfeld No. 1) is glued. The epoxy glue used is temperature stable up to 250 $^{\circ}\text{C}$ and resistant against most organic solvents including toluene, THF and chloroform. The two parts of the sample chamber are sealed using an indium wire for experiments with organic solvents and a rubber o-ring for aqueous samples. To minimise the consume of material and to provide fast heating and cooling the chamber has a volume of 40 μL .

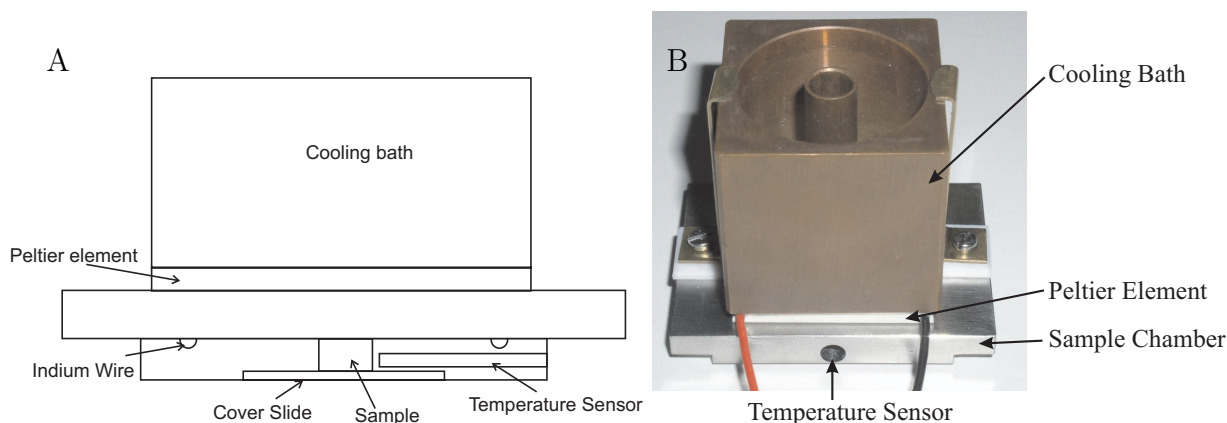


Figure 2.9: Scheme and photograph of a sample chamber with a fixed peltier element for temperature control.

2.4.2 Temperature Control Setup

FCS observes the motion of molecules on the length scale of a few nanometer. A temperature control setup therefore has to be mechanically stable and avoid any displacement of the sample. Hence thermostats working with liquid flux can not be used. We decided to use electrical heating by Peltier elements. These elements have the advantage that they provide fast heating and cooling of the sample. We fixed the element on top of the sample chamber as shown in the sketch in figure 2.9 A. To avoid damage of the element we have to make sure that the heat of the opposite site is dissipated. Therefore we put a cooling bath normally filled with water and ice on top. For good heat transport thermal conducting paste was filled between all components of the setup.

The control of the Peltier element was done by a PRG RS H 100 control unit produced by Peltron. To get a precise measure for the temperature of the sample a Pt-100 temperature sensor is placed near the sample. The signal of the sensor was measured by a Keitley 2000 multimeter. A LabView program was designed to read out the Keithley multimeter and to control the Peltier element via the PRG unit. Figure 2.10 show a typical curve

for a stepwise increase of the temperature from 35 up to 70° C. An magnification of one plateau of this result shows that the temperature of the sample can be controlled within about $\pm 0.1^\circ$ C. This setup was used to evaluate binding energies and thermodynamics of a protein–DNA interactions [Sch03] (see chapter 7).

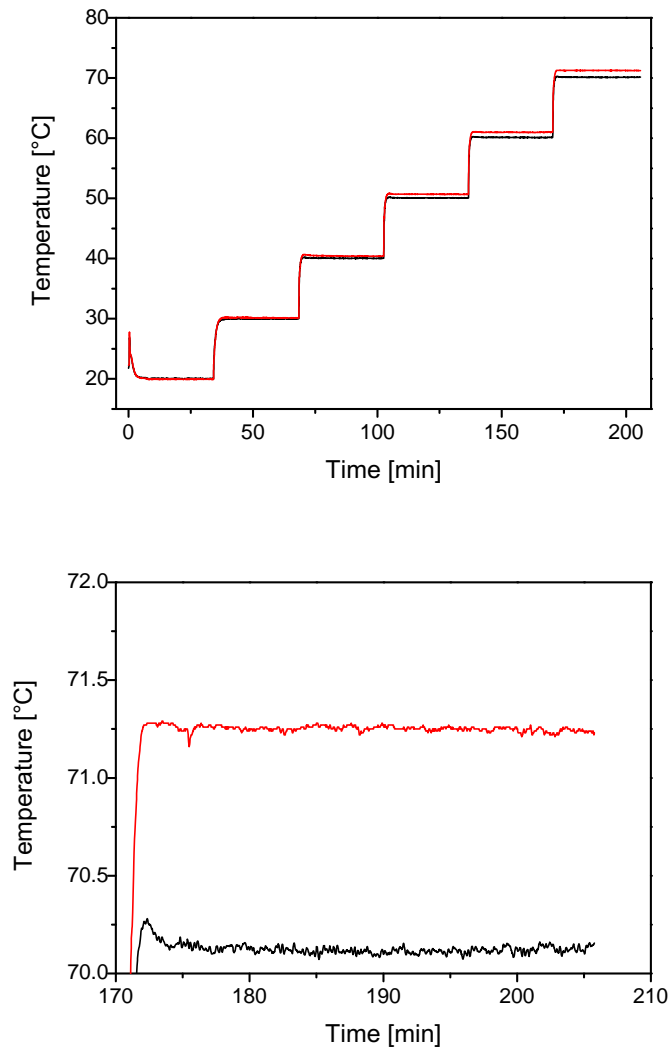


Figure 2.10: A characteristic heating curve of the described setup. The red line shows the temperature at the peltier element and the black curve shows the temperature inside the chamber.

Chapter 3

Determination of the Observation

Volume of the Fluorescence

Correlation Spectroscopy Setup for

Organic Solvents.

The importance of precise determination of the size and the shape of the FCS observation volume was emphasised in the previous chapter. For this purpose, calculations of the size and shape of the observation volume were presented in section 2.3. Furthermore, we have described the determination of the focal volume in aqueous solutions (section 2.3.2). However, for organic solvents there is so far no established procedure to determine the size of the focal volume. Hence in order to use the modified FCS setup in various organic solvents a new way for the determination of the size of the focal volume has to be found.

3.1 Possible Paths for the Determination of the Observation Volume

Fluorescent species that can be used for the determination of the observation volume have to fulfil several conditions. The particles have to be soluble in organic solvents and must not show aggregation in the respective solvent. To use an analogous procedure as described for water (section 2.3.2) the size or the diffusion coefficient of the fluorescent molecules has to be known. Furthermore the molecules should be monodisperse or should at least show a small distribution in molecular weight, otherwise the determination will show a large error and lead to imprecise values for the size of the focal volume [Sta99]. As for all FCS experiments the dye molecules have to be photostable to get correct values for the diffusion time.

We used several approaches to find proper molecules for the determination of the size of the observation volume. In analogy to the characterisation used for water we tested the dyes Rhodamine 6G, Rhodamine B, Sulforhodamine B and Cresyl Violet. All dyes have a low solubility in water and the dissolved particles show aggregation. Furthermore the diffusion coefficient of these molecules is unknown in toluene. To circumvent the problem of solubility we tested polyorganosiloxane nanoparticles labelled with Rhodamine B. These particles were synthesised by W. Schärfl from the University of Mainz. They have a diameter of around 20 nm and a spherical shape [Gra99]. The results of the measurements could not be used for the determination of the focal volume. The obtained diffusion times of two measurements of the same solution differed by more than 15% and the fitting procedure lead to very high values for the structure parameter S which seemed unphysical. We attribute the findings to the polydispersity of the small spheres and to slight swelling of the spheres in organic solvents.

To avoid swelling in organic solvents we tried to use inorganic fluorescent nanoparticles

for our measurements. CdSe nanoparticles show an intense fluorescence emission in the visible range of the spectra and can be excited easily by laser lines of 488 nm and 514 nm. The photostability is higher than shown by all organic dye molecules. The wavelength of the fluorescent light is strongly dependent on the size of the molecules. Therefore it is easy to distinguish different nanoparticles. However, in order to stabilise the particles in solvents a shell of organic ligands is necessary which modifies the size of the particle. Unfortunately, the number of ligands of the available nanoparticles differs strongly and therefore the size determination by the emission wavelength is no longer possible. FCS measurements of particles with core radii of 2.7 nm and 4.8 nm yielded the same diffusion time of $30 \mu\text{s}$ although we would expect a significant influence of the size. As R_h enters linearly into the diffusion time (equation 2.16 and 2.17) we conclude that the ligand shell is responsible for the unexpected diffusion time. Hence, also the nanoparticles can not be used for the determination of the focus size.

We received a good soluble fluorescent molecule by labelling polystyrene chains with single dye molecules. The diffusion behaviour and particularly the diffusion coefficient – molecular weight relationship is for polystyrene well investigated [Bug69, Mcd77, Rac80, Rac82, Rac83]. This system was used to measure the size of the focal volume. The polymerisation route, the labelling as well as the purification and characterisation will be described in detail in the following chapter. Furthermore FCS measurements and the derived waist radius are presented. The results of this chapter are published in the article “Fluorescence correlation spectroscopy of single dye-labelled polymers in organic solvents”. The paper is published in *Macromolecules* in 2004 [Zet04, Zet05a].

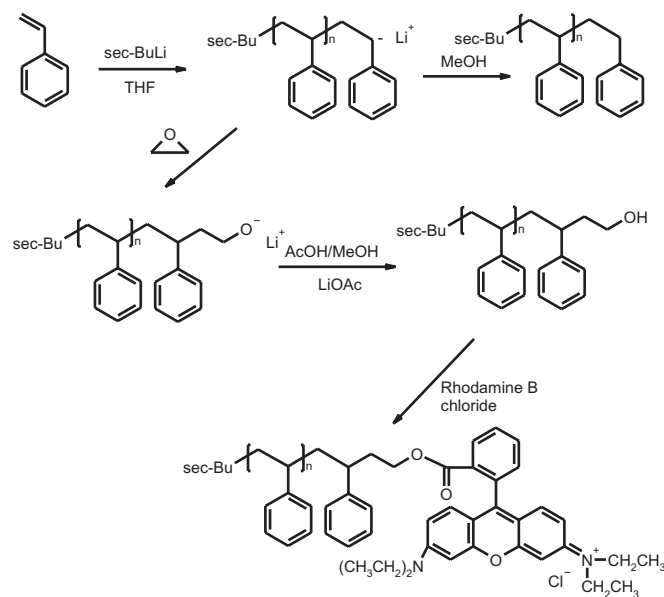


Figure 3.1: Scheme of the polymer synthesis and the subsequent polymer analogous coupling reaction.

3.2 Synthesis of Dye-labelled Polystyrene

3.2.1 Anionic Polymer Synthesis

The synthesis was performed using standard anionic polymerisation (Figure 3.1). The values for the synthesis of polystyrene with a molecular weight of 65 kg/mol are given in the following. 1 L freshly distilled THF was cooled down to $-78 \text{ }^\circ\text{C}$. 2.3 mL *sec*-BuLi (1.3 molar solution in *n*-hexane/cyclohexane) were injected before 20.31 g purified styrene were added. The polymerisation was allowed to proceed for 60 minutes, then the styryl anions were capped with 5 mL ethylene oxide (freshly distilled from CaH_2). The following day, the reaction was terminated with a 5 mL mixture of degassed AcOH/MeOH (5:1/v:v). The polymer was precipitated in 5 L methanol, redissolved in THF and reprecipitated two more times. The successful end-capping reaction was verified using MALDI-ToF mass spectrometry (see section 3.2.4).

3.2.2 Synthesis of the Acid Chloride of Rhodamine B

The synthesis of the acid chloride of the dye Rhodamine B was performed following a well known route [Bec96]. 2.1 mL thionylchloride and 0.1 mL dry pyridine were added to 0.83 g of Rhodamine B. The mixture was heated to 50 °C and boiled under reflux for four days. The dry pyridine is necessary to remove the hydrogenchloride formed during the reaction. Finally the excess of thionylchloride was removed by drying the product in vacuum at room temperature. The obtained product was characterised by IR-Spectroscopy. The IR-spectrum showed a characteristic change in the bands of the carbonyl and OH groups.

3.2.3 Coupling of the Polymer with the Dye Molecules

2 g of PS-OH were dissolved in 20 mL THF under nitrogen atmosphere. A two molar excess of the acid chloride of Rhodamine B was added. Subsequently 0.5 mL anhydrous pyridine were injected into the mixture. The reaction was allowed to proceed for 3 days at 40 °C before terminating with 1-2 mL of methanol. The resulting product was precipitated into 500 mL methanol and dried in a vacuum oven. We yielded a red-coloured powder. In order to use the labelled polymer for single-molecules experiments it is indispensable to quantitatively remove the unreacted dye molecules. The unreacted dye molecules and the labelled polymer chains differ strong in their diffusion times. For this purpose FCS is very efficient in verifying the quantitative removal of unreacted dye molecules. For the removal of the unreacted dye several techniques were tested. Dissolving the polymer and reprecipitating it into methanol was not successful. Ultrafiltration using a membrane with a cut-off molecular weight of 2000 g/mol was not successful either. Finally preparative gel permeation chromatography (prep-GPC) proved to provide a suitable purification procedure. For the

separation 100 mg of polymer were dissolved in 1 mL THF. The solution was injected in the preparative GPC. The purified polymer fraction was then dried under vacuum. After successful purification a white powder was received.

3.2.4 Characterisation of the Polymer by GPC and MALDI-ToF

In order to follow the polymer reaction at all intermediate states of the synthesis Matrix Assisted Laser Desorption Ionization Time-of-flight Mass Spectra (MALDI-ToF MS) of the low-molecular-weight polymers were recorded and analysed. Figure 3.2 shows the MALDI-

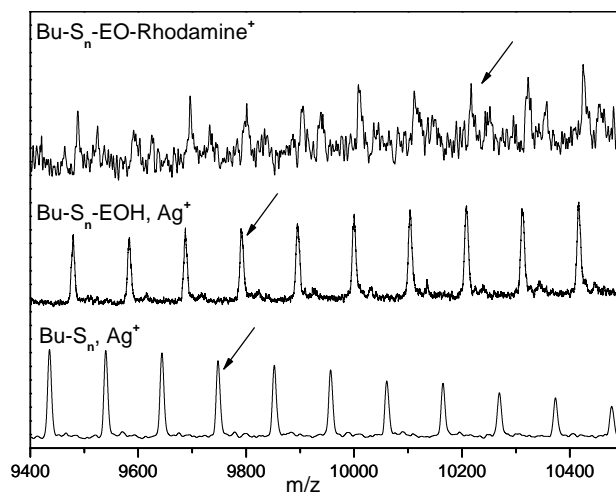


Figure 3.2: MALDI-ToF mass spectra of the PS precursor (bottom), the OH-end-functionalised PS (middle), and the dye-labelled PS-chains, respectively. The arrows indicate a polymer chain with 93 Styrene units ($n=93$).

ToF spectra of the 11k PS precursor, the OH-endgroup-capped polymer chain and the dye-labelled polymer. The measurements were performed on a Bruker Reflex II spectrometer equipped with a nitrogen laser (337 nm). To improve the resolution of the spectra the reflection mode of the instrument was used. An acceleration voltage of 20 kV and a reflector voltage of 23 kV together with matrix / low-mass suppression up to 3000 g/mol were used. 1000 laser shots were added for all spectra. Polymer sample (10 mg/mL), matrix (dithranol,

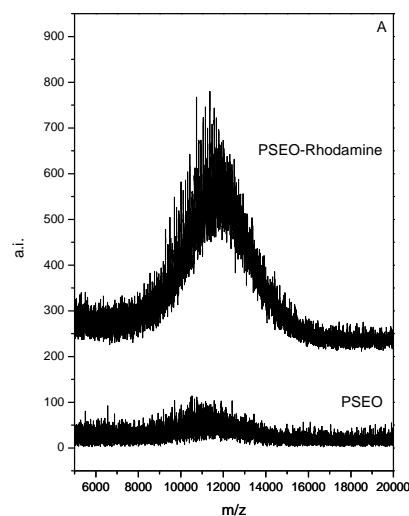


Figure 3.3: MALDI-ToF mass spectra of the dye-labelled PS-chains (top) and OH-end functionalized PS (bottom) measured without addition of Ag-salt. The dye labelled polystyrene shows an eight times higher intensity compared to the unlabelled polystyrene.

20 mg/mL) and silver trifluoroacetate as salt (10 mg/mL) were dissolved in THF and mixed at a volume ratio of 20:5:1 (matrix:sample:salt). 1 mL of this mixture was placed on the target and allowed to dry. The spectra of the ethyleneoxide-functionalised polystyrene (PS-OH) show a shift to higher mass compared with the pure polystyrene (PS). The difference between the main peaks is 44 g/mol, which fits to the mass of a C_2H_4O unit. The same analysis should be possible with the dye-labelled PS. However, when silver triflate was used as cationising agent two series of signals were obtained. The mass of the most intense signal does not correspond to the expected mass of the target molecule PS-RhB carrying one Ag^+ attached to the main chain but rather shows the same mass signal as the precursor. Also the second series does not exactly correspond to the mass of the target molecule but shows a mass which is slightly higher than expected. Polystyrene is usually measured by using a dithranol matrix and silver trifluoroacetate as cationising agent. However, a comparison of the MALDI-ToF spectra of the precursor molecule (PS-OH) and the dye-labelled polymer (PS-RhB) without adding salt to either species to enhance cationization

Table 3.1: Molecular weight and polydispersity of the Polystyrene samples.

Abbreviation	M_n [kg/mol]	M_w [kg/mol]	PD
PS 4	3.6	3.9	1.10
PS 11	11.2	11.5	1.03
PS 17	16.8	17.3	1.03
PS 67	67.4	70.2	1.05
PS 264	258.8	263.7	1.02
PS 1550	1465.2	1550.0	1.06

shows an eight times higher intensity for the dye-labelled product (Figure 3.3). Under these conditions no or only a very weak signal is expected for neutral species. Since Rhodamine B is an organic cationic salt the result of the measurement leads to the conclusion that the coupling of Rhodamine B to the polymer was successful and that the dye causes an intrinsic cationisation of the polymer chain. This notion is corroborated by the fact that the experimentally observed mass signals are in agreement with the expected mass signals for such species (Figure 3.2).

Additionally a GPC analysis was performed to obtain the molecular weight and the polydispersity of the synthesised polystyrenes. The GPC measurements were conducted using a set of 30 cm SDV-gel columns. The columns have a particle size of $5\ \mu\text{m}$ and pore sizes of 10, 10^2 , 10^3 and 10^4 nm. For detection a refractive index detector and a UV-detector were used. The polymers were dissolved in THF and analysed with an elution rate of $1\ \text{mL}/\text{min}$. The columns were calibrated with a set of polystyrenes with narrow molecular weight distribution. Table 3.1 shows the results of the analysis.

3.3 Observation Volume in Organic Solvents

The dye labelled polystyrenes were used to measure the diffusion of single chains by FCS. The experiments were conducted on the modified FCS setup described in chapter 2.2. For the measurement the Rhodamine B label of the chain was excited by an Ar-ion laser at 514 nm. The fluorescence light was separated from scattered light by a 514 nm beamsplitter. An additional long-pass filter with a cut-off wavelength of 560 nm was used to suppress the remaining scattered excitation light. For every measurement the polymer solutions were freshly prepared with toluene p.a. grade and filled in the sealed sample chamber described in section 2.4.1. Three autocorrelation curves with a recording time of 5 min were measured for each molecular weight.

Figure 3.4 shows the curves obtained for 10^{-8} M polymer solutions of four different

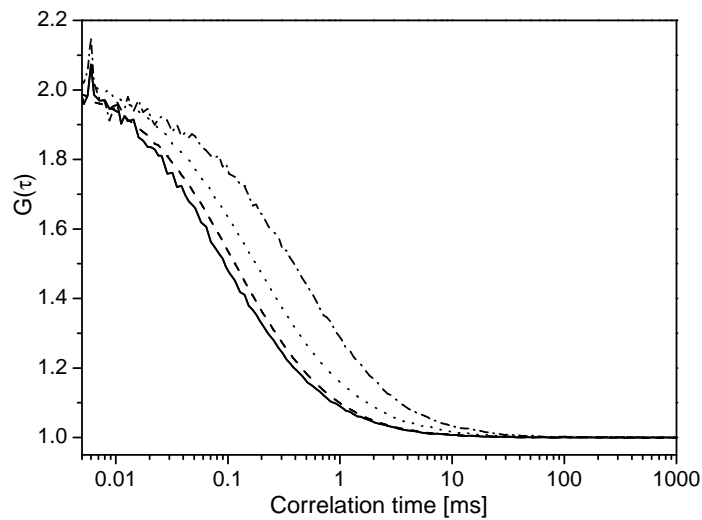


Figure 3.4: Normalized FCS autocorrelation curves for 10^{-8} M solutions of different labelled polystyrenes in toluene. The molecular weight of the polystyrenes is from left to right: 11.5k, 19k, 63k, and 285k.

molecular weights. For increasing molecular weight the autocorrelation curves show a clear increase in the diffusion time. The diffusion times τ_{Diff} were extracted by a fit of equation 2.21 to the data. The obtained diffusion times were plotted versus the molecular weight

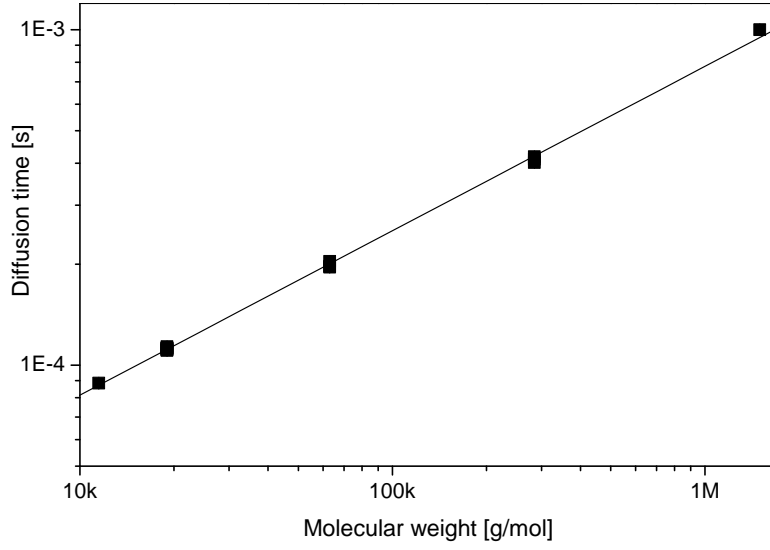


Figure 3.5: Single molecule diffusion times as a function of molecular weight as determined from least squares fits to the data. The straight line shows a linear fit to the data.

(figure 3.5). We recall that the diffusion times τ_{Diff} are correlated to the waist radius by $\tau_{\text{Diff}} = \frac{w^2}{4D}$ as described in equation 2.16. A double-logarithmic presentation of our experimental data shown in figure 3.5 reveals a power law dependence between molecular weight and diffusion time. The fitting procedure yields the exponent and prefactor of the diffusion time – molecular weight relationship.

$$\tau(M_w) = k \cdot M_w^a \Rightarrow \log \tau(M_w) = (-6.050 \pm 0.021) + (0.498 \pm 0.0043) \cdot \log M_w \quad (3.1)$$

$$D(M_w) = \frac{w^2}{4\tau(M_w)} = \frac{w^2}{4k} \cdot M_w^{-a} \Rightarrow D(M_w) = \frac{w^2}{4 \cdot 8.912 \cdot 10^{-7}} \cdot M_w^{-0.498} \quad (3.2)$$

Bugdahl studied the molecular weight dependence of the diffusion coefficient for polystyrene in toluene by dynamic light scattering [Bug69] and found the following scaling law:

$$D(M_w) = (2.15 \cdot 10^{-4}) \cdot M_w^{-0.53} = b \cdot M_w^{-a} \quad (3.3)$$

By comparison of the prefactors of the equations 3.2 and 3.3 the waist radius of the observation volume in toluene can be extracted.

$$b = \frac{w^2}{4 \cdot 8.912 \cdot 10^{-7}} \Rightarrow w = \sqrt{4 \cdot 8.912 \cdot 10^{-7} \cdot b} = 277 \text{ nm} \quad (3.4)$$

For toluene a waist radius of $w_{\text{toluene}} = 277 \text{ nm}$ was obtained. This value differs significantly from the value of the waist radius in water, which was determined to be $w_{\text{water}} = 212 \pm 4 \text{ nm}$ by the Rhodamine 6G measurements described earlier.

As outlined in chapter 2.3 theoretical considerations of the focus size can only be done by exact wave-optical calculations. In figure 3.6 the calculated MDF is shown and the measured waist radius of our observation volume is represented by a black bar. It is clearly seen that the region of high intensity from the calculated MDF and the measured waist radius are identical. Only with the new synthesized polymer system for the determination of the observation volume we were able to measure the size of the observation volume precisely and achieve a high agreement with the theoretical calculated size of the focus volume.

In summary, a procedure was developed to determine reliably the size of the observation volume in organic solvents with different refractive indices. Therefore polymers with a single dye molecule coupled to the end of the chain were synthesised and characterised by MALDI-ToF and GPC-measurements. To achieve narrow distributions in molecular weight all polymers were synthesised by anionic polymerisation. This fact and the use of five different molecular weights in a range of 10 to 1550 kg/mol enable FCS measurements with high validity. Hence a waist radius of the focus volume in toluene was received which is in excellent agreement with calculations based on wave-optical considerations. The successful combination of polymer synthesis *and* modifications of the FCS setup enable high quality FCS measurements in organic solutions.

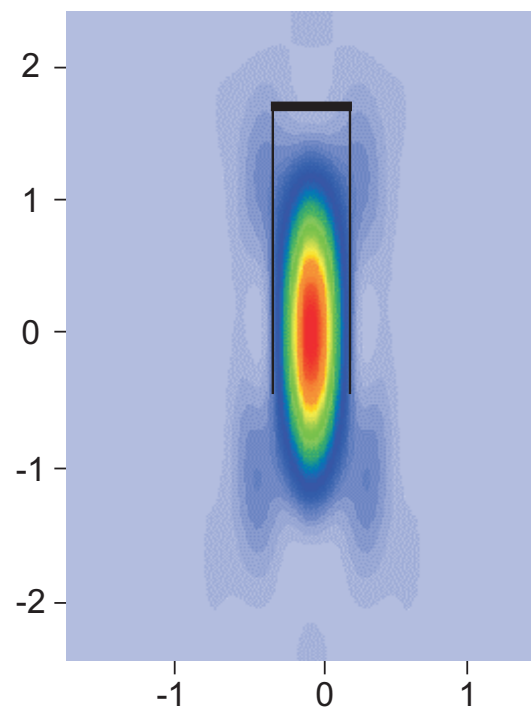


Figure 3.6: Calculated intensity distribution for an objective with a numerical aperture of 0.9 used for measurements in toluene. The black line indicates the waist radius w_{xy} determined from measurements with dye labelled polystyrenes of different molecular weights.

Chapter 4

Determination of the Crossover between Dilute and Semi-Dilute Polymer Solutions

Polymer solutions constitute an important part of polymer science. Often synthesis, characterisation and processing of polymers take place in solutions of different concentrations. In some cases like synthesis and spin casting the polymer concentration varies in a broad range during the experiment. Phase diagrams of polymer solutions yield information about the relation between concentration, molecular weight, temperature and composition of polymers. Variation of the parameters leads to changes in the physical properties of the solution. Phase diagrams which cover a broad range in molecular weight and concentration can so far only be measured by using various methods for the investigation of the physical properties of the polymer solutions in the different concentration regimes and for the different molecular weights. Thus, it will be very helpful to devise an experimental method which covers the full range of concentration regimes for largely difficult molecular weights. Single molecule methods often use tracer molecules to investigate the mobility of single

polymer chains. Therefore they are not limited to a certain concentration. A superior signal to background ratio compared to DLS circumvents the restrictions in molecular weight. The high sensitivity of FCS for example on the change in the mobility of molecules allow to follow the onset of the beginning of the overlap of polymer chains with increasing concentration. The starting point of the overlap of polymer chains is localized in a concentration range which is hardly fully accessible by classical methods.

In the previous chapters we described how to modify a standard FCS setup for measurements in polymer solutions. It was shown by Liu et al [Liu05] that this technique allows to measure the mobility of single polymer chains in a broad concentration range. We use this advanced method to investigate polystyrene solutions within a broad range of concentrations and different molecular weights. These experiments will yield information about mobility changes of single polymer chains at the crossover between dilute and semi-dilute polymer concentrations.

4.1 Dilute and Semi-Dilute Polymer Solutions

Polymer solutions are categorized in three different concentration regimes. In phase diagrams dilute, semi-dilute and concentrated polymer concentrations are distinguished. The locus of the crossover between the different regimes depends on the concentration and on the chain dimensions. In the following chapter we will concentrate on the dilute and semi-dilute regime and especially on the crossover between these two regimes.

At very high dilution the single polymer chains move separately from each other and do not show any interaction. This regime is called the dilute state. With increasing polymer concentration the chains start to touch each other. This concentration is called the *overlap concentration* (c^*). By increasing the polymer concentration even more the polymer chains start to interpenetrate (figure 4.1) and the semi-dilute regime is reached. The

overlap concentration usually is not a sharp transition due to polydispersity. It refers to a concentration range between the dilute and semi-dilute region. For the understanding of polymer solutions it is very useful to investigate the scaling properties of c^* with the molecular weight. The basic definition of the overlap concentration is given by de Gennes [Gen79] and by Strobl [Str97]: The monomer concentration in the solution has to be the same as the monomer concentration in the volume occupied by a single polymer coil. Though the

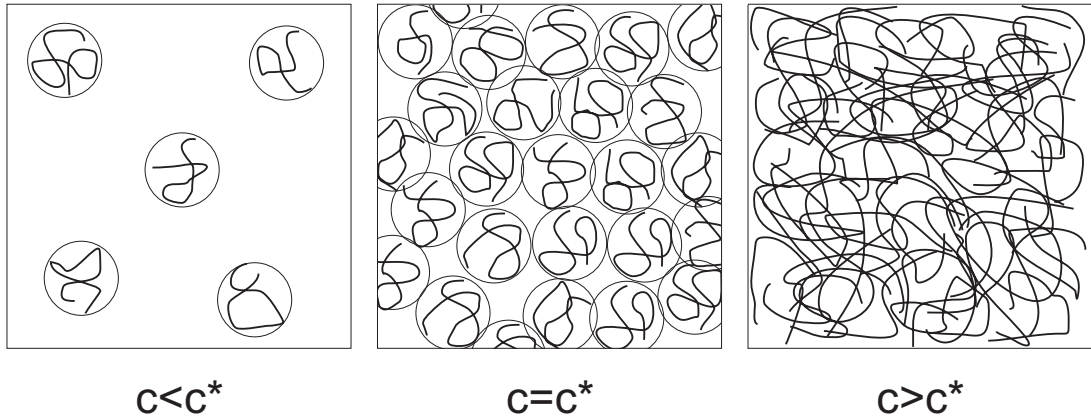


Figure 4.1: Concentration regimes of polymer solutions. Dilute regime $c < c^*$ and semi-dilute regime $c > c^*$. In the semi-dilute regime the polymer chains overlap. The crossover occurs when the volume of the individual chains is the same as the sample volume. At that point the concentration of monomers inside the volume of a single chain is the same as the monomer concentration in the entire polymer solution $c_m = c_m^*$.

crossover takes place in a concentration range Strobl suggests for expanded chains an exact concentration defined by:

$$c^* = \frac{N}{R_F^3} \quad (4.1)$$

where N is the degree of polymerisation and R_F is the “Flory radius”. This radius is a measure for the volume occupied by a polymer chain in the corresponding solvent. With this expression it is possible to give a scaling law for the dependence of the overlap concentration

on the degree of polymerisation. The scaling of R_F is given by

$$R_F = a_F \cdot N^\nu \quad (4.2)$$

a_F denotes the effective length of a single monomer unit. The exponent ν describes the shape of the polymer chains. The Flory-Huggins theory gives for chains in a Θ -solvent $\nu = \frac{1}{2}$ and for coiled chains in a good solvent ν reaches $\frac{3}{5}$. Inserting equation 4.2 in 4.1 yields the scaling law for the overlap concentration.

$$c^* = \frac{N}{a_F^3 \cdot N^{3\nu}} = \frac{N^{1-3\nu}}{a_F^3} \quad (4.3)$$

Using the relation between the degree of polymerisation N and the weight average of the molecular weight M_w of the polymer sample and the molecular weight of a monomer unit M :

$$N = \frac{M_w}{M} \quad (4.4)$$

the scaling law can be rewritten as:

$$c^* = \frac{1}{a_F^3 \cdot M^{1-3\nu}} \cdot M_w^{1-3\nu} \quad (4.5)$$

It is convenient to define the volume fraction of a polymer in solution.

$$\phi = v_m \cdot c_m \quad (4.6)$$

v_m is the volume of a monomer. With this definition equation 4.5 reads:

$$\phi^* = v_m \cdot c_m^* = \frac{v_m}{a_f^3 \cdot N^{1-3\nu}} \quad (4.7)$$

The concentration range of the overlap concentration is difficult to reach by conventional methods typically used in polymer science. Rheology and scattering methods do not give direct access to the overlap concentration. Moreover rheology measurements always disturb the system by shearing and do not give direct information about the undisturbed system. For scattering methods there are too many scattering centres in the semi-dilute concentration regime. Besides light scattering experiments are restricted to molecular weights higher than 15 kg/mol. To get information about the overlap concentration often geometrical considerations are used. Graessley for example measured the intrinsic viscosity of polystyrene solutions. From the achieved values he calculated the overlap concentration of the polymer chains [Gra80]. The results of his calculations are shown in figure 4.2. Other groups calculated the overlap concentration with hydrodynamic radii determined by light scattering experiments. None of these studies based on geometrical calculations measures the overlap concentration directly.

Brown *et al.* [Bro88] measured the change of the diffusion coefficient for three molecular weights and extracted from the change of the diffusion coefficient the overlap concentration. The proof of the scaling law given in equation 4.5 was only possible in a range of molecular weight ranging from 100 to 2900 kg/mol. Hervet *et al.* [Her79] used forced Rayleigh light scattering to investigate changes in the mobility of polymers. They investigated only the two molecular weights 123 and 245 kg/mol. Hence, they only determined the overlap concentration and did not proof any scaling law with their results.

A more direct determination of the crossover between the dilute and the semi-dilute regime by investigating the mobility of single polymer chains in a broad range of molecular weights would give a more detailed insight in the behaviour of the polymers at this crossover. Single molecule methods give the possibility to avoid all these restrictions mentioned above. Working with highly diluted tracer molecules allows the direct observation of the behaviour of single polymer chains. From the change of the mobility of single polymer

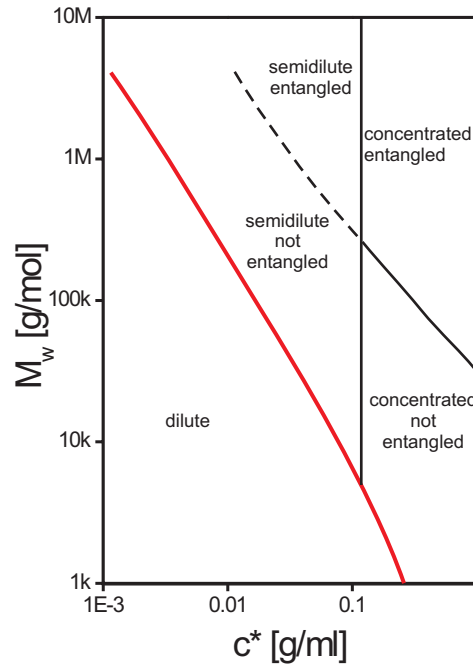


Figure 4.2: Concentration versus molecular-weight for polystyrene in a good solvent. The crossover between the dilute and the semi-dilute concentration was calculated from intrinsic viscosity data by Graessley [Gra80].

chains the overlap concentration can directly extracted.

4.2 Determination of the Overlap Concentration of Polystyrene with FCS

We want to determine the overlap concentration of polystyrene dissolved in toluene. For the experiments we used the same polymers as for the analysis of the shape and size of the observation volume (chapter 3.2). For the experiments solutions of dye-labelled polystyrenes of a concentration of 10^{-8} M were prepared. For the measurement a low dye concentration is needed (see theory chapter 2.1). To vary the polymer concentration and keep the dye concentration constant unlabelled polymer from the same synthesis batch is added to the

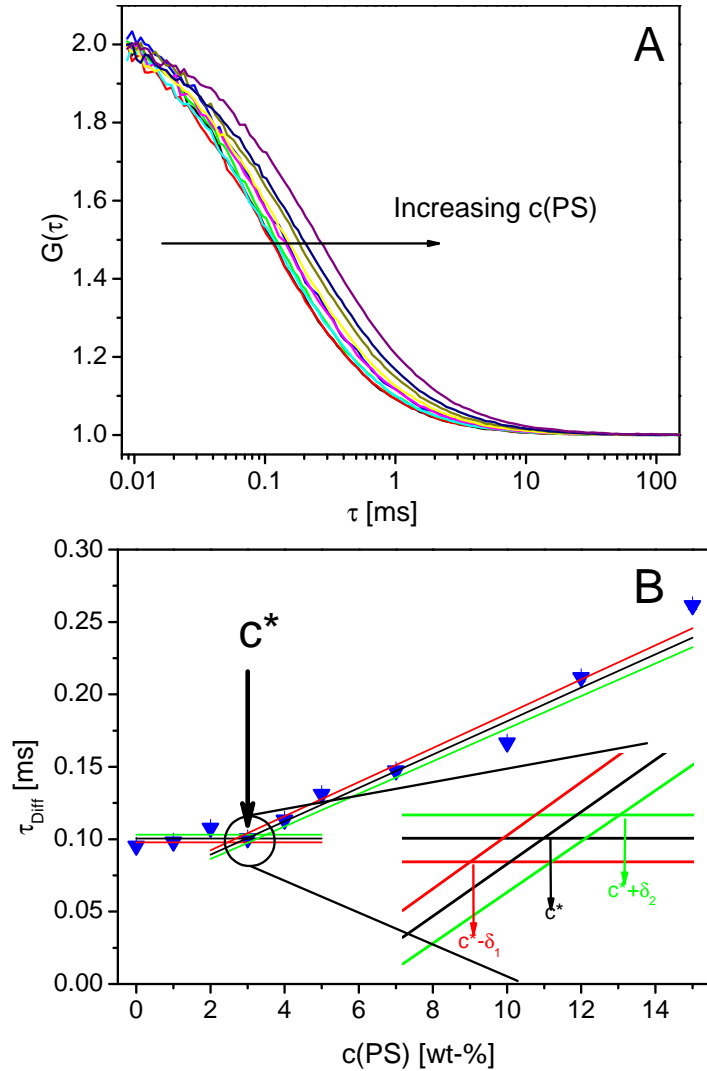


Figure 4.3: Normalised FCS autocorrelation curves in graph A show the 17k PS in a concentration range of 0 wt% up to 15 wt% of unlabelled polystyrene added to the solution. With increasing polymer concentration the diffusion time of the tracer molecules increases. A fit to the data yields the respective diffusion time τ_{Diff} . Graph B illustrates the concentration dependence of τ_{Diff} . Two linear fits (black lines) to the data yield the overlap concentration. The red line and the green line illustrate the error of the fit. Due to this we estimated the error of our overlap concentration as shown.

dilute solutions of dye labelled polystyrene. With that procedure we make sure to analyse solutions with different concentrations of polystyrene but with a *constant* concentration of labelled polymer.

In the following, a detailed description of the measurement and analysis procedure is given for the sample PS 17. For the experiments ten solutions with concentrations of unlabelled polymer in a range of 0 up to 14.5 wt% were prepared. Every solution was measured for 30s and each measurement was repeated thirty times. To avoid evaporation of the solvent all samples were measured in the sealed sample chambers described in section 2.4.1. For the data analysis the average of the three measurements was built. A fit of equation 2.21 to the data yields the respective diffusion times τ_{Diff} . The received normalised autocorrelation curves in figure 4.3A do not show a significant change for polymer concentrations up to 3 wt%. Above this concentration the curves are shifted to higher τ -values. As expected from the theory of polymer solutions presented in the previous chapter the diffusion time does not change in the low concentration regime (below 3 wt%) because the polymer chains are separated and do not influence each other. Increasing the polymer concentration above 3 wt% leads to a linear increase in the diffusion time with increasing polymer concentration. We define the polymer solutions below 3 wt% as dilute solutions and above as semi-dilute. To define a precise value of the overlap concentration we apply linear fits to both concentration regimes and calculate the point of intersection of the fitting lines. To get an indication for the quality of the overlap determination we estimated an error which is extracted from the error of the fits as shown in figure 4.3B.

This procedure was repeated for each of the synthesised polymers and the resulting diffusion times are plotted in figure 4.4. As predicted (equation 4.3), c^* shifts to lower concentrations for higher molecular weights. The double logarithmic plot of the overlap concentration over the molecular weight reveals a clear power-law dependence over a range

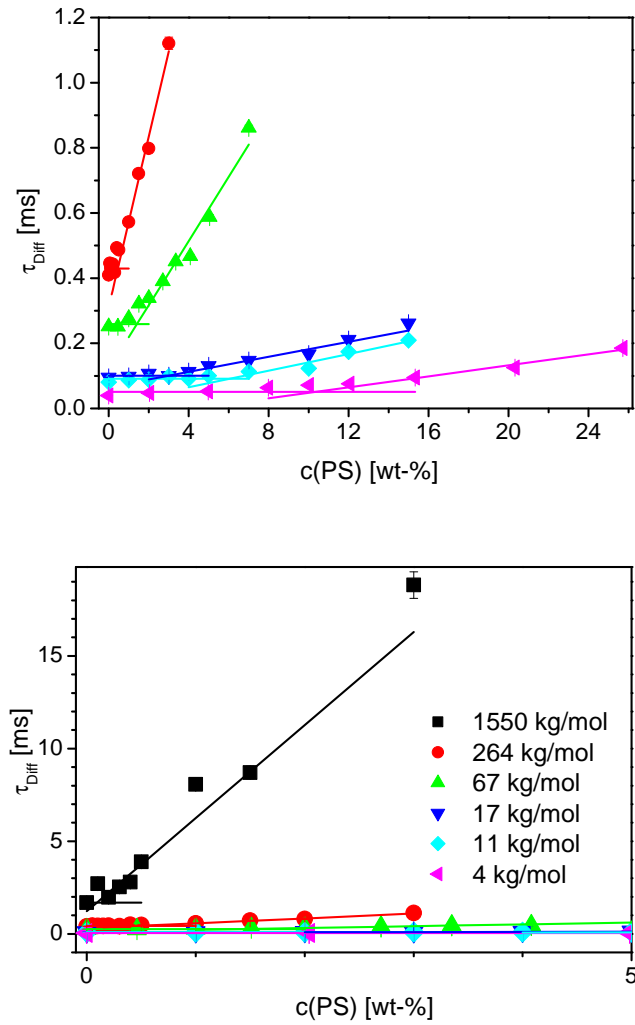


Figure 4.4: Concentration dependence of the diffusion time for all measured polystyrenes. To each set of data the two linear fits used for obtaining c^* were plotted. In the right graph the PS 1550 is presented.

of nearly three orders of magnitude. A fit to the data yields:

$$c^* = 10^{3.94(\pm 0.27)} \cdot M^{-0.78(\pm 0.057)} = \text{const} \cdot M^{1-3\nu} \quad (4.8)$$

with $\nu = 0.59$. This value is in excellent agreement with predictions made by the Flory-

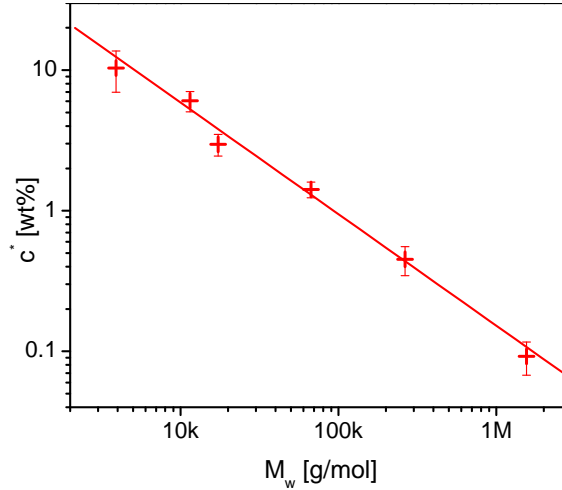


Figure 4.5: Change in the overlap concentration depending on the molecular weight of the polystyrene. With increasing molecular weight the diffusion time decrease linearly. A linear fit to the data yields the power law presented in equation 4.8.

Huggins theory for a polymer in a good solvent, which predict a value of $\nu = 0.6$ [Str97, Gen79]. In figure 4.6 we compare our results obtained from figure 4.4 with the calculations done by Graessley. We observe that the overlap concentration determined by FCS is slightly lower than Graessley's values for all molecular weights. This indicates that we sense a change in the dynamics of a single polymer chain before this is expected by the geometrical arguments described in chapter 4.1 and used in the investigations of Graessley. There is only one measurement determine the overlap concentration of polystyrene in toluene. Liu *et al.* measured the overlap concentration of a 390 kg/mol polystyrene by light scattering. They used the achieved Radius of gyration to calculate the overlap concentration and compared their results with FCS measurements. They found a good agreement between

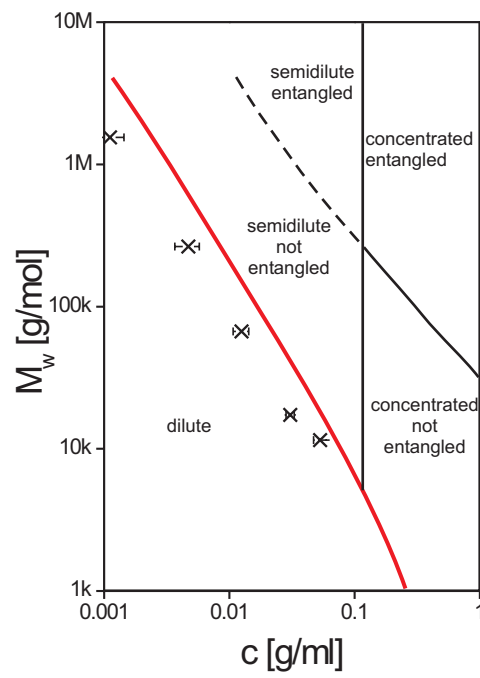


Figure 4.6: Calculated diagram for the molecular weight dependence of the overlap concentration deduced from rheology measurements [Gra80]. The black crosses indicate our data determined by FCS.

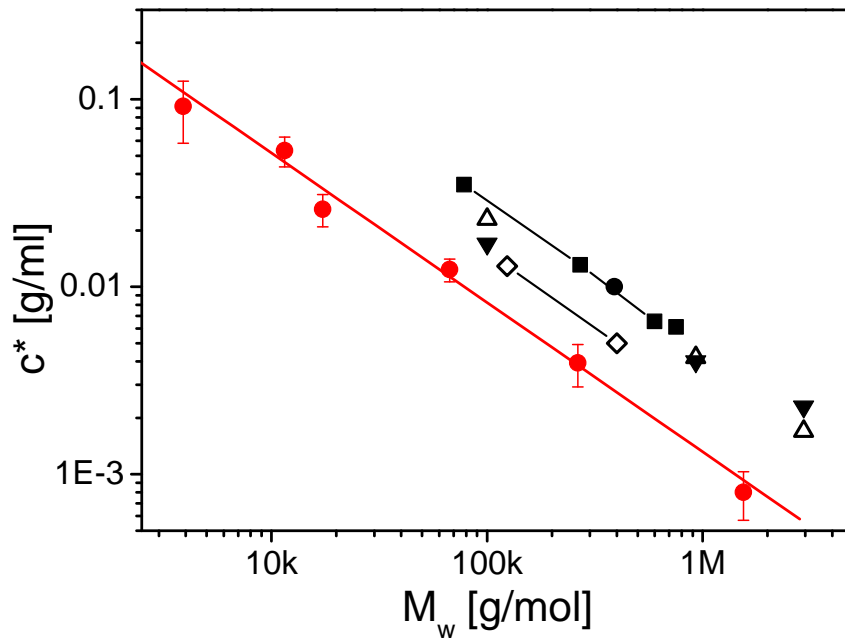


Figure 4.7: Comparison of our data (red) with published values of c^* for other good solvents. \blacksquare is a determination of c^* by forced Rayleigh light scattering measurements of polystyrene in benzene [Her79]. The \blacktriangledown show quasi elastic light scattering experiments in dichloromethane [Bro88]. For the same solvent Brown calculated the overlap concentration from intrinsic viscosity measurements (\triangle) [Bro88]. Raspaud measured the radius of gyration and calculated from this the overlap concentration (\diamond) [Ras95]. \bullet is the overlap concentration measured in toluene with light scattering by Liu *et al.* [Liu05]. They compared their data with FCS measurements on the same system.

the two methods [Liu05]. Because of there are no more data available in the literature our results with data on the overlap concentration of polystyrene in dichlormethane and in benzene. These two solvents are good solvents for polystyrene as well. The overlap concentrations were measured by forced Rayleigh light scattering [Her79] and by quasi-elastic light scattering [Bro88]. These two methods analyse the changes in the dynamics of the polymer chains. Another possibility are geometrical considerations. Raspaud *et al.* [Ras95] and Brown [Bro88] calculated the overlap concentrations from a measurement of the radius of gyration in the dilute regime. Hence interactions by changes in the conformation and size of the chains near c^* are neglected. Figure 4.7 shows the mentioned published data and our results. In contrast to the values published so far our method enable us to analyse the dynamic behaviour of single polymer chains in a range of molecular weights from 4 to 1550 kg/mol. This is twice the range accessible with alternative methods.

We conclude our results on the physics of polymer solutions. With an improved FCS setup we were able to get new insights in the dynamics of single polymer chains with different dimensions and at different concentrations. We were able to verify the power law describing the molecular-weight dependence of the overlap concentration in a range of three orders of magnitude in the molecular weight. Our experiments demonstrate that FCS works well in both the highly-dilute and in the semi-dilute regime. Furthermore this method works without perturbing the system.

Chapter 5

Aggregation of Surfactants investigated by FCS

Self-aggregation of surfactants is a key issue in a variety of industrial processes such as cleaning, pharmaceutical formulation, and emulsion polymerisation. In this context, precise knowledge of the size of the aggregates and a quantitative determination of the critical micelle concentration (*cmc*) is indispensable. A detailed analysis of the formation of the micelles can give new insights in the physical properties of surfactant solutions.

In the previous chapters the high sensitivity of FCS for the analysis of polymer solutions was shown. This high sensitivity can be used as well to study the aggregation of small surfactant molecules. For FCS studies it is necessary to find a suitable method to label the aggregates. One possibility is to covalently label a part of the aggregating molecules and to blend them with unlabelled molecules in a similar way as described in chapter 4.2 for the overlap studies. This method has already been used for studies of surfactant aggregation in aqueous solutions [Nor99, Pet86, Pal87]. However, this method requires the synthesis of corresponding molecules with fluorescent labels. Such a synthesis is always costly and time consuming. Hence, it is not the best way for developing a fast and easy method to

analyse the aggregation of molecules.

Many surfactant molecules have a polar and an unpolar part. In polar solvents like water micelles with an unpolar core and a polar shell are formed. In unpolar solvents like toluene, THF and chloroform inverse micelles with a polar core and an unpolar shell are formed. Insoluble dye molecules tend to change their environment and are often incorporated in the micelles respectively in the inverse micelles. By choosing a polar dye molecule for unpolar solvents and vice versa a labelling of the aggregates without any synthetic work is possible. By attaching unpolar side chains to dye molecules the “insolubility” can be increased and the efficiency of labelling rises in polar solvents [Sch00a].

In the following chapter we will describe a new non-covalent labelling for ionic surfactant molecules. We utilise the Coloumb interaction between ionic surfactant molecules and ionic dyes for labelling micelles.

5.1 Theoretical Basis for the Aggregation of Surfactant Molecules.

Typical low molecular weight surfactant molecules are composed of a polar head group that is compatible with water and a unpolar part which is incompatible with water. The unpolar part is mostly a hydrocarbon chain. The polar headgroup can be an ionic group like sulfonic acid, carboxylic acid or amino groups or is a polar oligomer of e.g. ethyleneoxide. Depending on the structure of the single surfactant molecules the formed micelles can have different shapes like spheres, discs, rods or ellipsoids. For further discussions we consider spherical micelles. The forces that keep the micelles together are mostly van der Waals interactions, hydrophobic interactions and hydrogen-bonding. Due to these weak interactions the surfactant micelles show liquid like behaviour and the complete aggregation

behaviour is strongly influenced by changes of the micelle environment.

The thermodynamics of micelle formation is described in many reports in the literature. An overview of concepts can be found in the books of Tanford [Tan80], Israelachvili [Isr91] and Evans [Eva99]. In the following a short description of the basics is given. In order to reach thermodynamic equilibrium the chemical potential μ of the surfactant molecules in the micelles and the chemical potential of non-associated surfactant molecules have to be identical.

$$\mu = \underbrace{\mu_1^0 + kT \ln X_1}_{\text{monomer}} = \underbrace{\mu_2^0 + \frac{1}{2} kT \ln \frac{1}{2} X_2}_{\text{dimers}} \dots \quad (5.1)$$

where X_1 is the concentration of single surfactant molecules and X_2 is the concentration of molecules which form dimers. The concentrations used in the following considerations are always given in mole fractions of the corresponding molecules. For an aggregate with N surfactant molecules we yield a chemical potential of

$$\mu = \mu_N = \mu_N^0 + \frac{kT}{N} \ln \left(\frac{X_N}{N} \right) = \text{constant} \quad (5.2)$$

where μ_N is the chemical potential of a molecule in a aggregate with the aggregation number N . μ_N^0 is the standard chemical potential in these aggregates and X_N is the concentration of surfactant molecules located in aggregates formed by N surfactant molecules. To obtain the concentrations of molecules which are aggregated equation 5.1 is used.

$$X_N = N \left(X_1 e^{(\mu_1^0 - \mu_N^0)/kT} \right)^N \quad (5.3)$$

The total concentration of surfactant molecules in the solution is the sum over all concentrations described by equation 5.3:

$$C = X_1 + X_2 + X_3 + \dots = \sum_{N=1}^{\infty} X_N \quad (5.4)$$

As all considerations are done for solutions the total concentration C and therefore all X_N can never exceed unity.

The formation of stable aggregates requires the condition that $\mu_N^0 < \mu_1^0$ for some value of N . The variation of μ_N^0 with N determines many of the physical properties of the micelles, such as the aggregate size and their polydispersity. Since X_N as defined in equation 5.6 is a distribution function and may peak at more than one value of N more than one size of aggregates can occur in thermodynamic equilibrium. In order to get an idea of the concentration at which the aggregate formation starts an energetic description of the micelles is necessary. For this we define an energy αkT describing the intermolecular interaction between two surfactant molecules. For a spherical micelle we then get a chemical potential of

$$\mu_N^0 = \mu_\infty^0 + \frac{\alpha kT}{N^{1/3}} \quad (5.5)$$

A combination of equation 5.3 and 5.5 leads to

$$X_N = N \left(X_1 e^{\alpha(1-1/N^{1/3})} \right)^N \approx N (X_1 e^\alpha)^N \quad (5.6)$$

This equation clearly shows that the concentration of molecules located in the aggregates only depends on the parameter α which again depends on the intermolecular interactions between two surfactant molecules. For sufficiently low surfactant concentrations X_1 the term $X_1 e^\alpha$ is much less than one for all $N > 1$ and therefore all molecules are isolated monomers. With increasing surfactant concentration C the concentration of isolated monomers will increase in this regime. However since X_1 reaches a value of $e^{-\alpha}$ the concentration of isolated monomers can not grow any more and the additionally added surfactant

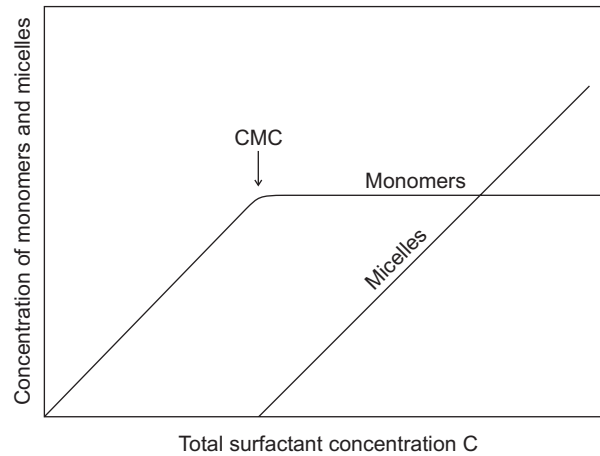


Figure 5.1: Concentration of isolated surfactant molecules (monomers) and micelles depending on the total surfactant concentration [Isr91]. The concentration of monomers increases linear with increasing surfactant concentration up to the cmc. Above the cmc the monomer concentration remains constant and the micelle concentration increases.

forms aggregates. The monomer concentration at this point is called the *critical micelle concentration* (cmc).

$$(X_1)_{cmc} = \text{cmc} \approx e^{-\alpha} \quad (5.7)$$

Here an increase in C is followed by formation of aggregates. Figure 5.1 illustrates the dependence of the monomer and the micelle concentration on the total surfactant concentration. With increasing surfactant concentration the concentration of isolated surfactant molecules (monomers) increases up to the cmc. After the cmc the monomer concentration remains constant and the concentration of micelles increases with increasing surfactant concentration.

5.2 Experimental Methods for the CMC Determination

The physical properties of surfactant solutions show an abrupt change upon reaching the cmc. This change in macroscopic properties is used to determine the cmc. Usually the data are drawn from light scattering, surface tensiometry, conductivity or osmotic pressure measurements [Eva99]. These techniques, however, are limited in sensitivity, need considerable amounts of material, and are time consuming. In addition, at least 10% of the molecules have to be in micelles to be detected by these methods [Isr91, Eva99]. These conditions are insufficient for detailed studies on the aggregation of molecules. A single molecule method is much more sensitive for these kind of investigations and gives the chance to follow the formation of the very first micelles.

5.3 Aggregation Studies of Surfactants with FCS

The results presented in this chapter are published in the paper “Investigation of Micelle Formation by Fluorescence Correlation Spectroscopy” in the “Journal of Physical Chemistry B” [Zet05b].

The following chapter demonstrates the potential of fluorescence correlation spectroscopy (FCS) as an alternative method to characterise the self aggregation behaviour of surfactants, using a non-covalently attached dye as fluorophore. As at the beginning of this chapter already mentioned rely previous FCS studies of surfactant systems on the synthesis of dye-labelled molecules, which were blended with the bare molecules under consideration [Pet86, Pal87]. With increasing surfactant concentrations micelles were formed and the dye-labelled molecules were incorporated as shown in figure 5.2 A.

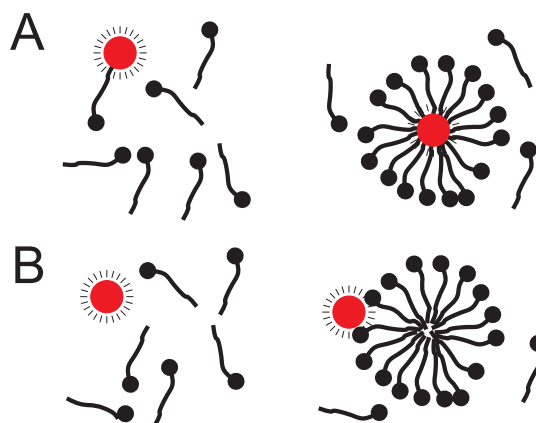


Figure 5.2: (A) Investigation of micelle formation with covalently labelled surfactant molecules. (B) Sketch describing the studies made with associated dye molecules. In the left half the situation for low surfactant concentrations is shown and in the right side the situation above the cmc is presented.

In the following chapter we will show that the synthetic work of labelling surfactant molecules can be circumvented if a Coulomb interaction between surfactant molecules and dye molecules is utilised. This physical aggregation of the dye molecules to micelles enables as well an efficient labelling (see figure 5.2 B). A systematic study of the ability of free dye molecules to act as a label in aggregate-forming systems is shown here. A suitable choice of commercially available dyes allow a straightforward determination of both the aggregate size and the critical micelle concentration. The results compare well to values determined by the “classical” techniques mentioned above.

5.3.1 Sample Preparation

In our experiments, three surfactants, hexadecyltrimethylammonium chloride (CTAC), sulfosuccinic acid bis(2-ethylhexyl) ester sodium salt (AOT) and pentaethylene glycol monododecyl ether ($C_{12}E_5$) were used as purchased from Fluka. The dyes Sulforhodamine G, Sulforhodamine B and Rhodamin B Base were purchased from Sigma-Aldrich GmbH. Rho-

damin 6G and Cresyl Violet were obtained from Lambda Physics. All chemicals were used without further purification. In figure 5.3 the chemical structure of the investigated surfactants and dyes are shown.

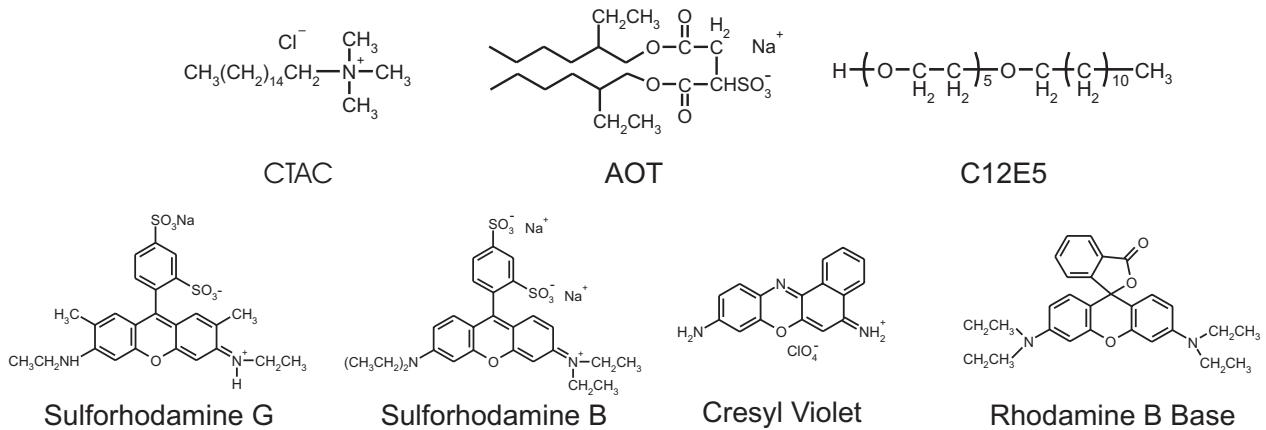


Figure 5.3: Chemical structures of the investigated surfactants and the used dyes.

The solutions were prepared with Milli-Q water. The same water was used as immersion medium for the objective.

All surfactant solutions were prepared with a constant dye concentration of 10^{-8} M. The FCS measurements were performed on droplets of $40 \mu\text{L}$ placed onto a coverglass. The focus of the objective was placed $200 \mu\text{m}$ above the coverglass to avoid interactions between the glass surface and the investigated molecules. For the measurements a $40\times$ water immersion objective was used. The dye molecules were excited by an Ar-ion laser at 514 nm. Further details of the experimental setup are described in chapter 2.2. Each FCS measurement with a duration of 60 s was repeated three times. The three achieved autocorrelation curves were averaged and analysed by fitting.

5.3.2 Results of the FCS Measurements

In the following sections we will discuss the results of the measurements on the three different surfactants separately.

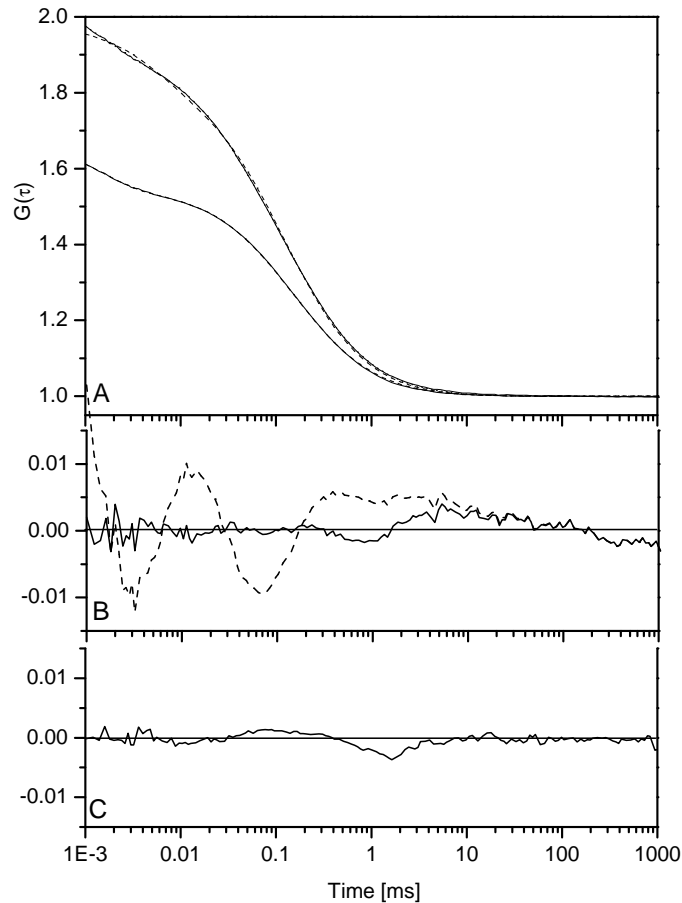


Figure 5.4: (A) The experimental autocorrelation curves (—) of the two CTAC concentrations $8.0 \cdot 10^{-4}$ M and $1.5 \cdot 10^{-3}$ M with an amplitude of 2.0 and 1.6 are plotted together with the single-particle fit (---). (B) Residuals of the single particle and two-particle fits at a CTAC concentration of $8.0 \cdot 10^{-4}$ M, respectively. The residuals of the single-particle fit (---) are considerably larger than the ones of the two particle-fit (—). (C) Residuals of the single-particle fit to the data at $1.5 \cdot 10^{-3}$ M are shown. For this concentration a single-particle fit is sufficient.

Cationic surfactant

The cationic surfactant CTAC was measured with the anionic dyes Sulforhodamine B and Sulforhodamine G and the cationic dye Cresyl Violet. We start discussing the results obtained with the anionic dyes. Figure 5.4 A shows two typical autocorrelation functions for CTAC concentrations of $8.0 \cdot 10^{-4}$ M and $1.5 \cdot 10^{-3}$ M, respectively. Figure 5.5 (top) shows the diffusion time as a function of CTAC concentration obtained by single-particle fits throughout the entire concentration range. The dashed vertical line indicates the published value of the *cmc* obtained using classical techniques. We observe an increase of the diffusion time starting at a surfactant concentration of $5.0 \cdot 10^{-4}$ M, i.e. at a concentration considerably below the *cmc*. Note that a single-particle fit assumes all dye molecules to diffuse at the same average speed. In case of aggregate formation this implies that all dye molecules have associated to aggregates of the same size. In order to check whether different fractions of dye molecules are present in the solution, the autocorrelation functions were also fitted with a two-particle model ($i = 2$ in equation 2.21) and an F-test was applied to determine which of the two models is more suitable to represent the experimental data. The main criterion of the F-test is the value of χ^2 , which leads to an intuitive understanding of the F-test; only if the residuals (and thus χ^2) are significantly lowered, the model with more free fitting parameters is justified. For $c(\text{CTAC}) = 8.0 \cdot 10^{-4}$ M χ^2 is 0.015 for the single-particle fit and 0.00075 for the two-particle fit. This means that the two-particle model improves χ^2 by a factor of twenty and therefore this model has to be chosen. Not surprisingly, also the F-test favours the two-particle model. Repeating this procedure for the whole concentration range, it turns out that for the CTAC system a two-particle fit is needed between $5.0 \cdot 10^{-4}$ M and the *cmc* resulting from classical techniques. Below and above this concentration range, a single-particle fit is sufficient. To further visualise this procedure, we compare in figure 5.4 B the residuals of a single-particle and a two-particle fit to an autocorrelation function obtained in the intermediate concentration regime. Here,

the two-particle fit clearly leads to smaller residuals. In figure 5.4 C, we show the residuals for a single-particle fit to an autocorrelation function obtained above the *cmc*. Here, the residuals are considerably smaller and a two-particle model does not lead to a significant improvement. Figure 5.5 (bottom) shows the results for the diffusion times resulting from two particle fits in the intermediate CTAC concentration regime.

The two particles represent free dye molecules (dominant at low CTAC concentrations) exhibiting a diffusion time of $\tau_1 \approx 30 \mu\text{s}$ and a dye molecules bound to a micelle (dominant at high CTAC concentrations) exhibiting a diffusion time of $\tau_2 \approx 150 \mu\text{s}$. This value is nearly constant up to a CTAC concentration of $1.5 \cdot 10^{-3} \text{ M}$. At intermediate concentrations slightly below the *cmc*, both free dye molecules and dye molecules bound to micelles coexist. The diameter of the micelles calculated from τ_2 according to equations (2.16) and (2.17) yields 6.3 nm. This is in good agreement with the value of 7.9 nm reported by Lindman and coworkers [Lin84]. Figure 5.6 shows the increase of the fraction of dye molecules associated to micelles as a function surfactant concentration.

In a third series of experiments, the cationic CTAC system was also studied together with the cationic dye Cresyl Violet (figure 5.5 open triangles). The results of the single-particle fits show considerably smaller increase in diffusion time signalling for a large number of free dye molecules even well above the *cmc*. The F-test indicates a much broader concentration range in which two fractions of particles coexist. Consistently, the fraction of dye molecules associated with micelles, which is obtained from the two-particle fit, is quite small (Figure 5.6). It is very likely that repulsive electrostatic interaction is the origin of the ineffective physical aggregation of Cresyl Violet to the CTAC micelles.

To get a more detailed insight in the aggregate formation the concentration range between $2 \cdot 10^{-4} \text{ M}$ and $2 \cdot 10^{-3} \text{ M}$ is studied in more detail with the anionic dye Sulforhodamine B. Figure 5.7 show the diffusion behaviour of the dye molecules. For the concentrations between $3 \cdot 10^{-4} \text{ M}$ and $1 \cdot 10^{-3} \text{ M}$ a two particle fit is necessary. In the right part of the

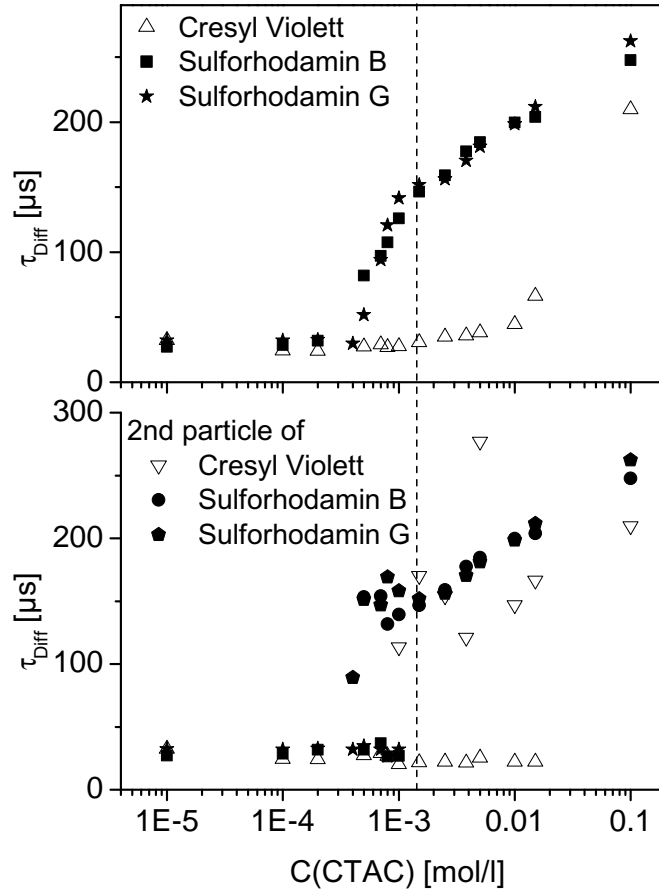


Figure 5.5: Diffusion times determined for CTAC solutions of different concentrations. The data result from fitting equation (2.19) to the experimental FCS autocorrelation functions. The dashed line indicates the *cmc* value determined by classical methods. The top graph shows the results obtained for single-particle fits ($K = 1$). The bottom graph shows data obtained when using a two particle fit. In order to determine whether a single or a two-particle fit should be used, we applied a hypothesis test (F-test) with a 5% confidence level. In case of anionic dye molecules the two-particle fit was required only at concentrations below the dashed vertical line. For the cationic dye molecule the two-particle fit was necessary up to a concentration of $1.5 \cdot 10^{-2}$ M.

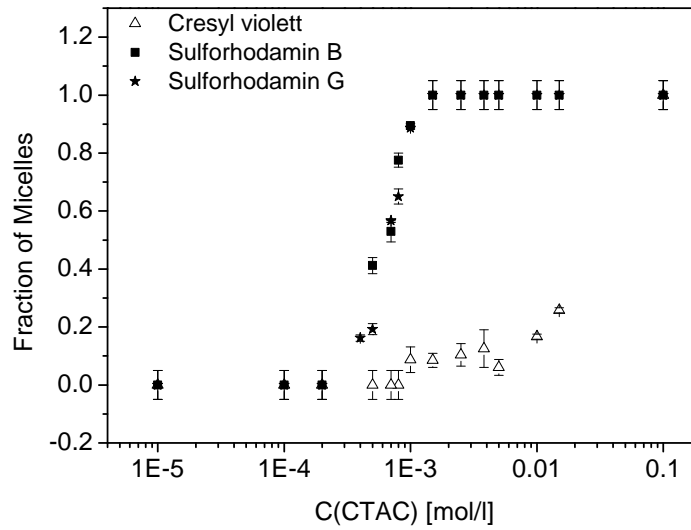


Figure 5.6: Fraction of dye molecules associated with micelles. Whenever a two-particle fit was required, the value of the fraction was taken from the fit. When using the single-particle model, the value was set to 0 at low and to 1 at high concentrations and an error of 5% was assumed. For the anionic Sulforhodamines we obtain a much faster increase than for the cationic dye Cresyl Violet.

figure the fraction of dye molecules associated to micelles is plotted. With increasing concentration of surfactant molecules we find a linear increase in the number of dye molecules associated to micelles. The diffusion time detected for the micelles is almost constant over the whole concentration range. This shows that we obviously detect the first micelles and can follow the increase in the number of micelles present in the solution. At the concentration $3 \cdot 10^{-4}$ M 10% of the dye molecules are associated to micelles. This means that we have a “micelle concentration” of 10^{-9} M. This behaviour of micelle formation is in good agreement with theoretical predictions made by Tanford [Tan80] and Israelachvili [Isr91] which were already presented in chapter 5.1.

Anionic surfactant

The anionic surfactant AOT was analysed with each of the dyes Cresyl Violet and Sulforhodamine B.

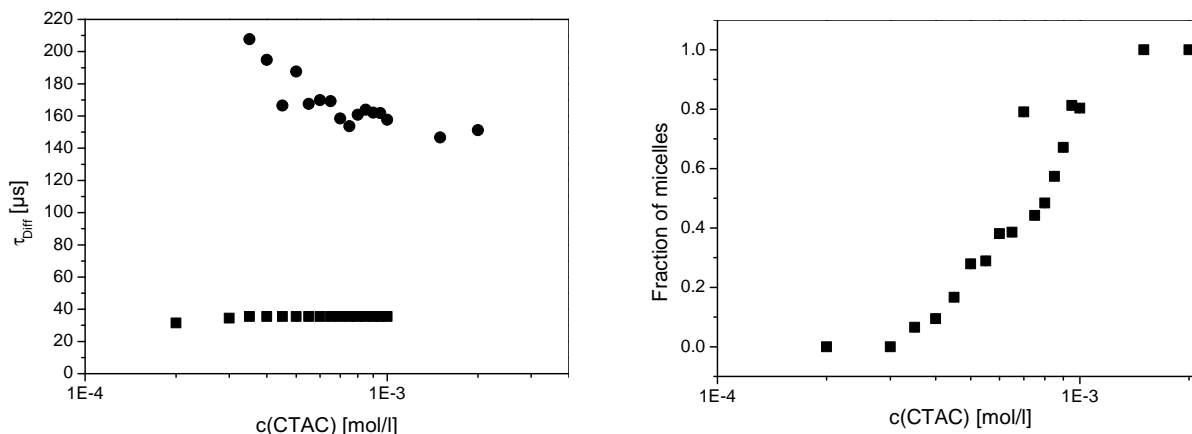


Figure 5.7: Detailed study of the micelle formation below the classical *cmc*. At a concentration of one third of the *cmc* in FCS a second fraction of particles with higher diffusion times is observed. This we define as the first micelles formed by surfactant molecules.

Figure 5.8 shows the normalised autocorrelation curves of AOT analysed with Cresyl Violet in an AOT concentration range of $2.3 \cdot 10^{-5}$ M to $1.5 \cdot 10^{-2}$ M. At concentrations below $1.5 \cdot 10^{-3}$ M the autocorrelation signal is independent of surfactant concentration and resembles that of pure dye solutions. At concentrations between $1.5 \cdot 10^{-3}$ M and $3.8 \cdot 10^{-3}$ M the autocorrelation curves shift to higher diffusion times, indicating the beginning of the micelle formation. At $1.5 \cdot 10^{-3}$ M free dye molecules and micelles coexist. At high surfactant concentrations the autocorrelation signal is, again, independent of surfactant concentration, indicating that all dye molecules are attached to micelles. The evaluation of the data leads to the concentration dependence of the diffusion time shown in figure 5.9. At AOT concentrations below $1.5 \cdot 10^{-3}$ M the fit clearly yields a single fraction of molecules and thus, the observed diffusion time is attributed to free Cresyl Violet molecules. At $1.5 \cdot 10^{-3}$ M a second fraction of particles with a diffusion time of $91 \pm 9 \mu\text{s}$ is observed. At and above $2.5 \cdot 10^{-3}$ M the data are, again, well represented by a single fraction with a characteristic diffusion time, which increases from a value of $48.4 \pm 0.2 \mu\text{s}$ up to $104.9 \pm 0.2 \mu\text{s}$ with increasing surfactant concentration. Thus, we find a one-to-one correspondence to the CTAC system measured with anionic dyes but with the polarities inverted: At low

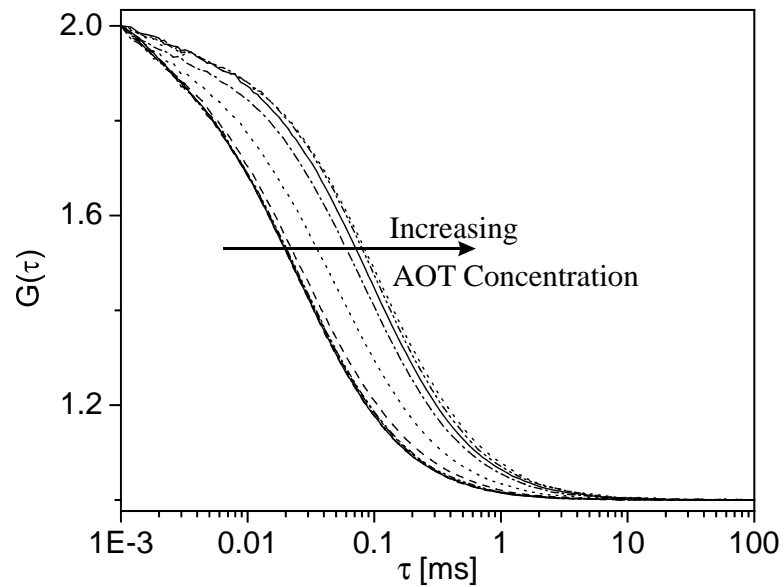


Figure 5.8: Normalised autocorrelation curves of AOT measured with Cresyl Violet. The five curves (—), corresponding to AOT concentrations of $2.3 \cdot 10^{-5}$ M to $8.0 \cdot 10^{-4}$ M do not differ in shape and cannot be distinguished. At an AOT concentration of $1.5 \cdot 10^{-3}$ M (---) the diffusion time starts to increase. The curve at *cmc* ($2.5 \cdot 10^{-3}$ M) (···) shows a diffusion time much larger than that of the free dye. With increasing AOT concentration the diffusion time converges to an upper limit of $\approx 100 \mu\text{s}$.

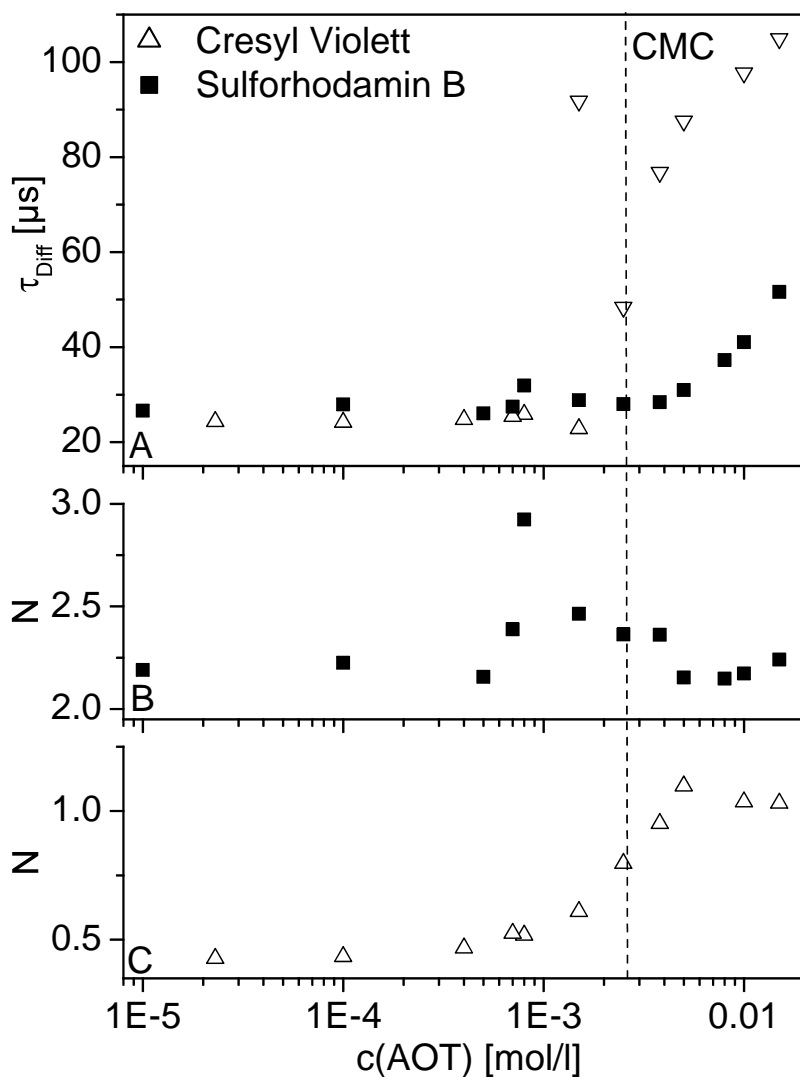


Figure 5.9: Characteristic diffusion times (A) and number of dye molecules in the excitation volume (B, C) for AOT solutions measured with Cresyl Violet and Sulforhodamine B, respectively. At low AOT concentrations only free Cresyl Violet molecules with a diffusion time of $\approx 25 \mu\text{s}$ are detected. At an AOT concentration of $1.5 \cdot 10^{-3}$ M a second fraction of particles with a diffusion time of $90 \mu\text{s}$ appears. At higher AOT concentrations, a single fraction of particles is observed with a diffusion time significantly longer than that of the free dye. The solution with Sulforhodamine B shows an increase in the diffusion time at $5 \cdot 10^{-3}$ M. Figures B and C show the change in the number of fluorescent particles in the excitation volume. This number increases with increasing surfactant concentration for Cresyl Violet (C) but does not display any distinct trend for Sulforhodamine B (B).

surfactant concentrations only free dye molecules are observed, while above the “classical” *cmc* all dye molecules are bound to micelles. At concentrations slightly below the *cmc* both free dye molecules and dye molecules bound to micelles are present in the solution. Along the same lines the data obtained with the anionic dye Sulforhodamine B resemble the scenario observed for CTAC with the cationic dye Cresyl Violet. The data can be fitted with a single fraction of particles throughout the entire concentration range. The diffusion time increases only slightly and even above the classical *cmc* predominantly free dye molecules are observed.

We now turn to the discussion of the number of particles N within the excitation volume, which is the second important fitting parameter. According to equation (2.19) N is proportional to $1/(G(0) - 1)$ for single particle systems. Figure 5.9 C shows the concentration dependence of the number of particles of Cresyl Violet. Although all solutions were prepared with identical dye concentration we observe an increase in the number of particles at the very concentration at which the diffusion time starts to increase. In other words, the concentration of dye molecules increases exactly at the onset of micelle formation. We attribute this to the ability of micelles to dissolve dye molecules that at low surfactant concentrations (below *cmc*) are adsorbed at the surfaces of the sample chamber.

Measuring the same surfactant with Sulforhodamine B, we do not observe a significant change in the number of particles beyond the statistical scatter in the data points (figure 5.9 B).

Non-ionic surfactants

The non-ionic surfactant $C_{12}E_5$ shows a different behaviour than the ionic species. This surfactant could only be investigated by FCS with Rhodamine B Base. All other dyes studied with this surfactant did not show any change in diffusion time with increasing surfactant concentration. For Rhodamine B Base we detect a single fraction of particles

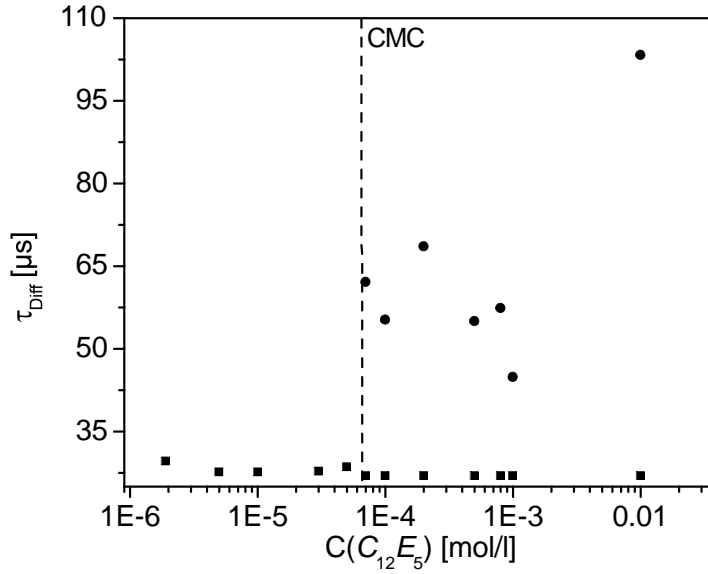


Figure 5.10: For the non-ionic surfactant up to a concentration of $6.5 \cdot 10^{-5}$ M no interaction with the Rhodamine B Base can be noted. At this concentration a second particle with a longer diffusion time of $62 \pm 5 \mu\text{s}$ and a fraction of 12% appears. With increasing surfactant concentration the fraction of this particle increases up to 80%.

surfactant	<i>cmc</i> [M]		
	cationic	anionic	conductivity
CTAC	7×10^{-3}	1.5×10^{-3}	1.46×10^{-3}
AOT	2.5×10^{-3}	4×10^{-3}	2.4×10^{-3}

Table 5.1: *cmc* values for the ionic surfactant systems as obtained from conductivity measurements and from FCS measurements with anionic and cationic dyes.

(free dye molecules) at surfactant concentrations below $6.5 \cdot 10^{-5}$ M. At this concentration a second fraction of particles appears with a characteristic diffusion time of $\approx 60 \mu\text{s}$. The fraction of this species is 12%. With increasing surfactant concentration the fraction increases up to 80%. The scatter in diffusion time of the micelles is relatively large and therefore its value is not specified.

5.3.3 Discussion

For all ionic surfactants studied here, we find a quite general behaviour. Well below the *cmc* only free dye molecules are observed. At and above the *cmc* value obtained by classical techniques, micelles are observed provided that the dye molecules are chosen to have the opposite polarity of the surfactant (see table 5.1). Well below and above the classical *cmc* the FCS autocorrelation function can be fitted by assuming a single fraction of particles corresponding to free dye molecules (at low concentrations) and to dye molecules bound to micelles (at high concentrations), respectively. In the concentration range between about one third of the *cmc* and the actual *cmc* the situation is more complex and indeed more interesting. Here, the FCS data clearly indicate the coexistence of two fractions of dye molecules, one characterised by the diffusion time of the free dye and the other one characterised by a considerably larger diffusion time. This finding suggests the formation of aggregates already below the *cmc*. The width of the concentration range below the *cmc*, where aggregate formation is observed, varies slightly from system to system. However, the observation of aggregate formation below the *cmc* is a distinct result of the FCS experiments. In addition, for dye molecules suitable for *cmc* analysis a systematic increase of the number of particles within the excitation volume is observed when approaching the *cmc*. It is assumed that dye molecules located at the glass surface (and therefore not accessible to FCS) will be dissolved on the onset of micelle formation.

One may argue that the formation of micellar aggregates at surfactant concentrations below the classical *cmc* may be induced by the presence of the dye molecule and thereby be considered an artefact of the FCS technique [Niu92]. In order to test this hypothesis, we have quantified the influence of Sulforhodamine G and Cresyl Violet on the micelle formation in CTAC solutions by conductivity measurements. The results are summarised in table 5.2. Irrespective of the polarity of the dye the addition of up to $1 \cdot 10^{-4}$ M of dye molecules did not lead to any measurable change of the *cmc*. Only at a dye concentration

Dye Conc. [M]	<i>cmc</i> [M]	
	Sulforhodamine G	Cresyl Violet
0	1.43×10^{-3}	1.43×10^{-3}
1×10^{-7}	1.4×10^{-3}	1.4×10^{-3}
1×10^{-4}	1.5×10^{-3}	1.4×10^{-3}
1×10^{-3}	3.0×10^{-3}	1.9×10^{-3}

Table 5.2: *cmc* values for the cationic surfactant CTAC with different concentrations of Sulforhodamine G and Cresyl Violet. The values are measured by conductivity.

of $1 \cdot 10^{-3}$ M a slight shift of the *cmc* is observed. We note that this concentration is five orders of magnitude larger than the concentration used for the FCS experiments. The shift is independent of the polarity of the dye molecule. In addition, the *cmc* happens to shift to higher concentrations in contrast to the observation of aggregation at concentrations *below* the *cmc*. Therefore it seems unlikely that the *pre-cmc* aggregation is induced by the dye. Thus, it is rather probable that a small number of aggregates is indeed formed below the *cmc*. The sensitivity of the FCS technique requires no more than $1 \cdot 10^{-9}$ M of aggregates in order to lead to the observed results. Such small number of aggregates can not be detected by the techniques commonly used for *cmc* determination.

The observation of pre-micellar aggregation may also raise the question of how to determine a critical micelle concentration from FCS experiments. For most practical purposes, we may define a *cmc* from FCS experiments as the lowest surfactant concentration at which the FCS autocorrelation function can be well represented by a single fraction of dye molecules bound to micelles. Because of the inherent experimental errors typical of the classical techniques for *cmc* determination, this value is in quantitative agreement with the published *cmc* values.

As for the choice of the dye molecules, the experiments indicate that different polarity between surfactant head group and dye molecule is advantageous. Indeed, the clearest results are obtained when anionic surfactants are combined with cationic dyes and *vice*

versa. If the same polarity is chosen for surfactant and dye, the results are ambiguous and hardly any conclusions on the value of the *cmc* can be drawn. The experiments further indicate that the ionic interaction between dye and surfactant rather than the solubility of the dye is the crucial parameter for a successful *cmc* measurement by FCS [Sch00a]. This fully accords with the finding that for non-ionic surfactants the detection of a *cmc* is more difficult and the change in the diffusion time is not as large as in ionic surfactants (see figure 5.10). In this case a second fraction of particles appears at $6.5 \cdot 10^{-5}$ M, which coincides with the *cmc* value obtained by classical methods.

Here we will conclude our results on the investigation of the three different surfactant systems. We have explored the potential of fluorescence correlation spectroscopy (FCS) for the characterisation of surfactant aggregation in aqueous solution. Rather than using covalently dye-labelled surfactant molecules, we have investigated the physical aggregation of dye molecules to micelles. Our results show that FCS can be used for *cmc* determination in ionic surfactant systems provided that attractive ionic interactions are present. In consequence, the advantages characteristic of FCS (small sample volume, fast measurements) apply and make this technique an attractive alternative to the classical methods for *cmc* detection. We note that the high sensitivity of the technique (typical dye concentrations in the 10^{-8} M regime) allows the detection of *cmcs* in concentration regimes, which are not accessible by any of the classical techniques [Erh01b] (see section 6.3). Our results also show the beginning of the aggregations already below the *cmc* determined by classical methods. This finding give for the first time an insight in the formation of the first micelles.

Chapter 6

Aggregation of Block Copolymers investigated by FCS

In the previous chapters modifications of an FCS setup are described which allow the observation of single fluorescent molecules in organic solutions. In addition new methods for the investigation of aggregation with the FCS technique were shown in chapter 5. The possibilities of these new developments are demonstrated with measurements of model systems like small molecular weight surfactants and polystyrene solutions. To give an insight in the big potential of this enhanced technique and the new areas that has been made available several systems synthesised and studied by co-workers were investigated as well. In the following sections only a short description of the investigated systems is given. A detailed description of the synthesis and the characterisation of them is given in the respective PhD thesis and publications. Here the focus is put on the FCS measurements accomplished during this thesis.

6.1 Theoretical basis for the aggregation of polymers

Aggregation of molecules is mostly shown by amphiphilic molecules. Therefore block copolymers are an important class of this kind of molecules. These polymers consist of two different immiscible polymers. If the solubilities of the two polymers are sufficiently different the polymer shows aggregation in dilute solution. The shape of the aggregates depends on the size of the two different blocks and is characterized by the number of monomer units N per chain. The thermodynamic description of the interactions taking place in polymer solutions are described by the “Flory-Huggins” interaction parameter χ . In the case of diblock copolymers three different χ values are distinguished. χ_{AB} describes the interaction between the two different polymer blocks A and B. χ_{AS} represents the interaction between the A-block of the polymer and the solvent and in analogy χ_{BS} is the interaction between the B-block and the solvent. A combination of the two parameters χ_{AB} and N is used to describe the phase separation behaviour of block copolymers. Polymers which are in the strong segregation limit where $\chi_{AB} \cdot N \gg 10$ form micelles in solution. In this case the core of the micelles contains only A blocks and the shell is formed by the B block. This block is swollen with solvent. The solvent phase contains for this kind of block copolymers no A blocks.

6.2 Aggregation of Polystyrene-block-Amylose in THF

The results of this section are published in the paper “Micellar Aggregates of Amylose-*block*-polystyrene Rod-Coil Block Copolymers in Water and THF” in *Macromolecules* in the year 2005 [Loo05, Loo01].

6.2.1 Investigated sample

We investigated an asymmetric A-B diblock copolymer consisting of a short Amylose block and a much longer polystyrene block. The Amylose block shows a helical secondary structure and forms hydrogen bonds between neighbouring segments. This type of block copolymers has a high Flory-Huggins interaction parameter χ_{AB} . This parameter quantifies the incompatibility of the two blocks. Hence, rod-coil diblock copolymers form at relatively small degrees of polymerisation already aggregates. In our case we investigated a diblock copolymer with a small blocksize of amylose ($N_{\text{Amylose}} = 60$) and a much longer block of polystyrene ($N_{\text{PS}} = 740$). The chemical structure of this polymer is shown in figure 6.1. This amphiphilic structure leads to the formation of micelles in THF. These micelles have an amylose core and a polystyrene shell and are often designated as star micelles. The

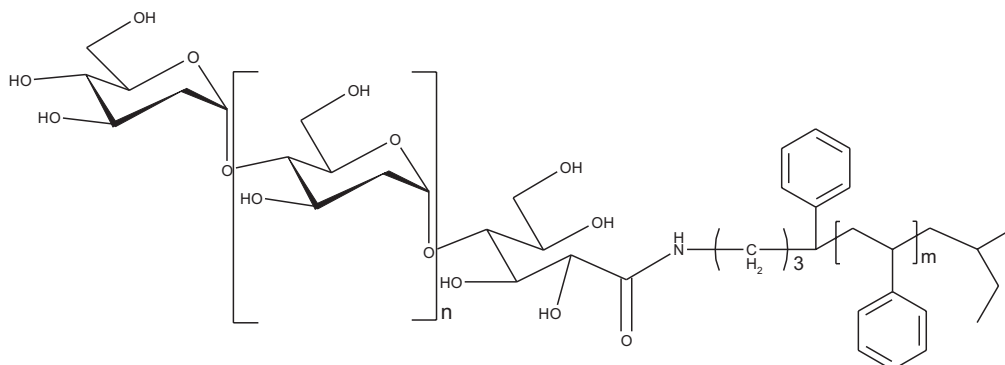


Figure 6.1: Chemical structure of the investigated diblock copolymer. In our case the block length of the Amylose block is $n = 60$ and the block length of the polystyrene block is $m = 740$.

polymer is made by sequential anionic and enzymatic polymerisation. The details of this synthesis are described by Loos et al [Loo97, Loo02]. By simply dissolving the polymer in THF star micelles are obtained. For labelling the micelles Rhodamine B was added. This dye is hardly soluble in THF and therefore tends to locate inside the formed micelles. The polymer solutions have a constant dye concentration of 10^{-8} mol/L. For the investiga-

tions the sealed sample chambers described in chapter 2.2 were used. All measurements were performed at room temperature without any temperature control. Each sample was measured three times 20 min each. Equation 2.21 was fitted to the obtained autocorrelation curves. The results of every polymer concentration were analysed by using a single component and a two component fit model. By applying an F-test the correct model was chosen.

6.2.2 Results and Discussion

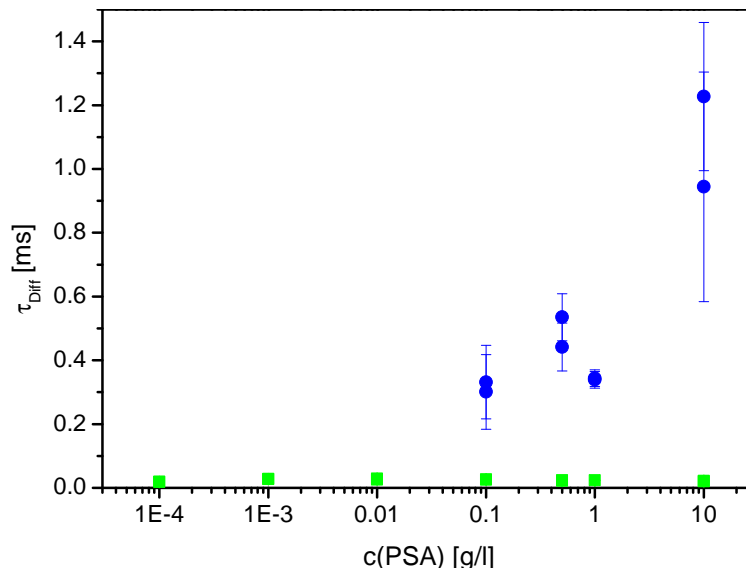


Figure 6.2: Concentration dependence of the measured diffusion time. The green squares represents the free dye molecules. The blue circles are the a second fraction of particles showing a much slower diffusion time. This particle we define as polymer micelles labelled by dye molecules.

The autocorrelation functions received for polymer concentrations below 0.1 g/mol can be evaluated using the single component model. From the fit we get the diffusion time τ_{Diff} with a value of 25 μs . This value is typical for the diffusion time of a single dye molecule. For concentrations at and above 0.1 g/L a satisfying result can only be achieved using a two component model. The diffusion time τ_{Diff} achieved for the fast component corresponds to

the diffusion time of the free dye molecule as received for polymer concentrations below 0.1 g/L. The second particle with a diffusion time of 300 μs is diffusing much slower than the free dye molecule. We assign this large diffusion time to polymer micelles. The results of the fits are summarized in figure 6.2. From these results we conclude that micelle formation starts at a critical micelle concentration in the range between 0.01 g/L and 0.1 g/L.

In the same concentration range the amplitude $G(0)$ of the measured autocorrelation

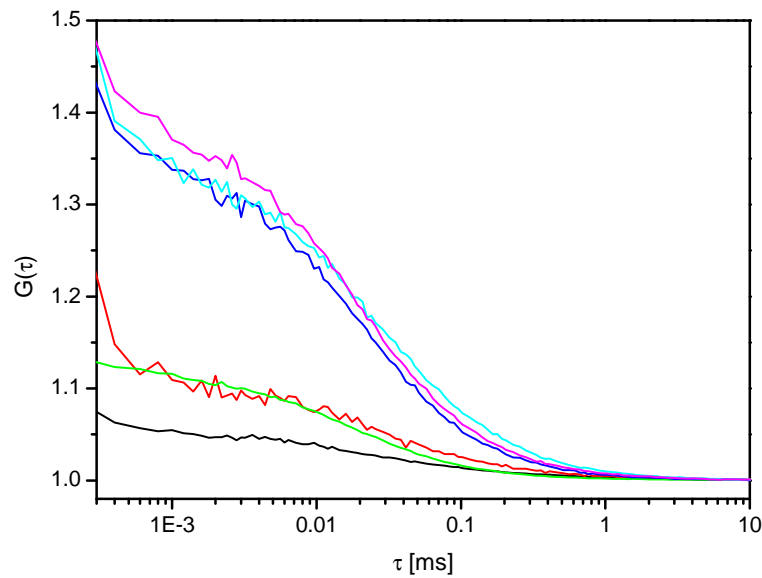


Figure 6.3: Experimental autocorrelation functions for different polymer concentrations. At low polymer concentrations (light blue, blue and pink) the curves look nearly identical and have a high amplitude. With increasing polymer concentration the amplitude of the measured autocorrelation curves decrease and indicating that the number of fluorescent particles in the observation volume increases.

functions decreased significantly (figure 6.3). Since $G(0)$ scales inversely with the number of dye molecules in the observation volume N we have a measure for the dye concentration in the solution ($G(0) = \frac{1}{N_{dye}} + 1$). This finding indicates an increase in the number of observed dye molecules. This increase can be explained by an improved solubilization of dye molecules with starting micelle formation. The polymer micelles dissolve dye molecules absorbed at the walls of the sample chambers and the cover glass.

6.3 Aggregation of Janus micelles in THF

In analogy to the amylose-polystyrene block copolymer a triblock copolymer forming “Janus micelles” with a very low critical aggregation concentration was examined. The results shown in this chapter are published in the paper “Janus micelles” [Erh01b, Erh01a] in *Macromolecules*.

6.3.1 Investigated polymer

The term “Janus micelles” describes particles exhibiting amphiphilic properties consisting of one hydrophobic half sphere and one hydrophilic half sphere. In our case Janus micelles consisting of one half sphere of polystyrene (PS), one half sphere of polymethylmethacrylate (PMMA) and a core of crosslinked polybutadiene (PB) were synthesised using anionic polymerisation. In thin films this polymer forms a morphology of lamellae formed by the outer blocks and spheres of the inner blocks located at the interface between the lamellae. The sphere forming PB middle block of this triblock copolymer can easily be crosslinked. By redissolving the crosslinked polymer in a good solvent a solution of Janus micelles is obtained. A detailed description of this procedure is given by Erhardt et al [Erh01b]. The dissolved Janus micelles form superaggregates (figure 6.4). The determination of the critical aggregation concentration was not possible by light scattering experiments.

The FCS measurements were performed in a similar way as already described in section 6.2 for the PSA polymer. The solutions for the measurements were prepared by dissolving the Janus micelles in THF. The concentration of the polymer was varied in a range between $50 \mu\text{g/L}$ and 1 g/L . All polymer solutions had a constant Rhodamine B concentration of 10^{-8} mol/L . The dye molecule was excited by a He-Ne-laser operating at a wavelength of 543 nm. The scattered laser light was separated from the fluorescence light by a dichroic mirror with a cut off wavelength of 543 nm and a long pass filter with a cut off wavelength

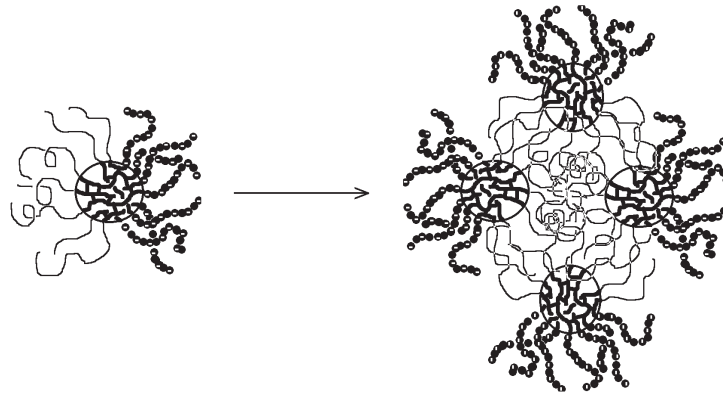


Figure 6.4: Sketch of the supermicelles formed by the Janus micelles above the cac.

of 560 nm. The pinhole used in this configuration had a diameter of $78\ \mu\text{m}$. Each solution was measured for 20 min and each measurement was repeated 3 times.

Rhodamine B has a low solubility in THF and in the presence of Janus micelles some dye molecules are located inside the micelles. The measured autocorrelation functions are evaluated using equation 2.21. In case of the Janus micelles a two component fit was necessary over the whole concentration range in order to describe the data sufficiently.

6.3.2 Results and Discussion

For concentrations below $8\ \text{mg/L}$ we got for all polymer solutions two components with constant diffusion times. The fast component shows a diffusion time of $25\ \mu\text{s}$. This time corresponds very well to diffusion times measured for dye solutions without any polymer. The second particle is much slower and has a diffusion time of around $200\ \mu\text{s}$. We associate this component to single Janus micelles carrying a dye molecule. At the concentration of $8\ \text{mg/L}$ the diffusion time of the second particle increases. The diffusion time of the free dye molecule stays constant for all polymer concentrations. The diffusion time of the second particle increases with increasing polymer concentrations up to a value of 1.1 ms. In figure 6.5 the change in diffusion time with increasing polymer concentration is shown. In contrast

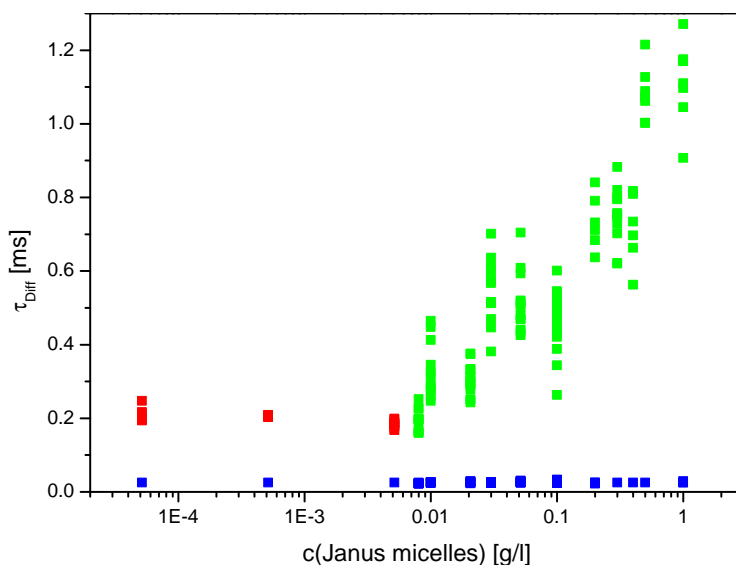


Figure 6.5: The blue squares indicate the free dye molecules, the red ones are single Janus micelles and the green squares represent the super aggregates. Above a concentration of Janus micelles of 7 mg/L the diffusion time of the slower particle increases. We define this concentration as the starting point for the formation of the super aggregates.

to other methods it is possible to follow the aggregation of Janus micelles using FCS. We define the critical aggregation concentration (cac) as that point where the diffusion time of the second particle increases. Though we yield a cac of $7 \pm 2 \text{ mg/L}$. Such low cac are only detectable by highly sensitive methods like FCS.

6.4 Amphiphilic Janus Micelles

The two half spheres of the Janus micelles presented in the previous section have nearly identical solubility parameter. The reason for the observed aggregation is still not understood. To achieve molecules with an amphiphilic character the ester groups of the PMMA half sphere are hydrolysed. A micelle with a hydrophobic PS-part and a hydrophilic polyacrylic acid (PAA) part is received. The details of the synthesis and characterisation of this polymer is given in the article “Amphiphilic Janus Micelles with Polystyrene and

Poly(methacrylic acid) Hemispheres” published in the Journal of the American Chemical Society (JACS) [Erh03, Erh01b].

6.4.1 Experimental Setup

The polymer is synthesised by alkaline hydrolysis of the Janus micelles in dioxane. Via dialysis the polymer is transferred to aqueous solutions with a NaCl content of 1 wt%. The salt circumvent a stretching of the polyelectrolyte chains. To the solutions used for the FCS investigations the dye Cresyl Violet was added. The concentration of the dye was for all investigated samples constant 10^{-9} M. To avoid evaporation and therefore a change in the concentration during the measurement the samples were investigated in a sealed sample chamber (sketch see section 2.4). The dye molecules were excited by an He-Ne-laser at 543 nm. Each measurement took 5 min and was repeated 5 times. The received autocorrelation curves were averaged and fitted to equation 2.20.

6.4.2 Results and Discussion

The normalised autocorrelation curves (figure 6.6) are for polymer concentrations below $5 \cdot 10^{-3}$ g/L identical. This autocorrelation curves can be fitted well by assuming one fraction of dye molecules. The obtained diffusion time of $27 \mu\text{s}$ corresponds very well to free dye molecules. At higher polymer concentrations the curves are shifted to higher τ -values. In addition the shape of the autocorrelation curves changes in a characteristic way. At short correlation times we observe a fast decay of $G(\tau)$ (region I in figure 6.6), which is characteristic for triplet losses, indicative for the change in the micro environment of the dye molecules. At higher τ -values $G(\tau)$ develops two shoulders at around 1-10 ms (region II) and at 100-1000 ms (region III). These two shoulders correspond to two different kind of aggregates. The first shoulder can be reproduced by a fit assuming two fractions with

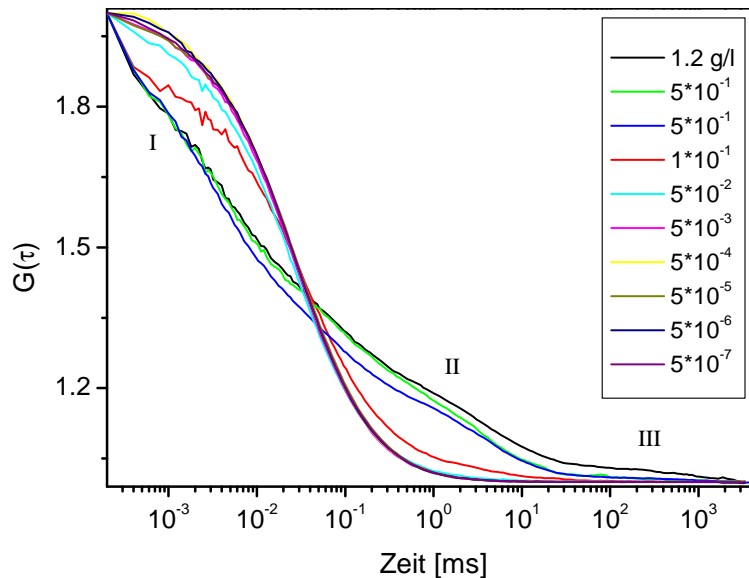


Figure 6.6: Normalised autocorrelation curves of hydrolysed Janus micelles. For low polymer concentrations we see identical autocorrelation curves typical for freely diffusing dye molecules. Polymer concentrations above 0.1 g/L show three different relaxation times and can be separated in three parts. Part I in the range of 1 to $10 \mu\text{s}$: In this fast decay photophysical effects like triplet relaxation occur. Part II in the range of 1 to 10 ms : In this range the diffusion of aggregates formed by the Janus micelles is seen. Part III with relaxation times of more than 100 ms : This time represents very huge aggregates.

different sizes. One corresponds to free dye molecules (black squares in figure 6.7) and the second corresponds to dye molecules incorporated in aggregates formed by the Janus micelles (red circles). In contrast, the second shoulder is difficult to model as no well defined value for $G(\tau) \rightarrow \infty$ is available and the fraction of molecules with this high diffusion time is very low. From the amplitude of $G(\tau)$ in region III an estimation yields a fraction of 3% for a polymer solution with a concentration of 1.2 g/L . As in chapter 2.1 mentioned it is difficult to determine fractions below 10%. Therefore the model assuming two different fractions of molecules is also used for the high polymer concentrations. From the results shown in figure 6.7 the critical aggregation concentration (c_{ac}) is located between 0.01 and 0.1 g/L . Above this concentration the molecular dissolved Janus micelles (unimers) aggregate to polymolecular “supermicelles” (multimers). The hydrodynamic radius of the

multimers is determined to 54 nm using equation 2.16 and 2.17 and the measured diffusion time. In addition to the supermicelles huge aggregates with hydrodynamic radii of several hundreds of nanometer up to microns are observed (region III). A more detailed study of these big aggregates was not possible. This huge aggregates are interpreted as frozen micelles. These frozen structures develop during the preparation of the polymer solution via dialysis and due to the high glass transition temperature of the polystyrene core is their breakup kinetically hindered. None the less can small molecular weight dye molecules diffuse in the frozen micelles.

In summary the cac of the saponified Janus micelles could be determined to be between

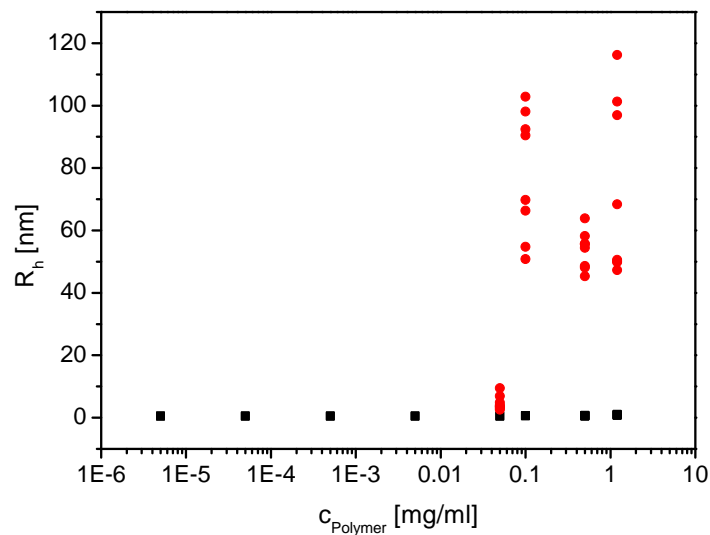


Figure 6.7: The black squares indicate free dye molecules with a hydrodynamic radius of around 0.5 nm. The red circles indicate a second fraction of particles with a bigger hydrodynamic radius ranging from 10 to 100 nm. These second particles are the saponified Janus micelles which aggregate to bigger structures with a broad distribution in size. These findings were already discussed with the measured autocorrelation curves.

0.01 and 0.1 g/L polymer. The normalised autocorrelation curves indicate clearly three different fractions of fluorescent molecules. One fraction is remaining free dye molecules.

Another are dye molecules associated to multimers and the last fraction are dye molecules incorporated in huge aggregates – probably frozen micelles. A quantitative analysis of the third fraction was not possible during these experiments.

Chapter 7

Temperature dependent

Measurements in Biophysics

Frank Schubert studied in his PhD thesis among other things the binding kinetics and thermodynamics of a protein to single stranded DNA (ssDNA) [Sch05]. FCS enables to study this interaction with a high sensitivity and low amount of material. The setup developed for temperature dependent measurements (description see section 2.4) enables to determine activation energies, reaction constants and reaction enthalpies. The following chapter demonstrates the possibilities of the enhancement of FCS made during this thesis. The results of his measurement are published in Biochemistry in the paper “Comparative thermodynamic analysis of DNA-protein interactions using surface plasmon resonance and fluorescence correlation spectroscopy” [Sch03, Sch05].

7.1 Binding of protein to DNA

In the following experiments the binding properties of the Replication Protein A (RPA) are investigated. This protein is involved in the replication and recombination processes of

DNA molecules. It plays an important role in the pathway of DNA repair [Lao99, Wol97]. It binds with low sequence specificity and high affinity to single stranded DNA molecules [Mit93, Kim94]. The experiments were conducted using ssDNA molecules with a dye label at one end. The used dye molecule Cy5 can be well excited at 633 nm. All measurements were conducted with the sample chamber developed for temperature dependent measurements presented in section 2.4.1 including the capability for sample exchange. With increasing protein concentration the normalised autocorrelation curves shift to higher τ -values (figure 7.1). The diffusion times of free and protein bound ssDNA were determined from the autocorrelation curves with no protein (black curve in figure 7.1) and an excess of protein in the solution (blue curve). The respective autocorrelation curves were fitted using equation 2.21 and assuming a one component model. From this a diffusion time $\tau_{\text{DNA}} = 152.1 \pm 2.4 \mu\text{s}$ for the free DNA and $\tau_{\text{complex}} = 450.8 \pm 5.2 \mu\text{s}$ for the complex could be obtained at 25 °C.

To study the progress of complex formation the bound fraction and from that the equilibrium constant of the reaction was determined. Therefore a reverse titration of RPA against ssDNA was performed. The resulted autocorrelation curves were fitted using equation 2.18 for two different fractions of particles, i.e. ssDNA molecules and RPA-DNA complex. The two diffusion times τ_{DNA} and τ_{complex} obtained from measurements of the free ssDNA and at saturating protein concentrations were kept fix for this fitting procedure. The fraction of complex $\theta = \phi_1$ is the only free parameter of the fit and was determined at every titration point. This fitting parameter of the autocorrelation curve is identical with the degree of binding.

The law of mass action links the degree of binding to the equilibrium constant of the dissociation.

$$K_{\text{D}} = \frac{(1 - \theta)[B]([A] - \theta[B])}{\theta[B]} \quad (7.1)$$

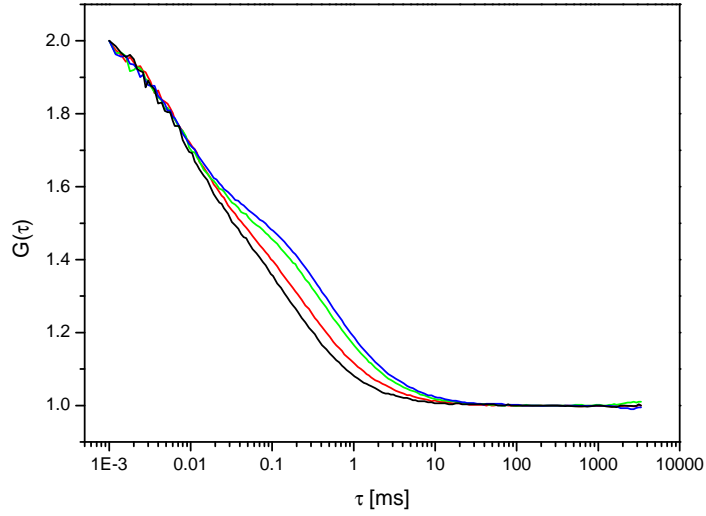


Figure 7.1: Normalized autocorrelation functions for different RPA concentrations at 25 °C. The percentage of complex was determined by a two component fit to each function. Curves for 0% (—), 40% (—), 81% (—) and 100% (—) ssDNA–RPA complex are shown. An increase in diffusion time with increasing complex fraction can clearly be seen.

where $[A]$ is the RPA concentration, $[B]$ is the concentration of ssDNA, and K_D is the equilibrium constant for the dissociation. Rearranging this equation, solving the quadratic formula and replacing $\alpha = [A] + [B] + K_D$ yields to:

$$\theta = \frac{\alpha - \sqrt{\alpha^2 - 4[A][B]}}{2[B]} \quad (7.2)$$

The degree of binding determined from the FCS measurements at three different temperatures as a function of RPA concentration and the corresponding fit of the data to equation 7.2 is depicted in figure 7.2. The obtained K_D -values range from 0.64 to $8.52 \cdot 10^{-10}$ M in the studied temperature range. The determined dissociation constants were used to perform a van't Hoff analysis of the complex formation (figure 7.3). This analysis yields for the reaction enthalpy ΔH a value of -66.5 ± 8.9 kJ/mol.

The presented experiments show for the first time the determination of reaction constants

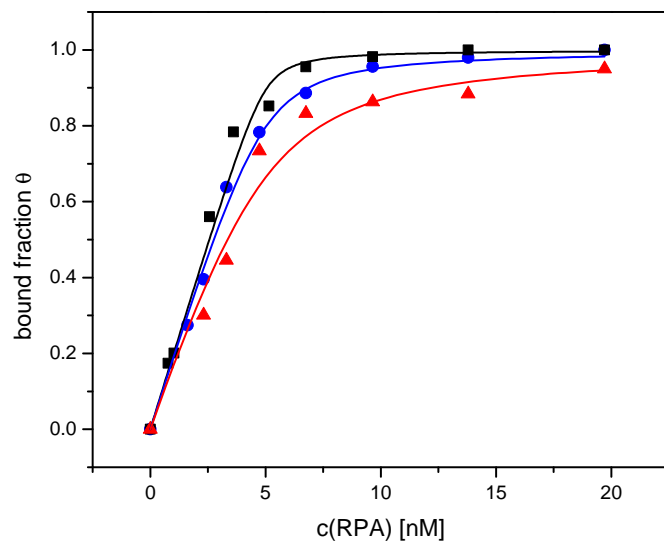


Figure 7.2: Titration curves derived from the autocorrelation functions for a DNA concentration of 5 nM at 10°C (■), 25°C (●) and 40°C (▲).

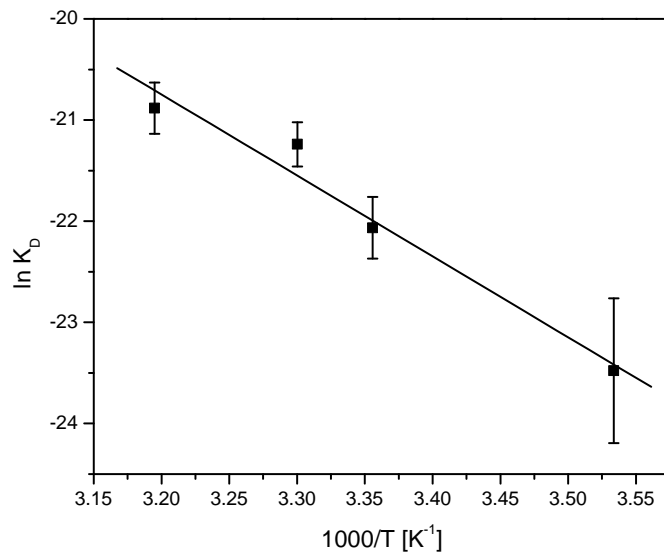


Figure 7.3: van't Hoff plot of the ssDNA–RPA interaction obtained from titration curves at 5 nM DNA concentration. The slope yields a reaction enthalpy of -66.5 ± 8.9 kJ/mol

and reaction enthalpy on the basis of a single molecule experiment. This enables to study complex formation and other thermodynamically driven processes in life science at low concentration with a minimum amount of material.

Chapter 8

Summary

In this work we have developed new concepts for the usage of fluorescence correlation spectroscopy. A classical FCS setup was modified in such a way that fluorescent species in aqueous as well as organic environments can be studied at varying temperature. We have synthesised a set of dye-labelled polymers that served as a well-defined system to study polymer diffusion and that was used to characterise the beam path and focal volume in environments with refractive indices different from that of water. Furthermore a new method for the labelling of ionic species was developed.

The adaptation of the microscope optics to non-aqueous environments was done by replacing the present microscope objective by a multi-immersion objective. Secondly, a sample chamber was developed that was not only resistant to organic solvents in all parts but also allowed temperature control of the solution.

Determining diffusion coefficients of polymers in solution and their concentrations requires the exact knowledge of shape and size of the observation volume. For this purpose we have synthesised a set of polystyrenes with molecular weights ranging from 4 to 1550 kg/mol each chain being labelled with a single dye molecule. All species were anionically polymerised in order to grant a very low polydispersity and with this a high reliability in the determination

of the observation volume. This concept can be transferred to other solvents and, hence, shows an easy way to calibrate fluorescence correlation microscopes to different solvents and to investigate non-aqueous solutions.

Furthermore, we have shown exemplarily for polystyrene that FCS is capable of determining the crossover between the dilute and the semi-dilute concentration regime. Dye-labelled polymer chains were mixed with unlabelled polymer chains of the same length and their mobility was measured by FCS for different mixing ratios. The change of the mobilities leads to the respective overlap concentrations, which are shown to follow a scaling law ($c^* \propto M^{1-3*0.59}$) in a range of molecular weights from 4 to 1550 kg/mol. This is in excellent agreement with the predictions made by Flory and Huggins ($c^* \propto M^{1-3*0.6}$). The data shown demonstrate that FCS can measure diffusion properties in ranges that were not accessible before.

Another part of this work focusses on concepts to monitor the aggregation of molecules by FCS. Taking low-molecular-weight surfactants as an example it is shown that with the help of Coulomb interaction cationic surfactants can be labelled with anionic dye molecules and vice versa. Moreover, micelle formation is observed already at concentrations slightly below the critical micelle concentration found with classical methods. This findings are in excellent agreement with the predictions made by Israeliachvili in the 1990ies.

Additionally, it was demonstrated that by using insoluble dye molecules, which are incorporated by the forming aggregates, aggregate formation can be followed by FCS on a single-molecule level. This procedure was shown to work in both aqueous and organic polymer solutions. The high sensitivity of FCS permitted to determine the critical aggregation concentration of Janus micelles in THF to the very low value of 8 mg/L. No other experimental method available today is capable of determining aggregation concentrations in such a low concentration regime. In the same way the critical aggregation concentration of block copolymer polystyrene-Amylose in THF was determined.

Finally, temperature-dependent correlation curves allowed the determination of reaction constants and enthalpies. This is of particular interest in biochemical contexts, as the amount of available material can be minute. Exemplarily, the binding enthalpy of an RPA protein to a single-stranded DNA strain is determined by temperature-dependent correlation curves.

The modifications made to a classical FCS setup were shown to enhance the spectrum of possible applications to new experimental fields. The methods and concepts developed in the framework of this thesis are expected to play an important role in meeting future challenges of polymer physics and microbiology.

Kapitel 9

Zusammenfassung

In dieser Arbeit wurde die Einzelmolekültechnik Fluoreszenzkorrelationsspektroskopie (FCS) zur Untersuchung von Polymerlösungen und für temperaturabhängige Messungen an biologischen Systemen eingesetzt. Für die Durchführung dieser Messungen war es notwendig, den zur Verfügung stehenden kommerziellen Aufbau zu modifizieren und zu erweitern. Des Weiteren sind für die Messungen neue mit Farbstoff markierte Polymere synthetisiert und eine neue Methode für die Farbstoffmarkierung von ionischen Molekülen und Aggregaten entwickelt worden.

Durch den Einbau eines Spezialobjektives konnte das zur Verfügung stehende Fluoreszenzkorrelationsmikroskop so modifiziert werden, dass es für Messungen an Polymerlösungen mit sehr unterschiedlichen Brechungsindizes geeignet war. Für Messungen mit organischen Lösungsmitteln und für temperaturabhängige Studien wurde eine Probenkammer mit Temperaturregelung entwickelt. Die Materialien für die Kammer und die Verbindungen zwischen den Einzelteilen wurden so gewählt, dass sie eine hohe Widerstandsfähigkeit gegen die meisten organischen Lösungsmittel aufweisen.

Um aus den FCS Messungen die Diffusionskoeffizienten der Polymere und deren Konzentration zu bestimmen war eine genaue Form- und Größenbestimmung des Beobachtungsvolu-

mens notwendig. Dafür wurde eine Reihe von Polystyrolpolymeren mit Molekulargewichten zwischen 4 und 1550 kg/mol synthetisiert, die am Ende der Kette genau ein Farbstoffmolekül tragen. Alle Polymere wurden mittels anionischer Polymerisation hergestellt, was die Polydispersität sehr gering hält und damit die Genauigkeit der Volumenbestimmung erhöht. Das in diesen Messungen eingesetzte Konzept ist auch auf andere Lösungsmittel übertragbar. Das bedeutet, dass auf diesem Weg Fluoreszenzkorrelationsmikroskope für verschiedene Lösungsmittel geeicht und so Lösungen mit ganz unterschiedlichen Brechungsindizes untersucht werden können.

Ferner wurde am Beispiel von Polystyrol gezeigt, dass FCS in der Lage ist, den Übergang zwischen dem verdünnten und dem halb verdünnten Konzentrationsbereich von Polystyrolösungen zu bestimmen. Dazu wurden die farbstoffmarkierten Ketten mit nichtmarkierten Polystyrolketten gleicher Länge gemischt und die Beweglichkeit der Ketten mittels FCS gemessen. Die Auswertung der Beweglichkeit der Ketten bei verschiedenen Mischungsverhältnissen führt zur Überlappungskonzentration. Als Ergebnis erhält man ein Skalierungsgesetz für die Überlappungskonzentration in Abhängigkeit des Molekulargewichts ($c^* \propto M^{1-3*0.59}$) im Molekulargewichtsbereich von 4 bis 1550 kg/mol. Der Vergleich mit den Vorhersagen der Flory-Huggins-Theorie ($c^* \propto M^{1-3*0.6}$) zeigt eine hervorragende Übereinstimmung. Dieses Experiment zeigt, dass FCS in Konzentrations- und Molekulargewichtsbereiche vordringt, die bisher nicht experimentell zugänglich waren.

Schließlich wurden in dieser Arbeit Konzepte entwickelt, wie mit Hilfe von FCS die Aggregation von Molekülen verfolgt werden kann. Anhand von niedermolekularen Tensidmolekülen wurde gezeigt, dass sich durch die Coulomb Wechselwirkung kationische Tenside mit anionischen Farbstoffen und umgekehrt markieren lassen. Bereits unterhalb der mit klassischen Methoden bestimmten kritischen Mizellenkonzentration wurden mit FCS Mizellen nachgewiesen. Dieses Ergebnis bestätigt experimentell die Vorhersagen, die von Israeliachvili im Jahr 1991 getroffen wurden.

Desweiteren wurde gezeigt, dass die Verwendung von unlöslichen Farbstoffmolekülen, die in sich bildende Aggregate eingelagert werden, Aggregatbildung für FCS sichtbar macht. Diese Variante wurde sowohl für wässrige als auch für organische Polymerlösungen verwendet. Durch die niedrigen Farbstoffkonzentrationen, die in FCS-Experimenten verwendet werden, konnte die Kritische Aggregationskonzentration (c_{ac}) von Janus-Mizellen in THF von $\approx 8 \text{ mg/L}$ noch bestimmt werden. Keine andere derzeit verfügbare Methode kann in einem so niedrigen Konzentrationsbereich die Aggregation von Molekülen nachweisen. Auf die gleiche Weise wurde die kritische Aggregationskonzentration des Block-Copolymer Polystyrol-Amylose in THF und die der verseiften Janus-Mizellen in Wasser bestimmt. Schliesslich erlaubt die temperaturabhängige Messung von Korrelationskurven die Bestimmung von Reaktionsenthalpien und Reaktionskonstanten. Dies ist insbesondere in der Biochemie aufgrund des äußerst geringen Materialverbrauchs sehr gefragt. In dieser Arbeit wurde mit Hilfe temperaturabhängiger FCS-Messungen die Bindungsenergie des Proteins RPA an eine Einzelstrang-DNS bestimmt.

Durch die Modifizierung und Erweiterung des vorhandenen Fluoreszenzkorrelationsmikroskops und durch die Synthese neuer Polymere konnten neue Einsatzbereiche für die Fluoreszenzkorrelationsspektroskopie erschlossen werden. Es ist zu erwarten, dass die in dieser Arbeit entwickelten Methoden und Konzepte sowohl in der Polymerphysik als auch in der Mikrobiologie eine wichtige Rolle spielen werden.

List of Publications

H. Zettl, Y. Portnoy, M. Gottlieb, and G. Krausch.

Investigation of micelle formation by fluorescence correlation spectroscopy. *J Phys Chem B*, 109(27):13397–13401, 2005.

H. Zettl, W. Häfner, A. Böker, H. Schmalz, M. Lanzendorfer, A. H. E. Müller, and G. Krausch.

Fluorescence correlation spectroscopy of single dye-labeled polymers in organic solvents. *Macromolecules*, 37(5):1917–1920, 2004.

Rainer Erhardt, Alexander Boeker, Heiko Zettl, Hakon Kaya, Wim Pyckhout-Hintzen, Georg Krausch, Volker Abetz, and Axel H.E. Mueller.

Janus micelles. *Macromolecules*, 34(4):1069–1075, 2001.

A. Böker, H. Elbs, H. Hänsel, A. Knoll, S. Ludwigs, H. Zettl, V. Urban, V. Abetz, A. H. E. Müller, and G. Krausch.

Microscopic mechanisms of electric-field-induced alignment of block copolymer microdomains. *Phys. Rev. Lett.*, 89(13):–, 2002.

H. Hänsel, H. Zettl, G. Krausch, C. Schmitz, R. Kisselev, M. Thelakkat, and H. W. Schmidt.

Combinatorial study of the long-term stability of organic thin-film solar cells. *Appl. Phys. Lett.*, 81(11):2106–2108, 2002.

R. Erhardt, M. F. Zhang, A. Böker, H. Zettl, C. Abetz, P. Frederik, G. Krausch, V. Abetz, and A. H. E. Müller.

Amphiphilic Janus micelles with polystyrene and poly(methacrylic acid) hemispheres. *J Am Chem Soc*, 125(11):3260–3267, 2003.

F. Schubert, H. Zettl, W. Häfner, G. Krauss, and G. Krausch.

Comparative thermodynamic analysis of DNA-protein interactions using surface plasmon resonance and fluorescence correlation spectroscopy. *Biochemistry*, 42(34):10288–10294, 2003.

H. Hänsel, H. Zettl, G. Krausch, R. Kisselev, M. Thelakkat, and H. W. Schmidt.

Optical and electronic contributions in double-heterojunction organic thin-film solar cells. *Adv Mater*, 15(24):2056–+, 2003.

A. Böker, H. Elbs, H. Hänsel, A. Knoll, S. Ludwigs, H. Zettl, A. V. Zvelindovsky, G. J. A. Sevink, V. Urban, V. Abetz, A. H. E. Müller, and G. Krausch.

Electric field induced alignment of concentrated block copolymer solutions. *Macromolecules*, 36(21):8078–8087, 2003.

K. Loos, A. Böker, H. Zettl, A. F. Zhang, G. Krausch, and A. H. E. Müller.

Micellar aggregates of amylose-block-polystyrene rod-coil block copolymers in water and THF. *Macromolecules*, 38(3):873–879, 2005.

J. T. Russell, Y. Lin, A. Böker, L. Su, P. Carl, H. Zettl, J. B. He, K. Sill, R. Tangirala, T. Emrick, K. Littrell, P. Thiyagarajan, D. Cookson, A. Fery, Q. Wang, and T. P. Russell. Self-assembly and cross-linking of bionanoparticles at liquid-liquid interfaces. *Angew Chem Int Edit*, 44(16):2420–2426, 2005.

K. Schmidt, A. Böker, H. Zettl, F. Schubert, H. Hänsel, F. Fischer, T. M. Weiss, V. Abetz, A. V. Zvelindovsky, G. J. A. Sevink, and G. Krausch.

Influence of initial order on the microscopic mechanism of electric field induced alignment of block copolymer microdomains. *Langmuir*, 21(25):11974–11980, 2005.

M. Lysetska, H. Zettl, I. Oka, G. Lipps, G. Krauss, and G. Krausch.

Site-specific binding of the 9.5 kilodalton DNA-binding protein ORF80 visualized by atomic force microscopy. *Biomacromolecules*, 6(3):1252–1257, 2005.

A. Böker, K. Schmidt, A. Knoll, H. Zettl, H. Hänsel, V. Urban, V. Abetz, and G. Krausch. The influence of incompatibility and dielectric contrast on the electric field-induced orientation of lamellar block copolymers. *Polymer*, 47(3):849–857, 2006.

H. Zettl, W. Häfner, A. Böker, H. Schmalz, M. Lanzendorfer, A. H. E. Müller, and G. Krausch.

Fluorescence correlation spectroscopy (FCS) of single dye-labeled polymers in organic solvents. (vol 37, pg 1917, 2004). *Macromolecules*, 38(15):6748–6748, 2005.

R. Erhardt, A. Böker, H. Zettl, H. Kaya, W. Pyckhout-Hintzen, G. Krausch, V. Abetz, and A. H. E. Müller.

Superstructures of Janus micelles. *Abstr Pap Am Chem S*, 221:U366–U366, 2001.

G. Krausch, A. Böker, H. Elbs, H. Hänsel, A. Knoll, S. Ludwigs, H. Zettl, V. Urban, V. Abetz, and A. H. E. Müller.

Macroscopic alignment of concentrated block copolymer solutions in electric fields. *Abstr Pap Am Chem S*, 224:U366–U366, 2002.

Danksagung

Während meiner Doktorarbeit habe ich von vielen Seiten Unterstützung erhalten. Dafür möchte ich mich bedanken.

Mein besonderer Dank gilt Prof Georg Krausch, der es mir ermöglicht hat dieses interessante Thema zu bearbeiten und mich immer wieder ermutigt hat auch neue Wege zu bestreiten und mich dabei auch unterstützt hat.

Bei Herrn Prof Axel Müller möchte ich für für viele Anregungen und Diskussionen über die Aggregation von Polymeren und über das Herstellen farbstoff-markierter Polymere bedanken.

Herrn Prof Matthias Ballauff möchte ich für viele interessante und anregende Diskussionen zum Thema Überlappungskonzentration von Polymeren danken.

Für seine Ideen zur Untersuchung der Mizellbildung mittels FCS von Tensiden möchte ich Herrn Prof Moshe Gottlieb danken. Auch die in seiner Gruppe durchgeführten Vergleichsmessungen halfen bei der Veröffentlichung des Papers.

Bei Herrn PD Dr Jörg Enderlein bedanke ich mich für die Rechnungen der MDF für die verschiedensten Objektive und Lösungsmittel und für die Diskussionen über die theoretischen Grundlagen von FCS, die mir viele neue Einblicke gewährt haben.

Mein Ansprechpartner für viele Fragen sowohl im Bereich der Optik als auch wenn es darum ging Programme in C zu schreiben oder wieder einmal längst vergessenes Inventar zu reaktivieren war Dr Wolfgang Häfner.

Helmut Hänsel danke ich für viele fruchtbare und kontroverse Diskussionen zu vielen wissenschaftlichen und nicht wissenschaftlichen Themen. Er war immer ein guter Ansprechpartner für Labview, Mathematika und sonstige Software und Computer Probleme. Er

hatte immer ein offenes Ohr für Probleme und war mir immer ein guter Freund.

Alexander Böker danke ich für seine große Hilfe bei der Synthese und Aufreinigung der farbstoffmarkierten Polymere, für viele unvergessliche Stunden am ESRF in Grenoble. Besonders danke ich ihm für seine langjährige Freundschaft.

Frank Schubert danke ich für seinen unermüdlichen Einsatz bei den Messungen biologischer Systeme und einen nicht immer funktionierenden Confocor Rechner am laufen zu halten. Ich danke ihm auch für viele gemeinsame Stunden beim Kochen, Grillen und verschiedene Besuche in Paderborn.

Bei Katja Loos und Rainer Erhardt danke ich, dass sie mir ihre Polymere für meine Messungen zur Verfügung gestellt haben, ohne sicher sein zu können, dass wir gute Ergebnisse erzielen.

Holger Schmalz danke ich für viele gute Ideen zur Synthese der endfunktionalisierten Polymere. Bei Anette Krökel bedanke ich mich für das farbstoff Markieren und Aufreinigen der Polymere.

Unserem "Hauselektroniker" Franz Fischer danke ich für die Ideen für eine elektrische Heizung der Probenkammern. Er ist immer gut für unkonventionelle aber effektive Lösungen.

Unsere Sekretärin Frau Sybille Zimmermann schafft mit ihrer offenen und liebenswerten Art ein sehr angenehmes Klima am Lehrstuhl. Auch die kontinuierliche Versorgung mit "Nervennahrung" hilft dabei so manche anstrengende Messreihe durchzuhalten.

Bei allen hier nicht namentlich genannten aktuellen und ehemaligen Mitgliedern des Lehrstuhls PCII möchte ich mich für die gute Arbeitsatmosphäre, die Hilfsbereitschaft und viele schöne gemeinsame Stunden, sei es bei Ausflügen, bei Grillfesten oder nur bei einer kurzen Kaffeerunde bedanken.

Ute danke ich, dass sie es wagte bei mir Diplomarbeit zu schreiben und viele Messungen zur Überlappungskonzentration in dieser Zeit gemacht wurden.

Bei meiner Familie möchte ich mich für die Unterstützung bedanken, die ich in all den Jahren während meines Studiums und während der Promotion erfahren habe.

Erklärung

Die vorliegende Arbeit wurde von mir selbstständig verfasst, und ich habe dabei keine anderen als die angegebenen Hilfsmittel und Quellen benutzt.

Ferner habe ich nicht versucht, anderweitig mit oder ohne Erfolg eine Dissertation einzureichen oder mich der Doktorprüfung zu unterziehen.

Bayreuth, den 12. Juni 2006

Heiko Zettl

Bibliography

- [Ara76] S. R. Aragon and R. Pecora. “Fluorescence Correlation Spectroscopy As a Probe of Molecular- Dynamics”. *J. Chem. Phys.*, **64** (4), 1791–1803 (1976)
- [Bec96] H. Becker. *Organikum : organisch-chemisches Grundpraktikum* (Barth, Heidelberg, 1996), 20., bearb. und erw. aufl. edition
- [Bev92] P. R. Bevington and D. K. Robinson. *Data reduction and error analysis for the physical sciences* (WCB McGraw-Hill, Boston, Mass., 1992), 2nd edition
- [Bro88] W. Brown and K. Mortensen. “Comparison of Correlation Lengths in Semidilute Polystyrene Solutions in Good Solvents by Quasi-Elastic Light-Scattering and Small-Angle Neutron-Scattering”. *Macromolecules*, **21** (2), 420–425 (1988)
- [Bug69] V. Bugdahl. “Diffusion measurements on solutions of high polymers studied with an interferometer”. *Kautschuk Gummi Kunststoffe*, **22** (9), 486–8 (1969)
- [Dei04] J. Deich, E. M. Judd, H. H. McAdams, and W. E. Moerner. “Visualization of the movement of single histidine kinase molecules in live *Caulobacter* cells”. *Proceedings of the National Academy of Sciences of the United States of America*, **101** (45), 15921–15926 (2004)
- [Dit01] P. S. Dittrich and P. Schwille. “Photobleaching and stabilization of fluorophores used for single-molecule analysis with one- and two-photon excitation”. *Appl. Phys. B-Lasers Opt.*, **73** (8), 829–837 (2001)
- [dlT01] M. H. de la Torre, R. Forni, and G. Chirico. “Brownian dynamics simulations of fluorescence fluctuation spectroscopy”. *Eur Biophys J Biophys*, **30** (2), 129–139 (2001)

- [Dun02] A. W. Dunn, E. D. Svensson, and C. Dekker. “Scanning tunneling spectroscopy of C-60 adsorbed on Si(100)-(2 x 1)”. *Surf. Sci.*, **498** (3), 237–243 (2002)
- [Egg98] C. Eggeling, J. Widengren, R. Rigler, and C. A. M. Seidel. “Photobleaching of fluorescent dyes under conditions used for single-molecule detection: Evidence of two-step photolysis”. *Analytical Chemistry*, **70** (13), 2651–2659 (1998)
- [Egg05] C. Eggeling, A. Volkmer, and C. A. M. Seidel. “Molecular photobleaching kinetics of rhodamine 6G by one- and two-photon induced confocal fluorescence microscopy”. *Chemphyschem*, **6** (5), 791–804 (2005)
- [Ehr74] M. Ehrenberg and R. Rigler. “Rotational Brownian-Motion and Fluorescence Intensity Fluctuations”. *Chem Phys*, **4** (3), 390–401 (1974)
- [Ehr76] M. Ehrenberg and R. Rigler. “Fluorescence correlation spectroscopy applied to rotational diffusion of macromolecules”. *Quarterly Reviews of Biophysics*, **9** (1), 69–81 (1976)
- [Eig94] M. Eigen and R. Rigler. “Sorting single molecules: application to diagnostics and evolutionary biotechnology”. *Proceedings of the National Academy of Sciences of the United States of America*, **91** (13), 5740–5747 (1994)
- [Els74] E. L. Elson and D. Magde. “Fluorescence Correlation Spectroscopy .1. Conceptual Basis and Theory”. *Biopolymers*, **13** (1), 1–27 (1974)
- [End00] J. Enderlein. “Theoretical study of detection of a dipole emitter through an objective with high numerical aperture”. *Opt Lett*, **25** (9), 634–636 (2000)
- [End03] J. Enderlein and M. Bohmer. “Influence of interface-dipole interactions on the efficiency of fluorescence light collection near surfaces”. *Opt Lett*, **28** (11), 941–943 (2003)
- [End04] J. Enderlein, I. Gregor, D. Patra, and J. Fitter. “Art and artefacts of fluorescence correlation spectroscopy”. *Curr Pharm Biotechno*, **5** (2), 155–161 (2004)
- [Erh01a] R. Erhardt. *Janus-Micellen: Amphiphile oberflächenkompartimentierte Polymermicellen mit vernetztem Kern*. Ph.D. thesis, Universität Bayreuth (2001)

- [Erh01b] R. Erhardt, A. Boeker, H. Zettl, H. Kaya, W. Pyckhout-Hintzen, G. Krausch, V. Abetz, and A. H. Mueller. “Janus micelles”. *Macromolecules*, **34** (4), 1069–1075 (2001)
- [Erh03] R. Erhardt, M. F. Zhang, A. Boker, H. Zettl, C. Abetz, P. Frederik, G. Krausch, V. Abetz, and A. H. E. Muller. “Amphiphilic Janus micelles with polystyrene and poly(methacrylic acid) hemispheres”. *J Am Chem Soc*, **125** (11), 3260–3267 (2003)
- [Eva99] H. Evans, D.F.; Wennerstrom. *The Colloidal Domain where Physics, chemistry and Biology meet* (Wiley-VCH, New York, 1999)
- [Gal04] M. O. Gallyamov, B. Tartsch, A. R. Khoklov, S. S. Sheiko, H. G. Borner, K. Matyjaszewski, and M. Moller. “Real-time scanning force microscopy of a macromolecular conformational transitions”. *Macromol Rapid Comm*, **25** (19), 1703–1707 (2004)
- [Gee82] H. Geerts. “A Note on Number Fluctuations - Statistics of Fluorescence Correlation Spectroscopy as Applied to Brownian-Motion”. *J Stat Phys*, **28** (1), 173–176 (1982)
- [Gen79] P.-G. d. Gennes. *Scaling concepts in polymer physics* (Cornell University Press, Ithaca, N.Y., 1979)
- [Gon05] Y. I. Gonzalez and E. W. Kaler. “Cryo-TEM studies of worm-like micellar solutions”. *Curr Opin Colloid In*, **10** (5-6), 256–260 (2005)
- [Gra80] W. W. Graessley. “Polymer-Chain Dimensions and the Dependence of Viscoelastic Properties on Concentration, Molecular-Weight and Solvent Power”. *Polymer*, **21** (3), 258–262 (1980)
- [Gra99] C. Graf, W. Schaertl, K. Fischer, N. Hugenberg, and M. Schmidt. “Dye-labeled poly(organosiloxane) microgels with core-shell architecture”. *Langmuir*, **15** (19), 6170–6180 (1999)
- [Har01] G. S. Harms, L. Cognet, P. H. M. Lommerse, G. A. Blab, and T. Schmidt. “Autofluorescent proteins in single-molecule research: Applications to live cell imaging microscopy”. *Biophysical Journal*, **80** (5), 2396–2408 (2001)

- [Her79] H. Hervet, L. Leger, and F. Rondelez. “Self-Diffusion in Polymer-Solutions - Test for Scaling and Reptation”. *Phys. Rev. Lett.*, **42** (25), 1681–1684 (1979)
- [Hes02a] S. T. Hess, S. H. Huang, A. A. Heikal, and W. W. Webb. “Biological and chemical applications of fluorescence correlation spectroscopy: A review”. *Biochemistry*, **41** (3), 697–705 (2002)
- [Hes02b] S. T. Hess and W. W. Webb. “Focal volume optics and experimental artifacts in confocal fluorescence correlation spectroscopy”. *Biophysical Journal*, **83** (4), 2300–2317 (2002)
- [Ike01] S. Ikeda, V. J. Morris, and K. Nishinari. “Microstructure of aggregated and nonaggregated kappa-carrageenan helices visualized by atomic force microscopy”. *Biomacromolecules*, **2** (4), 1331–1337 (2001)
- [Isr91] J. N. Israelachvili. *Intermolecular and surface forces* (Academic Press, London, 1991), 2nd edition
- [Jan00] A. Janshoff, M. Neitzert, Y. Oberdorfer, and H. Fuchs. “Force spectroscopy of molecular systems - Single molecule spectroscopy of polymers and biomolecules”. *Angew Chem Int Edit*, **39** (18), 3213–3237 (2000)
- [Kam94] N. Kamenka, A. Kaplun, Y. Talmon, and R. Zana. “Interactions between Polysoaps and Surfactants in Aqueous-Solutions”. *Langmuir*, **10** (9), 2960–2964 (1994)
- [Kim94] C. Kim, B. F. Paulus, and M. S. Wold. “Interactions of human replication protein A with oligonucleotides”. *Biochemistry*, **33** (47), 14197–14206 (1994)
- [Kim02] Y. Kim, T. Komeda, and M. Kawai. “Single-molecule imaging and, repositioning of 1,3-butadiene adsorbed on Pd(110) surface”. *Jpn J Appl Phys 1*, **41** (7B), 4924–4927 (2002)
- [Kop74] D. E. Koppel. “Statistical Accuracy in Fluorescence Correlation Spectroscopy”. *Phys Rev A*, **10** (6), 1938–1945 (1974)
- [Kop76] D. E. Koppel, D. Axelrod, J. Schlessinger, E. L. Elson, and W. W. Webb. “Dynamics of fluorescence marker concentration as a probe of mobility”. *Biophysical Journal*, **16** (11), 1315–1329 (1976)

- [Kri02] O. Krichevsky and G. Bonnet. “Fluorescence correlation spectroscopy: the technique and its applications”. *Rep. Prog. Phys.*, **65** (2), 251–297 (2002)
- [Lao99] Y. Lao, L. Chang Geun, and M. S. Wold. “Replication protein A interactions with DNA. 2. Characterization of double-stranded DNA-binding/helix-destabilization activities and the role of the zinc-finger domain in DNA interactions”. *Biochemistry*, **38** (13), 3974–3984 (1999)
- [Lin84] B. Lindman, M. C. Puyal, N. Kamenka, R. Rymden, and P. Stilbs. “Micelle Formation of Anionic and Cationic Surfactants from Fourier-Transform H-1 and Li-7 Nuclear Magnetic-Resonance and Tracer Self-Diffusion Studies”. *J Phys Chem-Us*, **88** (21), 5048–5057 (1984)
- [Lin97] Z. C. Lin and C. D. Eads. “Polymer-induced structural transitions in oleate solutions: Microscopy, rheology, and nuclear magnetic resonance studies”. *Langmuir*, **13** (10), 2647–2654 (1997)
- [Liu05] R. G. Liu, X. Gao, J. Adams, and W. Oppermann. “A fluorescence correlation spectroscopy study on the self-diffusion of polystyrene chains in dilute and semidilute solution”. *Macromolecules*, **38** (21), 8845–8849 (2005)
- [Loo97] K. Loos and R. Stadler. “Synthesis of amylose-block-polystyrene rod-coil block copolymers”. *Macromolecules*, **30** (24), 7641–7643 (1997)
- [Loo01] K. Loos. *Hybridmaterialien mit Amylose durch enzymatische grafting from Polymerisation*. Ph.D. thesis, Universität Bayreuth (2001)
- [Loo02] K. Loos and A. H. E. Muller. “New routes to the synthesis of amylose-block-polystyrene rod-coil block copolymers”. *Biomacromolecules*, **3** (2), 368–373 (2002)
- [Loo05] K. Loos, A. Boker, H. Zettl, A. F. Zhang, G. Krausch, and A. H. E. Muller. “Micellar aggregates of amylose-block-polystyrene rod-coil block copolymers in water and THF”. *Macromolecules*, **38** (3), 873–879 (2005)
- [Lop98] G. P. Lopinski, D. J. Moffatt, D. D. Wayner, and R. A. Wolkow. “Determination of the absolute chirality of individual adsorbed molecules using the scanning tunnelling microscope”. *Nature*, **392** (6679), 909–911 (1998)

- [Lys02] M. Lysetska, A. Knoll, D. Boehringer, T. Hey, G. Krauss, and G. Krausch. “UV light-damaged DNA and its interaction with human replication protein A: an atomic force microscopy study”. *Nucleic Acids Research*, **30** (12), 2686–2691 (2002)
- [Lys05] M. Lysetska, H. Zettl, I. Oka, G. Lipps, G. Krauss, and G. Krausch. “Site-specific binding of the 9.5 kilodalton DNA-binding protein ORF80 visualized by atomic force microscopy”. *Biomacromolecules*, **6** (3), 1252–1257 (2005)
- [Mad76] D. Madge. “Chemical kinetics and fluorescence correlation spectroscopy”. *Quarterly Reviews of Biophysics*, **9** (1), 35–47 (1976)
- [Mag72] D. Magde, W. W. Webb, and E. Elson. “Thermodynamic Fluctuations in a Reacting System - Measurement By Fluorescence Correlation Spectroscopy”. *Phys. Rev. Lett.*, **29** (11), 705 (1972)
- [Mag74] D. Magde, E. L. Elson, and W. W. Webb. “Fluorescence Correlation Spectroscopy .2. Experimental Realization”. *Biopolymers*, **13** (1), 29–61 (1974)
- [Mai97] S. Maiti, U. Haupts, and W. W. Webb. “Fluorescence correlation spectroscopy: Diagnostics for sparse molecules”. *Proceedings of the National Academy of Sciences of the United States of America*, **94** (22), 11753–11757 (1997)
- [Mcd77] M. E. McDonnell and A. M. Jamieson. “Quasi-Elastic Light-Scattering Measurements of Diffusion-Coefficients in Polystyrene Solutions”. *J Macromol Sci Phys*, **B 13** (1), 67–88 (1977)
- [Mes99] U. Meseth, T. Wohland, R. Rigler, and H. Vogel. “Resolution of fluorescence correlation measurements”. *Biophysical Journal*, **76** (3), 1619–1631 (1999)
- [Mit93] P. G. Mitsis, S. C. Kowalczykowski, and I. R. Lehman. “A single-stranded DNA binding protein from *Drosophila melanogaster*: characterization of the heterotrimeric protein and its interaction with single-stranded DNA”. *Biochemistry*, **32** (19), 5257–5266 (1993)
- [Moe99] W. E. Moerner, E. J. Peterman, H. Sosa, S. Brasselet, R. M. Dickson, S. Kummer, R. Sakowicz, and L. S. B. Goldstein. “Single-molecule studies of fluorescent proteins and enzymes”. *Biophysical Journal*, **76** (1), A20–A20 (1999)

- [Mul02] D. J. Muller, H. Janovjak, T. Lehto, L. Kuerschner, and K. Anderson. “Observing structure, function and assembly of single proteins by AFM”. *Prog Biophys Mol Bio*, **79** (1-3), 1–43 (2002)
- [Niu92] S. Niu, K. R. Gopidas, N. J. Turro, and G. Gabor. “Formation of Premicellar Clusters of 2-Para-Toluidinonaphthalene-6-Sulfonate with Cationic Detergents”. *Langmuir*, **8** (5), 1271–1277 (1992)
- [Nor99] R. Norenberg, J. Klingler, and D. Horn. “Study of the interactions between poly(vinyl pyrrolidone) and sodium dodecyl sulfate by fluorescence correlation spectroscopy”. *Angewandte Chemie - International Edition*, **38** (11), 1626–1629 (1999)
- [Pal87] A. G. r. Palmer and N. L. Thompson. “Molecular aggregation characterized by high order autocorrelation in fluorescence correlation spectroscopy”. *Biophysical Journal*, **52** (2), 257–270 (1987)
- [Pet86] N. O. Petersen. “Scanning fluorescence correlation spectroscopy. I. Theory and simulation of aggregation measurements”. *Biophysical Journal*, **49** (4), 809–815 (1986)
- [Pfa99] A. Pfau, W. Schrepp, and D. Horn. “Detection of a single molecule adsorption structure of poly(ethylenimine) macromolecules by AFM”. *Langmuir*, **15** (9), 3219–3225 (1999)
- [Rac80] J. Raczek and G. Meyerhoff. “Determination of Molecular-Weight Distributions from Frequency-Analyzing (Dynamic) Light-Scattering”. *Macromolecules*, **13** (5), 1251–1254 (1980)
- [Rac82] J. Raczek. “Determination of Molecular-Weight Dependences and Characterization of Molecular-Weight Distributions”. *Eur Polym J*, **18** (5), 393–401 (1982)
- [Rac83] J. Raczek. “Error-Analysis for the Determination of Molecular-Weight Distributions by Dynamic Light-Scattering”. *Eur Polym J*, **19** (7), 607–615 (1983)
- [Ras95] E. Raspaud, D. Lairez, and M. Adam. “On the Number of Blobs Per Entanglement in Semidilute and Good Solvent Solution - Melt Influence”. *Macromolecules*, **28** (4), 927–933 (1995)

- [Ric59] B. Richards and E. Wolf. “Electromagnetic Diffraction in Optical Systems .2. Structure of the Image Field in an Aplanatic System”. *Proc R Soc Lon Ser-A*, **253** (1274), 358–379 (1959)
- [Rig79] R. Rigler, P. Grasselli, and M. Ehrenberg. “Fluorescence Correlation Spectroscopy and Application to the Study of Brownian-Motion of Biopolymers”. *Phys Scripta*, **19** (4), 486–490 (1979)
- [Rig01] R. Rigler and E. Elson. *Fluorescence correlation spectroscopy : theory and applications*. Springer series in chemical physics ; 65 (Springer, Berlin, 2001)
- [Saf03] S. Saffarian and E. L. Elson. “Statistical analysis of fluorescence correlation spectroscopy: The standard deviation and bias”. *Biophysical Journal*, **84** (3), 2030–2042 (2003)
- [Sak00] Y. Sako, S. Minoghchi, and T. Yanagida. “Single-molecule imaging of EGFR signalling on the surface of living cells”. *Nat Cell Biol*, **2** (3), 168–172 (2000)
- [Sch00a] H. Schuch, J. Klingler, P. Rossmannith, T. Frechen, M. Gerst, J. Feldthusen, and A. H. Mueller. “Characterization of micelles of polyisobutylene-block-poly(methacrylic acid) in aqueous medium”. *Macromolecules*, **33** (5), 1734–1740 (2000)
- [Sch00b] G. J. Schutz, M. Sonnleitner, P. Hinterdorfer, and H. Schindler. “Single molecule microscopy of biomembranes (review)”. *Mol Membr Biol*, **17** (1), 17–29 (2000)
- [Sch01a] P. Schwille. “Fluorescence correlation spectroscopy and its potential for intracellular applications”. *Cell Biochem. Biophys.*, **34** (3), 383–408 (2001)
- [Sch01b] P. Schwille and U. Kettling. “Analyzing single protein molecules using optical methods”. *Current Opinion in Biotechnology*, **12** (4), 382–386 (2001)
- [Sch03] F. Schubert, H. Zettl, W. Hafner, G. Krauss, and G. Krausch. “Comparative thermodynamic analysis of DNA-protein interactions using surface plasmon resonance and fluorescence correlation spectroscopy”. *Biochemistry*, **42** (34), 10288–10294 (2003)
- [Sch05] F. Schubert. *Visualization, Kinetics, and Thermodynamics of DNA-Protein Interactions*. Ph.D. thesis, Bayreuth (2005)

- [Sei01] G. Seisenberger, M. U. Ried, T. Endress, H. Buning, M. Hallek, and C. Brauchle. “Real-time single-molecule imaging of the infection pathway of an adeno-associated virus”. *Science*, **294** (5548), 1929–1932 (2001)
- [Sen01] T. J. Senden. “Force microscopy and surface interactions”. *Curr Opin Colloid In*, **6** (2), 95–101 (2001)
- [She97] C. Sheppard and P. Török. “An electromagnetic theory of imaging in fluorescence microscopy, and imaging in polarization fluorescence microscopy”. *Bioimaging*, **5**, 205–208 (1997)
- [Sta99] K. Starchev, J. Buffle, and E. Perez. “Applications of fluorescence correlation spectroscopy: Polydispersity measurements”. *Journal of Colloid and Interface Science*, **213** (2), 479–487 (1999)
- [Sti01] K. A. Stieglitz, B. A. Seaton, and M. F. Roberts. “Binding of proteolytically processed phospholipase D from *Streptomyces chromofuscus* to phosphatidylcholine membranes facilitates vesicle aggregation and fusion”. *Biochemistry*, **40** (46), 13954–13963 (2001)
- [Str97] G. R. Strobl. *The physics of polymers : concepts for understanding their structures and behavior* (Springer, Berlin, 1997), 2nd corr. edition
- [Tan80] C. Tanford. *The hydrophobic effect formation of micelles and biological membranes* (Wiley, New York, 1980), 2nd edition
- [Tor98] P. Torok, P. D. Higdon, and T. Wilson. “Theory for confocal and conventional microscopes imaging small dielectric scatterers”. *J Mod Optic*, **45** (8), 1681–1698 (1998)
- [Tor00] P. Torok. “Propagation of electromagnetic dipole waves through dielectric interfaces”. *Opt Lett*, **25** (19), 1463–1465 (2000)
- [Tro02] C. Tromas and R. Garcia. “Interaction forces with carbohydrates measured by atomic force microscopy”. *Top Curr Chem*, **218**, 115–132 (2002)
- [VR01] E. Van Rompaey, Y. Engelborghs, N. Sanders, S. C. De Smedt, and J. Demeester. “Interactions between oligonucleotides and cationic polymers investigated by fluorescence correlation spectroscopy”. *Pharmaceutical Research*, **18** (7), 928–936 (2001)

- [Web76] W. W. Webb. “Applications of fluorescence correlation spectroscopy”. *Quarterly Reviews of Biophysics*, **9** (1), 49–68 (1976)
- [Wid95] J. Widengren, U. Mets, and R. Rigler. “Fluorescence Correlation Spectroscopy of Triplet-States in Solution - a Theoretical and Experimental-Study”. *J Phys Chem-Us*, **99** (36), 13368–13379 (1995)
- [Wid00] J. Widengren and P. Schwille. “Characterization of photoinduced isomerization and back-isomerization of the cyanine dye Cy5 by fluorescence correlation spectroscopy”. *Journal of Physical Chemistry A*, **104** (27), 6416–6428 (2000)
- [Woh01] T. Wohland, R. Rigler, and H. Vogel. “The standard deviation in fluorescence correlation spectroscopy”. *Biophysical Journal*, **80** (6), 2987–2999 (2001)
- [Wol59] E. Wolf. “Electromagnetic Diffraction in Optical Systems .1. An Integral Representation of the Image Field”. *Proc R Soc Lon Ser-A*, **253** (1274), 349–357 (1959)
- [Wol97] M. S. Wold. “Replication protein A: a heterotrimeric, single-stranded DNA-binding protein required for eukaryotic DNA metabolism”. *Annu. Rev. Biochem.*, **66**, 61–92 (1997)
- [Zei01] Zeiss. *Applications Manual – LSM510 - ConfoCor 2* (Carl Zeiss Jena, 2001)
- [Zet04] H. Zettl, W. Hafner, A. Boker, H. Schmalz, M. Lanzendorfer, A. H. E. Muller, and G. Krausch. “Fluorescence correlation spectroscopy of single dye-labeled polymers in organic solvents”. *Macromolecules*, **37** (5), 1917–1920 (2004)
- [Zet05a] H. Zettl, W. Hafner, A. Boker, H. Schmalz, M. Lanzendorfer, A. H. E. Muller, and G. Krausch. “Fluorescence correlation spectroscopy (FCS) of single dye-labeled polymers in organic solvents.(vol 37, pg 1917, 2004)”. *Macromolecules*, **38** (15), 6748–6748 (2005)
- [Zet05b] H. Zettl, Y. Portnoy, M. Gottlieb, and G. Krausch. “Investigation of micelle formation by fluorescence correlation spectroscopy”. *J Phys Chem B*, **109** (27), 13397–13401 (2005)
- [Zha01] J. J. Zhao, S. C. Bae, F. Xie, and S. Granick. “Diffusion of polymer-coated nanoparticles studied by fluorescence correlation spectroscopy”. *Macromolecules*, **34** (10), 3123–3126 (2001)